Capillary Electrophoresis and Electrochromatography

Kathleen Anne McCormack

A thesis submitted in fulfilment of the requirements

for the degree of PhD

to the

University of Edinburgh

1991

Acknowledgements

I would like to thank my supervisor, Prof. J.H. Knox for his help and encouragement throughout the last four years.

I would also like to thank the University of Edinburgh for providing me with a studentship for the first three years, and Applied Biosystems, Inc., for providing funding in the final year.

The technical staff in the department were always helpful, and for that I am grateful.

Thanks to members of the chromatography group, in particular Qian, Iain and Madge, for their friendship and support.

And especially, thanks to Andrew, without whom I would never have got this far.

Abstract

Investigations into two capillary electroseparation techniques have been undertaken—capillary zone electrophoresis (CZE) and capillary electrochromatography (CEC). With CEC, in which propulsion of the eluent is by electrokinetic means, attempts were made to pack microbore capillaries with silica based packing materials, using both slurry packing and electrokinetic packing methods. Slurry packing was found to be the most effective. The formation of voids in the packed bed on application of high voltages was found to be the major limitation of the technique. Some separations of polyaromatic hydrocarbons are presented.

In CZE, the column temperatures were found to be up to 45°C above ambient under moderate conditions. Methods for calculating the buffer temperature in the capillary are shown. The excess temperature results in increased diffusion coefficients of samples. The observed curvature of plots of the number of theoretical plates against the linear velocity of the sample can be accounted for by the increased diffusion coefficients at higher temperatures and these plots can be linearised by including a temperature dependent factor.

The temperature excess can be minimised by the use of thick walled capillaries or forced convective cooling of the capillary. Liquid cooling is more effective for heat dissipation than air cooling.

To my parents

Contents

List of Figures

List of Tables

Chapter 1

Description of Electrophoresis

1.1 Introduction

Electrophoresis is the term employed to describe the movement of charged particles, ions or molecules under the influence of an electric field. The term was first used in 1909 by the German bacteriologist, Leonor Michaelis [1], in his investigation of the electrical transportation of enzymes . The principles of the method had been known however since the late 19th century, at which time it was known as cataphoresis. Initial studies were mostly concerned with the movement of colloidal particles in an electric field, first done by Picton and Linder in 1892 [2] on a variety of colloidal solutions, although Lodge [3] had measured the velocity of the hydrogen ion as early as 1886 using zone electrophoresis. Over a hundred years later, electrophoresis in its various forms is a major separation technique, used both as an analytical tool and for preparative scale separations, on a variety of samples ranging from simple ions to larger proteins and particles. In particular, electrophoresis has become one of the primary separation methods in the areas of biology and biotechnology for DNA and oligonucleotides. The future of the human genome project, mapping the DNA sequence of the human

genome, will depend to a large extent on the successful future development and speed of electrophoretic techniques.

The velocity of an ion or particle in an electric field is related to its charge and mass, in particular on the charge to mass ratio. Separation occurs when the charge to mass ratio is sufficiently different to allow the samples to draw apart in the time allowed for electrophoresis. Due to the nature of the separation process, electrophoresis is carried out in aqueous solutions, with or without the presence of a support. Electrophoretic techniques are complementary to another major analytical separation process–chromatography. Chromatographic techniques depend on the differential migration of analytes as a result of partitioning between two distinct phases moving relative to each other. In liquid chromatography, the moving phase or eluent is an aqueous or organic fluid, passing through or over a solid support which itself can be either polar or non-polar. In gas chromatography, the mobile phase is a gas and the stationary phase can be a liquid or a solid. Separation occurs when analytes have different affinities for the stationary phase and thus move at different velocities.

Although electrophoresis and chromatography are different techniques, occurring as a result of independent physical processes, similarities do exist, and recent work has shown [4, 5] that they can be combined to give a new technique—electrochromatography.

1.2 Basic Principles of Electrophoresis

An ion in an aqueous solution possesses an effective charge, q. When an electric field E is applied across the solution, the ion experiences a force F_e where

$$F_e = qE \tag{1.1}$$

As the ion accelerates as a result of this force, it experiences an opposing force due to the viscosity of the medium. The force is given by Stokes Law

$$F_v = 6\pi\eta a u \tag{1.2}$$

where u is the velocity of the ion, a is the effective radius of the ion and η is the viscosity of the medium. When these two forces are balanced, the ion reaches a steady state velocity given by equating equations 1.1 and 1.2,

$$u = \frac{qE}{6\pi\eta a} \tag{1.3}$$

The steady state velocity of the ion is thus seen to be directly related to the electric field strength and the charge on the ion, and inversely proportional to the size of the ion.

The velocity in an electric field can be expressed also as

$$u = \mu_{ep} E \tag{1.4}$$

where μ_{ep} is the electrophoretic mobility of the ion in question, and by comparison with equation 1.3

$$\mu_{ep} = \frac{q}{6\pi\eta a} \tag{1.5}$$

The electrophoretic mobility is a fundamental parameter in electrophoresis, the separation only occurring if the electrophoretic mobilities of the ions are sufficiently different in magnitude. The mobility is a signed quantity, as anions and cations move in opposite directions in an electric field.

1.3 Classic Forms of Electrophoresis

Electrophoretic techniques may be classified into two groups, Moving Boundary Electrophoresis (MBE) and Zone Electrophoresis. One of the limiting features of

electrophoretic techniques is the generation of Joule heat (discussed in Chapter 3) which can give rise to density gradients leading to convection currents and loss of separation. One method of preventing convective mixing is to carry out electrophoresis in a stabilising medium such as a gel. Electrophoresis can thus be further classified into free solution electrophoresis or supported electrophoresis.

1.3.1 Moving Boundary Electrophoresis (MBE)

As the name suggests, MBE is concerned with the movement of a boundary formed between a sol or solution and a pure fluid, and is a free solution technique. MBE is carried out in vertical U-shaped tubes of narrow rectangular shaped cross-section to improve heat dissipation and sensitivity of optical detection methods. This apparatus is referred to as a Tiselius type apparatus [6], named after Tiselius who developed it for the separation of proteins. Sample is applied as a uniform solution in a U-tube. The solution is contained in the lower part and pure solvent is laid over it in such a way as to form an initially sharp boundary. The system is thermostatted at 4 °C, at which temperature the solutions have maximum density and vary least with temperature, minimising the effect of convection currents which interfere with the sharpness of the boundary. The tube must be vertical for the same reason i.e. to minimise convective mixing. Migration of the boundary or boundaries is usually followed by Schlieren techniques which show the boundaries as peaks, but fluorescence and uv detection have also been employed. MBE has found wide application in the past for measuring electrophoretic mobilities and in the separation and identification of large molecules, in particular proteins. In fact the first application of MBE was to demonstrate that the component of blood serum originally identified as globulin consisted of a mixture of at least five proteins. It has also been useful in the

study of systems with concentration dependent interactions, as there is always a region where the concentration remains constant.

Complete separation and isolation of the components of a mixture is not possible. Each analyte in the solution, if they have different electrophoretic mobilities, will move at different rates and thus a boundary will eventually be formed for each component present in the mixture. However the only pure zones will be one at the beginning, with the fastest mobility, and one at the end corresponding to the component with the lowest mobility. As a result, MBE cannot be used as a preparative tool. MBE has now mostly been replaced as an analytical technique by zone electrophoresis in its various forms, a simpler and less expensive technique, but is still employed for the measurement of absolute electrophoretic mobilities and identification of the number and possibly type of components present. The experiments of Picton and Linder [2] and Lodge [3] already referred to were carried out using moving boundary techniques.

1.3.2 Zone Electrophoresis

With zone electrophoresis, the sample is applied as a relatively narrow zone or spot to the separating medium. Given sufficient time of analysis and given that the samples have different mobilities, complete separation is possible. Until recently, zone electrophoresis was most successful using a support. The horizontal rotating tube method of Hjerten [7] was developed to minimise the effects of convection currents in larger separation tubes, but has found little application. Free zone electrophoresis in a density gradient [8], developed using inert solutions such as sucrose, has had more success but, in general, electrophoresis utilising a support has been the most successful and finds widespread use in laboratories. The supports used vary from strips of paper and cellulose acetate to starch and

polyacrylamide gels.

Paper and Cellulose Acetate

Paper electrophoresis is the simplest and easiest form of supported electrophoresis. The paper strip is wetted with the buffer to be used, the excess buffer is removed, and the paper is placed on a horizontal sheet of glass with the ends of the paper dipping into vessels containing the buffer and electrodes. The sample is applied as a narrow streak or series of spots, the paper is covered with a sheet of glass to prevent evaporation of the buffer, and the voltage is applied at both ends. Paper electrophoresis may also be carried out with the paper suspended from a frame, or by supporting it in the middle and allowing the ends to hang down in the shape of an inverted 'V'. After separation is complete, or after a set time, the strip is removed, dried and treated with a reagent to locate and identify the substances separated. Whether the applied voltage is high or low depends on the size of the molecules to be separated. Small molecules e.g. amino acids and nucleotides obtained by hydrolysis of proteins and nucleic acids are best separated using high voltages of 50–200 V cm^{-1}. Low potential gradients are used to separate larger molecules such as proteins, enzymes and nucleic acids. Apart from organic ions, paper electrophoresis is useful in the separation of mixtures of inorganic ions and complexes.

The principles and methods of electrophoresis with cellulose acetate are similar to those used with paper, replacing the paper with a strip of cellulose acetate. With paper electrophoresis, direct connection of separating medium and applied voltage is possible, with the paper dipping into the electrode compartment. With cellulose acetate and the various types of gel electrophoresis discussed in the following section, connection is indirect via a wick. The stains and staining techniques used in identification and quantification differ from paper to cellulose

acetate. Quantification may be carried out using densitometers.

Cellulose acetate strips have advantages over paper electrophoresis—they adsorb proteins less, give better separations and allow the entire procedure to be carried out in less than two hours, but they are more expensive than paper strips.

Gel Electrophoresis

Gel electrophoresis is carried out on slabs of gels of the order of 1–10 mm thick. Due to the pores present in gels, a sieving mechanism occurs along with the electrophoretic process, and so introduces another separation mechanism to the technique, one based on size. Large molecules are restricted in their movement through the gel, and thus are held up for longer than smaller molecules which can pass straight through. By this method it was shown that the single α_2 globulin band from paper electrophoresis of blood serum gave ten sub-bands after starch gel electrophoresis.

A variety of gels have been used for gel electrophoresis, including silica, agar, starch and polyacrylamide. By far the most widespread used gel today is polyacrylamide, although agar and agarose gels are often used for larger molecules, being stronger than the most highly porous polyacrylamide gels.

Agar and agarose gels are made by warming and dissolving the granular material in the appropriate buffer, casting the gels and allowing them to set on cooling. The resolving power of the gels depends on the concentration of dissolved agar or agarose, dilute gels being used for very large molecules.,

Polyacrylamide gels are produced by polymerisation of a monomer (acrylamide) and a cross-linking agent ["BIS", (N,N'-methylene bisacrylamide)] which is initiated by free radicals produced by natural light in the prescence of sensitizers e.g. riboflavin, or peroxides. Addition of tertiary amines can improve the gelation e.g. "TEMED" (N,N,N',N'-tetramethylethylenediamine). The pore size

can be regulated by varying the concentration of acrylamide+BIS (w/v) (T) and the ratio of BIS concentration to BIS+acrylamide concentration (%) (C). A typical gel can have T=7.5 and C=5. Usually T is changed and C is kept constant at 5.

By varying T from 3 to 30, with C=5, a range of pore sizes can be obtained from 0. 5 to 3 nm and which will interact with analytes having molecular weights of 10^3 to 10^6.

The advantages of polyacrylamide gels are that they are transparent, flexible and versatile, but they are time consuming to prepare and can only be used once. Despite these disadvantages, polyacrylamide gels have found widespread use, particularily in the biological and clinical sciences, and are exclusively used in the separation of large molecules. A number of different techniques have been developed for use with polyacrylamide gels, although they can also be used with starch gels.

1. Disc electrophoresis was originally described by Ornstein [10] and Davis [11] in 1964. Electrophoresis is carried out in small glass or plastic cylinders, approximately 7.5 cm long with an inner diameter of 0.5 cm and an outer diameter of 0.7 cm. The name arises from the fact that the bands or zones stack up as a series of concentrated discs at the beginning of the procedure. This zone sharpening effect occurs as a result of discontinuities in the gel, placing a large pore gel (high migration rate) on top of a small pore gel (low migration rate), and by using multi-phasic buffers whose ions migrate at faster and slower rates than the analyte ions. Disc electrophoresis can be relatively simple, using just two different pore size gels, or more complicated, varying the buffer and/or pH also, depending on the application. Discs of sample obtained may be as narrow as 10 μm.

2. Gradient Gel Electrophoresis [12]. Using a gel with a continuous gradient

of pore size, by keeping C constant and varying T, can result in a much improved electrophoretic separation. As each component reaches its pore limit, it becomes trapped and so separation is more on the basis of size rather than mobility. As there is an inverse square root relation between T and pore size, the pore size gradient becomes very shallow at high values of T. Thus the use of a concave rather than a linear gradient of T is recommended. The sample can also be applied parallel to the pore gradient, and is run at right angles to it. The result gives a spectrum of separation profiles with various T values.

3. SDS-PAGE. Large molecules such as proteins and nucleic acids often have much the same charge to mass ratio and similar sizes, and so are difficult to resolve with straight electrophoresis. Addition of SDS to the buffer solution and gel causes denaturation of the sulfide and hydrogen bonds holding the protein together and complexes with it giving equal mass to charge densities for all proteins. The proteins are now effectively linear chains, and resolution is more easily accomplished by the sieving properties of the gel. It has been shown that under complete denaturing conditions, the electrophoretic velocity is a linear function of the log of the molecular weight. Thus by using suitable standards, the molecular weight of a protein can be determined from a single run, although in practice more runs are done for accuracy. This relationship has been found to hold true for oligonucleotides and proteins.

4. Immuno-electrophoresis was first suggested by Pierre Grabar in 1952. It is useful for biological material containing a complicated mixture of macromolecules with similar physico-chemical properties so that it may be difficult to distinguish between them. Components are distinguished and defined by a specific reaction i.e. their antigenic specificity. Electrophoresis is carried out in gels containing antibodies to the protein or proteins of interest in the mixture. When the protein and its antibody meet, precipitation occurs. The area enclosed by

the precipitate is proportional to the antigen-antibody ratio and is thus suitable for immunological identification and quantitation of antigens and/or antibodies. In crossed immuno-electrophoresis [13] electrophoresis is first carried out in an agarose gel, followed by electrophoresis perpendicular to this in an antibody containing gel. Rocket immuno-electrophoresis [14] is performed in an agarose gel with a mono-specific anti-serum, and allows the determination of a single protein in a protein mixture in a number of samples. The diluted samples to be compared are applied in circular wells side by side. Identification of the protein is by the rocket shaped precipitate formed. Quantification is based on the height of the precipitate.

5. Isoelectric Focussing (IEF). In IEF, a pH gradient is produced in the gel, parallel to the electric field gradient. The pH gradient is developed using high molecular weight polyamino polycarbonic acids. The sample, which must be zwitterionic, is placed at any point in the gel. If the local pH is greater than the sample's isoelectric point, it will be negatively charged and migrate towards the anode when the electric field is applied. The opposite occurs for samples placed where the pH is less than its isoelectric point. The sample migrates under the influence of the electric field until it reaches a point in the gel where the pH has the same value as its isoelectric point. At this position the sample has no charge and cannot move any further. Separation occurs therefore as a result of differences in isoelectric points and not as a result of differing mobilities. IEF produces very narrow zones, narrower than those expected from molecular diffusion. When a sample molecule diffuses out from the zone, it is pulled back by the restoring force of the pH gradient. IEF has been used in the study of amino acids, peptides and proteins.

Isotachophoresis

Isotachophoresis is a form of free zone electrophoresis which, unlike the previous methods described, is carried out in capillaries of 200–1000 μm i.d.. The ions to be analysed, either anions or cations but not a mixture of both, are injected onto the separation column as a zone between what are termed the leading and trailing electrolytes. The leading electrolyte contains an ion of the same charge as the sample ions, but with a higher mobility than any of the ions to be separated. The trailing electrolyte contains an ion of the same charge but lower mobility than any of the analyte ions. The ions all have identical counter ions. Under the influence of the applied field, a series of zones is generated in order of increasing mobility of ions. Each zone consists of ions of only one type (assuming all have different mobilities) with the common counter ion. The boundaries between the zones are extremely sharp.

1.4 Limitations of Classical Electrophoresis Techniques

The foregoing descriptions of the most commonly used electrophoretic techniques, and only a small proportion of the variety available, indicate the versatility of the technique. The most useful or used techniques necessitate the use of gels. As a result, the methods are time consuming and labour intensive. Automation is impossible. While resolution (chapter 3) is good to excellent, quantification is difficult. Quantification involves the use of densitometers, which measure the density of the eluted zone, and is not very accurate. The gels have to be stained with a specific reagent in order to see the separated components after the run. Hence the electrophoresis cannot be monitored in real time, only

trial and error allowing one to decide when the separation is complete. Recovery of the sample from the gel is also time consuming and difficult.

The problems with Joule heating were mentioned briefly at the beginning of the previous section. When an electric field is applied across a solution containing current carrying ions, power is generated and converted into Joule heat. The net result is an increase in the temperature of the electrolyte. As the heat can be dissipated only from the sides of the vessel, the temperature rise is greatest in the centre and decreases towards the sides. A temperature gradient across the system is the result. In free solution, the density of the buffer varies with the temperature and can result in convection currents which may destroy, or at least damage, the separation. Along with the density gradient, a vicosity gradient is also present. From equation 1.5 the electrophoretic mobility is inversely proportional to the viscosity. The viscosity gradient causes a velocity gradient in which the velocity of the sample will vary according to position in the separation chamber. Elimination of these effects, in particular density gradients, was achieved by using gels as stabilising media, and was the main reason for the success and widespread use and development of the described methods over the past forty to fifty years.

1.5 Modern Capillary Electroseparation Methods

In 1981, Jorgenson and Lukacs [15] carried out free solution electrophoresis in very narrow capillaries, producing well resolved narrow peaks in less than 20 minutes of a mixture of amino acids. Although up to 30 kV m^{-1} was applied to the capillary to effect the separation, the small inner diameter of the capillary was thought to allow effective dissipation of the Joule heat. The technique has since

become very popular, and resulted in a rebirth of electrophoresis as an exciting new topic for research. Since that paper, the development of what have come to be known as *capillary electroseparation methods* has been extremely rapid, with the development by manufacturers of complete systems and the emergence of new applications. At present, capillary electroseparation methods can be divided into 5 distinct techniques, some at a more advanced stage than others in their development.

1.5.1 Capillary Zone Electrophoresis (CZE)

In 1979, Mikkers et al [16] had carried out free zone electrophoresis in 200 μm i.d. teflon capillaries of inorganic and organic anions, with a separation showing about 36,000 plates (Chapter 3). However the true power and efficiency of CZE was illustrated by Jorgenson and Lukacs [15, 17, 18] in some papers in 1981 in which they obtained separations of amino acids and proteins in glass capillaries.

CZE is in fact a very simple technique. The basic apparatus is shown in figure 1.1 and consists of a high power voltage supply, two buffer reservoirs, a narrow separation capillary of 50–150 cm in length, a detector and ancillary equipment to record the electropherogram. Initially the capillaries used were of teflon, glass or quartz, but the most common material in use today is fused silica. The capillaries are generally in the order of 50–100 μm i.d., but with electrochemical detection capillaries as small as 2 μm have been used [19]. Up to 30 kV is applied across columns of 50–150 cm in length. With glass or fused silica columns electro-osmotic flow is usually present. Electro-osmosis (Chapter 2) arises as a result of the double layer which occurs when the surface is in contact with an aqueous solution. Electro-osmosis can be beneficial to the separation. The electro-osmotic velocity is superimposed on the electrophoretic velocity of

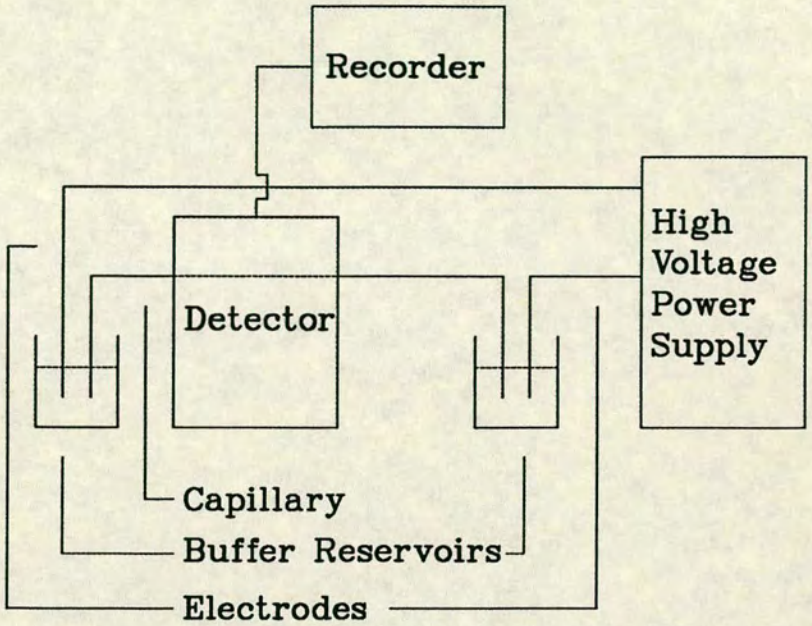

Figure 1.1. Basic apparatus for capillary zone electrophoresis.

the ions and sweeps all ions, regardless of charge, in the same direction. Thus analyses of anions and cations in a single run is possible, one of the advantages of CZE over alternative electrophoretic techniques previously described. The electro-osmotic flow may be suppressed if necessary by coating the inside of the capillary with a polymer layer [20], or reversed by adding $AlCl_3$ or CTAB (cetyl trimethyl ammonium bromide) to the buffer [21]. Injection and detection are both carried out on column, minimising dispersion of the analyte peaks (Chapter 3).

Injection may be carried out in one of three ways:

1. Hydrodynamic—the injection end of the capillary is placed in the sample

solution and raised a few cm above the level of the outlet reservoir. Poiseuille flow results in the deposition of sample on the capillary.

2. Electrokinetic—the injection end is placed in the sample container and a low voltage of 2–5 kV is applied for a few seconds (5–30). Sample is deposited on the column through a combination of electrophoresis and electro-osmosis.

3. Pressure—a positive pressure is applied at the injection end, or a vacuum at the outlet, to allow the sample to be pushed or sucked onto the column.

Detection in CZE is 'on-column' i.e. the column passes through the detector and sample zones are detected while they are still on the column. The majority of commercial instruments available to date use uv detection, as it is the most versatile, if the least sensitive (due to the small path length), of the methods available. Fluorescence detection is also becoming more readily available and with indirect detection [33] can be used to detect a wide variety of samples. In research laboratories a wide range of detection methods are routinely used, including amperometric [22], conductivity [23], thermal lens [24], laser induced fluorescence [25, 26] with circular dichroism [27] and charge coupled devices [28], refractive index [29], mass spectrometry [31, 32] and radioactivity [30], but the majority of these are likely to remain as research tools and not commercially available, at least in the near future.

CZE has been applied in a wide range of analyses, including peptides and proteins [34, 35, 42], simple inorganic [36, 37] and organic ions [37, 38], pharmaceutical products [39, 40], polystyrene particles [41], viruses [43] and red blood cells [44]. The beauty of CZE is in its simplicity and high efficiency, along with the fact that it uses very small volumes of sample (of the order of nl), particularly important in biological analyses where the amount of sample available is often very small. The speed of analysis (as compared to other modes of electrophoresis) and the fact that it can be easily automated makes it suitable for routine

analyses and more useful in an industrial environment. As the separation mode operates on different principles to chromatographic methods, it has become a complementary technique to methods such as HPLC and GC.

1.5.2 Micellar Electrokinetic Capillary Chromatography (MECC)

One disadvantage of CZE is that neutral compounds cannot be separated. In 1984, Terabe developed micellar electrokinetic capillary chromatography in an attempt to overcome this shortcoming [45]. In MECC, a micelle forming substance e.g. SDS (sodium dodecyl sulphate) is added to the buffer solution at a concentration greater than its critical micelle concentration. The SDS micelle is negatively charged and moves through the capillary at a velocity less than that of the bulk electro-osmotic flow. Neutral molecules are partitioned into the hydrophobic interior of the micelle and when there will move at the velocity of the micelle. The migration time or overall velocity of the neutral molecule will be altered, depending on its partition coefficient between the micelle and the surrounding solution. Thus a separation of neutral molecules can be brought about, based on a partition mechanism. The separation mechanism is a chromatographic one, not electrophoretic, but it developed from CZE and uses electro-osmotic flow to pump the fluid, and so is defined as an electroseparation method.

MECC may also improve the separation of charged compounds by adding an additional separation mechanism. As a result, charged compounds which have similar mobilities but different affinities for the interior of the micelle will show improved resolution if a micelle forming substance is added to the buffer [46].

Improvements have also been noted by using a mixed micellar solution e.g.

SDS and Brij35 instead of a single micellar sample [47] and by the addition of tetra-alkyl ammonium salts [48] and metal additives [49] to the micellar solution.

Chiral resolution with MECC has been achieved by adding bile salts to the micellar solution. Using SDS and sodium taurodeoxycholate, chiral resolution of drugs has been achieved [50] and optical resolution of amino acids has been achieved with the addition of a chiral additive, N-dodecanoyl-L-valine [51] to the micellar solution.

MECC has been used to separate a wide variety of compounds including phenols [52], vitamins [53], metal chelates [54], pharmaceuticals [55], nucleosides [56], gunshot and explosives [57] and illicit drug substances [58], and the range of applications is continuing to increase.

1.5.3 Complexation Electrophoresis

Addition of a charged complexing agent to the solution presents another method for the separation of neutral compounds. By complexing with the neutral sample, a charge is imparted to it and its migration velocity is altered, thus permitting separation if the selectivity of complexation is sufficiently different for the neutral samples present. There are not many examples in the literature of this type. Walbroehl and Jorgenson [59] added tetrahexyl ammonium perchlorate to the buffer solution and achieved a separation of organic aromatic hydrocarbons. Zare et al [60] added Cu^{2+} and aspartame to the buffer to form a chiral complex which was successful in effecting chiral resolution of a mixture of racemic amino-acids. Metal ions have been separated using on-column chelation with 8-hydroxyquinoline-5-sulphonic acid [61], and chiral resolution of drugs achieved by inclusion complexation with β-cyclodextrin [62].

This method is not as general as MECC, as the interaction between additive

and sample is a specific one, and so the additive may need to be tailored to suit the separation mixture. However, it does broaden the range of separation modes available.

1.5.4 Capillary Gel Electrophoresis (CGE)

Karger and co-workers were the first to develop capillary gel electrophoresis, when they filled a capillary with polyacrylamide gel to separate proteins [63]. Like the slab gel methods, CGE separates through a molecular sieve mechanism, separating on the basis of size. To date, CGE has been applied mostly to the resolution of polynucleotides, both natural and synthetic, where separation according to the number of nucleotide units is possible [64, 65, 66]. Schomburg has produced some excellent results with polynucleotides [68]. Chiral resolution of amino acids has been achieved by incorporating β-cyclodextrin into the gel [66].

CGE is a highly efficient technique, producing more plates per metre than CZE or MECC, with 30 million plates having been reported [66]. The high efficiency is due in part to the low diffusion coefficients of molecules in gels, compared to those in fluids.

Difficulties in production of the gel filled capillaries due to bubble formation are common, although Schomburg has reported a method for the production of bubble free gels [69]. Gel filled capillaries are now becoming commercially available and the manufacturers claim good reproducibility and stability. With this advance, CGE is likely to become more widely used. Hansen *et al* [70] have reported using entangled polymers such as methylcellulose or polyethylene glycol as additives which generate a molecular sieving effect in the separation of DNA standards. This method is more convenient and reproducible than use of gel filled capillaries.

Detection is on-column, and uv detection is most commonly used. Electrokinetic injection is the only injection mode that can be used.

1.5.5 Electrochromatography

Electrochromatography has been defined by Lecoq in 1944 [72] as *"chromatography carried out with the aid of an electromotive force"*. More recently, it has been redefined by Grant [73] as *"chromatography in which electro-osmosis is responsible for the flow of mobile phase"*. The latter definition will be used for the purpose of this thesis.

Pretorius suggested in 1974 [74] that it should be possible to propel fluid through a bed of particles by electro-osmotic flow and, due to the inherently flat flow profile (Chapter 2) compared to the parabolic flow profile of pumped flow, peak dispersion (Chapter 3) should be less, and so generate a more efficient chromatogram. Pretorius illustrated the improved efficiency of an unretained peak under electro-osmotic flow compared to pressure driven flow with a column packed with 75-125 μm Porasil particles. Strain had reported the combined use of electrophoresis and chromatography as early as 1939 [75] in the analysis of charged dyes. Tsuda has more recently used the term to describe separations in which a voltage was applied across a micro HPLC column of 2 mm i.d. in which the primary fluid pumping mechanism was pressure driven [5], but the efficiency was not improved due to the large diameter column used, although better resolution was obtained.

Jorgenson and Lukacs [18] reported a separation of aromatic hydrocarbons on 10 μm reversed phase material, but did not develop the technique any further. Knox and Grant [4] achieved separation of polyaromatic hydrocarbons on 5 μm

reversed phase materials, with 69,000 plates reported, which was the first illustration of the high efficiencies that could be produced for retained substances.

The use of electro-osmosis to propel fluid in open tubular liquid chromatography (OTLC) has also been investigated. Tsuda [76] derivitised the surface of a drawn glass capillary of 130 μm i.d. with octadecylsilane to obtain separations of aromatic hydrocarbons. While some improvement is possible over pressure driven flow [77] for unretained peaks, the effect diminishes as the compounds are more strongly retained on the surface (Chapter 3). Yeung [78] has shown that the electro-osmotic flow can be reversed to give a strong flow rate with the addition of CTAB to the mobile phase for electrically driven OTLC on an ODS derivitised capillary.

1.6 Aims of thesis

The previous sections have described the basic principles of electrophoresis and the derivitives available to date. The emergence of capillary electroseparation techniques has also been described. The aims of the work presented in this thesis are two fold.

1. To further develop the technique of electrochromatography and apply it to small particle packing materials.

2. To further develop an understanding of the Joule heating which may be present in capillary electrophoresis, to develop methods for the calculation of temperature rises within the capillary, and to understand the effect of temperature on the efficiency and resolution of the technique and to predict means by which it may be minimised.

Chapter 2 will discuss electrokinetic effects which are pertinent to both capillary electrophoresis and electrochromatography. Chapter 3 discusses the concepts of separation effiency, band broadening and dispersion, and resolution as applied to these techniques. Chapters 4 to 7 present the experimental work, results and conclusions.

Chapter 2

Electrokinetic Effects

In the previous chapter, mention was made of two important effects, namely electrophoresis and electro-osmosis, which are relevant to this thesis and, with two other phenomena, are grouped under the heading *electrokinetic effects.* Electrokinetic effects are defined as *"the relative movement, with respect to one another, of a solid and a liquid accompanied by certain electrical phenomena".* The four known electrokinetic effects are as follows:

1. Electrophoresis which is the movement of a charged ion or particle through a stationary medium induced by the prescence of an electric field.

2. Sedimentation potential which is the potential created when a charged ion or particle moves through a stationary fluid. Originally called the Dorn Effect and first studied by Dorn in 1880, this is the reverse of electrophoresis.

3. Electro-osmosis which is the movement of fluid relative to a stationary surface as a result of an applied electric field. The phenomenon was first observed by Reuss in 1809 when he noticed the movement of a liquid through the pores of a diaphragm under an electric field.

4. Streaming potential which is the potential which arises when a fluid is forced along a stationary surface. It is the opposite of electro-osmosis, and was

first observed by Quinck in 1859 when liquid was forced through a porous material.

Of the four effects described, electrophoresis and electro-osmosis have a strong bearing on the work in this thesis, and will be discussed in further detail. The phenomena all arise as a result of the double layer which can occur when two different phases come in contact with each other. The following description will concentrate on the solid/aqueous solution interface specifically, in particular glass or fused silica.

2.1 The Double Layer

When a solid e.g. glass or fused silica, is in contact with an aqueous solution, the surface develops a net negative charge, through either ionisation of the silanol groups on the surface, or through preferential adsorption of negative ions. To balance the charge on the surface, a net excess of positive ions exists in solution close to the solid surface. The layer of excess positive ions is what constitutes the double layer, and is directly responsible for the effects briefly described above.

The first theoretical description of the double layer was due to Helmholtz and Perrin, who placed all the excess positive ions in a plane parallel to the surface, with the locus of the ions a distance from the surface equal to the hydrated radius of the counter ion. The model was unsatisfactory in that it predicted perfectly parabolic electrocapillary curves (surface tension versus potential difference) and that the double layer capacity was independent of potential, neither of which were borne out by experiment. The Gouy-Chapman model described the counter ions as being spread out over a diffuse region, subject to both electrical and thermal forces, with the concentration of counterions decreasing with distance from the surface. The Gouy-Chapman model, however, predicted an inverted parabolic

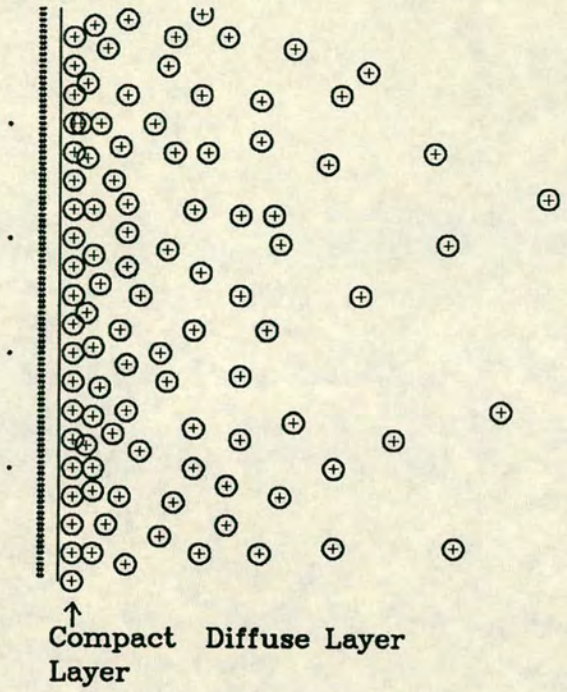

Figure 2.1. Stern model of the double layer.

dependence of the capacitance of the double layer with potential which was not found experimentally, and predicted a greater dependence of the capacitance on concentration than was observed.

Stern's treatment of the double layer combined both the Helmholtz-Perrin and Gouy-Chapman models. The double layer was described as having a fixed layer of hydrated counterions at a distance equal to the hydrated radius, with the remaining excess distributed in the solution in a cloud-like fashion. The double layer is now considered to be composed of a diffuse layer and a compact layer. Figure 2.1 illustrates the Stern model of the double layer, where only the excess charges are shown.

2.2 The Diffuse Layer

The diffuse layer consists of a spread out layer of excess charge, the ions of which are under the influence of thermal and electrical forces. To describe the variation of potential and charge density within this layer, use is made of the Poisson and Boltzmann equations. The Poisson equation is

$$\frac{d^2\psi}{dx^2} = \frac{-\rho}{\epsilon_o \epsilon_r} \tag{2.1}$$

where ψ is the potential at x and ρ is the excess charge density. ψ_o is the potential at the Outer Helmholtz Plane (OHP) i.e. between the compact layer and the bulk solution. If the surface is negatively charged

$$\rho = ze(n_+ - n_-) \tag{2.2}$$

where n_+, n_- are the numbers of positive and negative ions per unit volume at the point x in the double layer respectively, and e, z are the electronic charge and valence of the ion respectively.

Using the Boltzmann equation,

$$\begin{aligned} n_+ &= n_o \exp(ze\psi/kT) \\ n_- &= n_o \exp(-ze\psi/kT) \end{aligned} \tag{2.3}$$

Combining 2.2 and 2.3

$$\rho = +zen_o \left[\exp\left(+\frac{ze\psi}{kT}\right) - \exp\left(-\frac{ze\psi}{kT}\right)\right] \tag{2.4}$$

$$\rho = +2zen_o \sinh(ze\psi/kT) \tag{2.5}$$

Substituting into 2.1

$$\frac{d^2\psi}{dx^2} = \frac{-2zen_o}{\epsilon_o \epsilon_r} \sinh\left(\frac{ze\psi}{kT}\right) \tag{2.6}$$

At first sight, this is a complicated equation. However, using the Debye-Huckel approximation that if $ze\psi/kT \ll 1$

$$\sinh\left(\frac{ze\psi}{kT}\right) \sim \frac{ze\psi}{kT} \tag{2.7}$$

and making use of the mathematical rearrangement that

$$\frac{d^2\psi}{dx^2} = \frac{1}{2}\frac{d}{d\psi}\left(\frac{d\psi}{dx}\right)^2 \tag{2.8}$$

then

$$\frac{d}{d\psi}\left(\frac{d\psi}{dx}\right)^2 = -\frac{4z^2e^2n_o}{\epsilon_o\epsilon_r kT}\psi \tag{2.9}$$

Integrating

$$\left(\frac{d\psi}{dx}\right)^2 = -\frac{2z^2e^2n_o}{\epsilon_o\epsilon_r kT}\psi^2 + C \tag{2.10}$$

Using the boundary conditions that at $x = \infty, \psi = 0$ and $d\psi/dx = 0$, then $C = 0$. κ^2 is defined as

$$\kappa^2 = \frac{2z^2e^2n_o}{\epsilon_o\epsilon_r kT} \tag{2.11}$$

Substituting into 2.10, and taking square roots

$$\frac{d\psi}{dx} = -\kappa\psi \tag{2.12}$$

Integrating again, and using the boundary conditions that at $x = 0, \psi = \psi_o$

$$\psi = \psi_o \exp(-\kappa x) \tag{2.13}$$

Thus the potential at any point within the double layer is seen to vary exponentially with distance from the compact layer. The quantity κ in 2.13 and defined by 2.11 is known as the reciprocal double layer thickness, and is the thickness over which the potential decreases by a factor $1/e$. Alternatively $1/\kappa = \delta$ where

δ is the double layer thickness. Replacing n_o by cN_A where c is the concentration of the buffer and N_A is Avogadro's number,

$$\delta = \left(\frac{\epsilon_o \epsilon_r kT}{2z^2 e^2 N_A c} \right)^{1/2} \tag{2.14}$$

The double layer thickness is inversely dependent on the concentration of the buffer and on the charge of the counter ion. The derivation has assumed that the electrolyte is symmetrical, and requires for the Debye-Huckel approximation to hold with less than 10% error that $\psi < 20$ mV at $z = 1$, not common in CZE with aqueous buffers in a fused silica capillary.

[Appendix A gives a solution to the Poisson-Boltzmann equation without using the Debye-Huckel approximation. Using the final solution, it is seen that ψ can now be as high as 50 mV at $z = 1$, and that equation 2.13 is still valid to within 10%.]

2.3 The Compact Layer

In the simplest model of the compact layer, a certain proportion of the excess charges in solution are considered to be in a fixed plane parallel to the surface. The distance of this plane from the surface is generally considered to lie at a distance equivalent to the hydrated radius of the counterion. In fact, considering that the surface is also likely to have a layer of hydration, what is termed the Outer Helmholtz Plane (OHP) is likely to lie a little further out in the solution. The compact layer is equivalent to a parallel plate condenser. The potential varies linearly throughout the layer, from ψ_s on the surface to ψ_o on the OHP.

Figure 2.1 has shown the construction of the double layer due to Stern. Figure 2.2 shows the variation of potential throughout the double layer with distance from the surface, where ψ_s and ψ_o have been given arbitrary values.

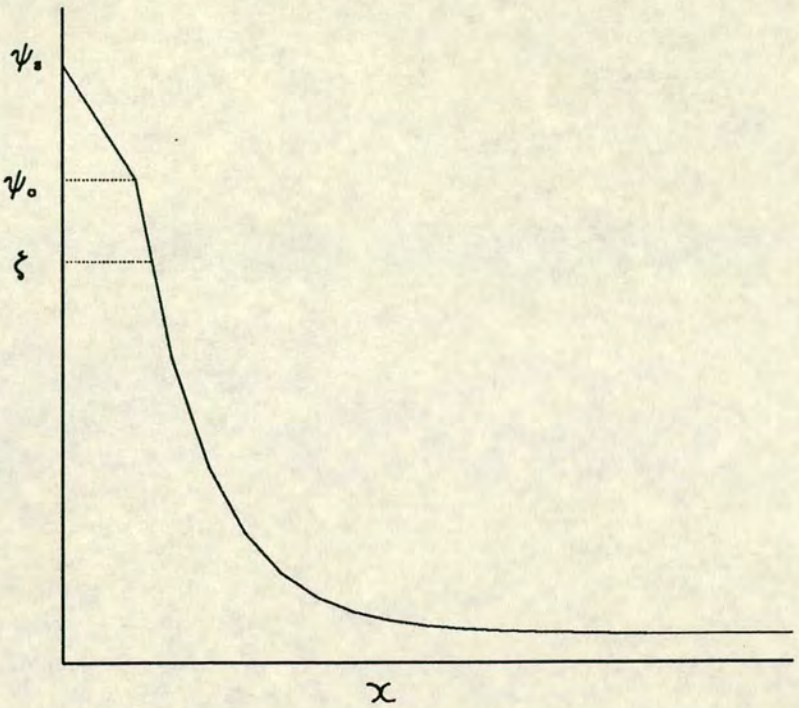

Figure 2.2. Variation of potential throughout the double layer.

This simple description of the excess charges in solution is based on that of Stern. However, the situation becomes more complicated depending on the nature of the buffer. It has been assumed in the simple description that the ions in solution are all hydrated, and so the closest distance of approach of these ions to the surface is equivalent to their hydrated radius. In fact, ions vary in their degree of hydration, the degree of hydration being inversely proportional to the volume charge density of the ion. Some anions and large cations are effectively unhydrated or very loosely hydrated in solution. As a result, these ions can approach closer to the surface and become specifically adsorbed on it, Specific or contact adsorption depends on the chemical nature of the ion, rather than on its charge. Because contact adsorption is relatively oblivious to the charge on the surface, anions can contact adsorb onto a negative surface, increasing the potential of the surface relative to the bulk solution. Contact adsorption

of cations results in a lowering of potential relative to the solution and, with superequivalent adsorption where the charge adsorbed is greater than the charge on the surface, the potential of the surface can be reversed. Thus addition of $AlCl_3$ to a buffer solution in contact with a glass surface results in reversal of the potential, and a net positive charge due to the superequivalent contact adsorption of the Al^{3+} ions on the surface. For a particular bulk concentration of a contact adsorbing species, the population of contact adsorbing ions in the inner layer changes as the charge on the surface changes. Contact adsorbed ions constitute the Inner Helmholtz Plane (IHP) with distance from the surface equal to the radius of the specifically adsorbed ions. Migration of an ion from the OHP to the IHP involves chemical interaction, interaction with the field arising from the surface charge q_s, and lateral interaction with an already settled population of contact adsorbed ions. The final expression is of the form

$$q_{CA} = C \exp(A q_s) \exp(-B q_{CA}^{3/2}) \tag{2.15}$$

where q_{CA} is the charge due to contact adsorbed ions, and A, B and C are constants.

2.4 The Zeta Potential

The zeta potential (ζ) is defined as the potential at the plane of shear of the double layer. As the ions in the compact layer are considered to be 'fixed' and unmoving, the plane of shear lies just outside the OHP in the diffuse layer. The magnitude of the ζ potential is then slightly less than the potential at the plane, ψ_o. The actual magnitude of the ζ potential depends on the thickness of the diffuse part of the double layer, $1/\kappa$. With a narrow double layer, or small $1/\kappa$, the potential drops from ψ_o to 0 over a shorter distance and therefore ψ_o and ζ can have quite different values. In very dilute solutions, $1/\kappa$ is large

and ζ approaches the value of ψ_o. As a result, $\zeta \propto 1/\kappa$. As $1/\kappa \propto 1/z\sqrt{c}$, large concentrations of buffers and/or ions with high valencies contribute to a lowering of the ζ potential.

The excess surface charge density at the OHP must be equivalent to the excess charge density in the bulk of the solution. Thus by integrating the excess charge density ρ over the bulk of the solution and applying the Debye-Huckel approximation an expression can be found relating ψ_o to σ_o as (Appendix B)

$$\psi_o = \frac{\sigma_o}{\epsilon_o \epsilon_r \kappa} \tag{2.16}$$

where σ_o is the surface charge excess at the OHP and ψ_o is the potential at that point. In dilute solutions, where $\zeta \sim \psi_o$ this gives

$$\zeta = \frac{\sigma_o}{\epsilon_o \epsilon_r \kappa} \tag{2.17}$$

The ζ potential is the most significant quantity in electrokinetic phenomena as it is the potential at the plane of shear and so is directly responsible for the magnitude of the electrokinetic effects observed. Similarily, it too is relatively easily measured from observation of electrokinetic effects, while the quantities ψ_s and ψ_o are difficult, if not impossible, to quantify.

2.5 Electro-osmosis

When an electric field is applied parallel to the double layer, the ions in solution begin to move, dragging their solvation sheaths with them. In the double layer, there is an excess of one ion over another, and so there is a net flow towards one electrode. With a fixed glass surface, in which the surface charge is generally negative, a bulk flow of liquid occurs towards the cathode as a result of the excess positive charge in the double layer. The velocity in the double layer increases from

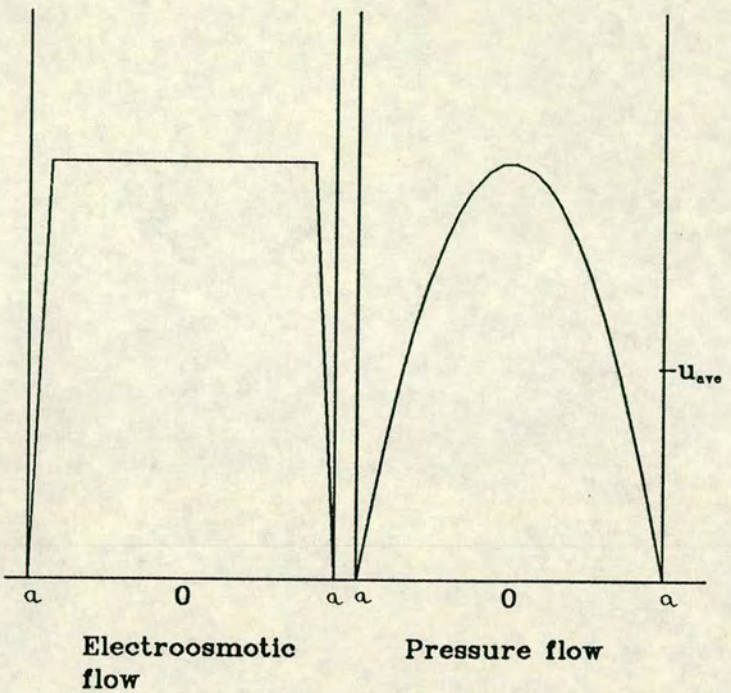

Figure 2.3. Comparison of electro-osmotic and pressure driven flow profiles.

zero at the shear layer to a constant velocity u in the bulk of the solution. Electro-osmotic flow is thus similar to plug flow (figure 2.3) when the ratio of capillary radius and double layer thickness is large. The von Smoluchowski equation is used to relate the fluid velocity (u) to the applied electric field E.

The net electrical force applied in the double layer is proportional to the excess charge density ρ and is given by

$$dF_e = EA\rho dx \tag{2.18}$$

where A is the area of the layer. The viscous force operating in the double layer is

$$dF_v = \eta A d(du/dx) \tag{2.19}$$

The viscous force is equal in magnitude to the electrical force. By equating

equations 2.18 and 2.19 and rearranging

$$\frac{d^2u}{dx^2} = \frac{E\rho}{\eta} \tag{2.20}$$

Substituting for ρ from the Poisson equation (equation 2.1)

$$\frac{d^2u}{dx^2} = \frac{-\epsilon_o\epsilon_r}{\eta} E \frac{d^2\psi}{dx^2} \tag{2.21}$$

Integrating twice, with the boundary conditions that in the bulk solution, $d\psi/dx = 0, du/dx = 0, u = u_{eo}$ and $\psi = 0$ and at the plane of shear $\psi = \zeta$ and $u = 0$, gives an expression for the electro-osmotic velocity as

$$u_{eo} = \frac{\epsilon_o\epsilon_r\zeta}{\eta} E \tag{2.22}$$

The derivation has assumed that the dielectric constant and viscosity remain constant throughout the double layer.

In contrast to pressure driven flow, where the fluid velocity is a function of the square of the channel diameter, electro-osmotic flow shows no dependence on the channel diameter. u_{eo} however is dependent on ζ, and as ζ has been shown to be dependent on the buffer concentration and the valence of the counter ion, u_{eo} is therefore very dependent on the electrolyte. In fact, u_{eo} is directly related to the double layer thickness. The magnitude of electro-osmotic flow can be tailored to suit requirements by correct choice of electrolyte. By making use of contact adsorption, the ζ potential can be eliminated or reversed. Altria and Simpson [21] were the first to use large organic quaternary ammonium cations to reduce or reverse electro-osmotic flow in CZE, but the effect of $AlCl_3$ and $ThCl_4$ on the electro-osmotic flow rate had been noticed as far back as 1915 by Powis. With large or high valence cations a relatively low concentration is needed to bring about a large change in ζ.

The fact that the electro-osmotic velocity is independent of channel diameter suggests that it should be possible to use electro-osmosis to pump fluid through

beds of fine particles, for which the required pressure gradient is too large to be practically useful. This would be of great benefit in chromatography where it has been shown that greater efficiency can be achieved with small particles. The independence of u_{eo} of channel diameter is not however strictly true. It has been shown that a velocity gradient occurs only in the double layer. Thus if the double layer thickness approaches the channel radius, there will be a large section of the channel in which there exists a velocity gradient, and a smaller or non-existent portion in which the velocity is constant. Rice and Whitehead [79] have carried out a theoretical study of the effect of double layer overlap. The velocity profile can be expressed by the following equations and is shown in figure 2.4 for various values of κa

$$u(x) = \frac{\epsilon_o \epsilon_r \zeta E}{\eta} \left[1 - \frac{I_o(\kappa x)}{I_o(\kappa a)} \right] \tag{2.23}$$

where I_o is the zero order modified Bessel function of the first kind and a is the capillary or channel radius. The diagram shows that at low values of κa, the velocity approaches that of a parabolic flow profile, with a maximum velocity much less than the classical value predicted by equation 2.22. As κa increases, the velocity profile becomes more plug like in appearance with a bulk flow rate close to that predicted by equation 2.22. In order to ensure that the flow profile is similar to a plug profile, conditions should be chosen such that

$$\kappa a > 10 \tag{2.24}$$

For symmetrical electrolytes at 25°C

$$\kappa = 0.329 \times 10^{10} (cz^2)^{1/2} \tag{2.25}$$

in which c is in mol dm^{-3}. For a concentration of 10^{-7} M of a 1:1 electrolyte in a 50 μm i.d. capillary, $\kappa a = 26.0$, so very dilute solutions can be reasonably used in CZE from the point of view of electro-osmotic flow. With a bed of 1

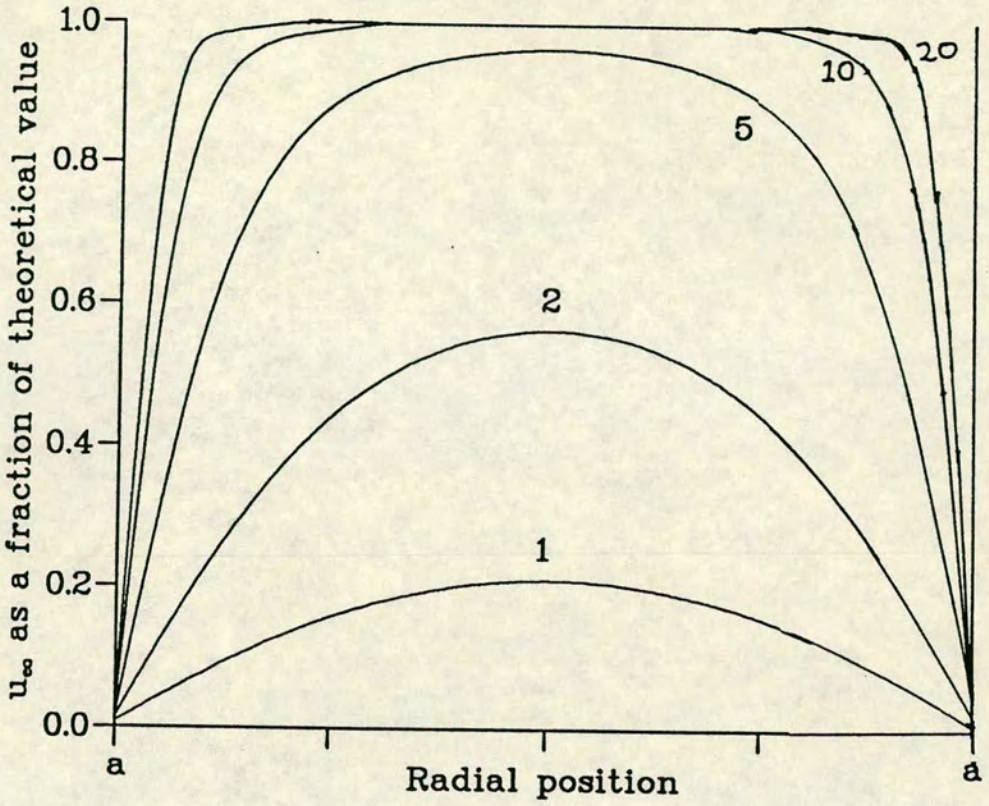

Figure 2.4. Effect of double layer overlap on the electro-osmotic flow profiles predicted by Rice and Whitehead. The value of κa is given next to each curve.

μm particles, the channel diameter is usually taken to be 1/3 of the particle diameter and so $a \sim 0.17$ μm. To fulfil condition 2.24, using equation 2.25 for a 1:1 electrolyte, the minimum concentration possible is 3.3×10^{-4} M. From the point of view of electro-osmotic flow, high electro-osmotic velocities can be expected in beds of small particles with a low concentration of electrolyte. This fact is very important for electrochromatography.

2.6 The Double Layer on Silica

The origin of the double layer on silica or glass has a particular relevance in the study of CZE and other electroseparation methods. The capillaries used in CZE are of quartz or, more commonly, fused silica and the resulting electro-osmotic flow is superimposed on the electrophoretic velocities of the analyte ions. In electrochromatography, the packing material is silica based or of surface modified silica (reversed phase materials). Many studies have been carried out in order to better understand the structure of the silica/electrolyte interface. There is every reason to believe that silica is unique among the oxides. The ζ potential—pH behaviour of silica is similar to other oxides, but the surface charge—pH and total capacitance behaviour of the oxide is very different to other oxides examined.

There appear to be two schools of thought as to the origin of the double layer on silica. One school considers the surface as a porous layer or permeable gel which can be penetrated by potential determining anions and counter ions. The other school sees it as a planar impenetrable barrier or array of surface sites which can dissociate to form charged groups and that may bind counter ions.

Whichever way the double layer is structured, it is generally accepted that the bulk of the surface charge is due to ionisation or hydrolysis of the surface silanols, which can be represented by

$$\equiv SiOH + H_2O \iff \equiv Si - O^- + H_3O^+$$
$$\equiv SiOH + H_2O \iff \equiv Si - OH_2^+ + OH^-$$

The effect of pH on the excess charge density of silica and, as a result, on the ζ potential can be understood in terms of the above equilibria with H^+ and

OH^- as the potential determining ions. At a particular bulk pH, there will be a point where there are equal numbers of positive and negative sites on the surface. This net zero charge condition, in the absence of specific chemical interactions, corresponds to a net zero surface potential termed the isoelectric point (i.e.p.). The pH at which the surface potential is zero is termed the isoelectric pH or pH_{iep}. Grieser *et al* [80] have shown that the pH_{iep} can be altered by thermal and radiation treatment of the surface. The magnitude of the ζ potential relative to the i.e.p. is unchanged for thermally treated glass/water interfaces but is decreased for silica/water interfaces above pH 7 which have been thermally treated above 800 °C, and for the glass/water interface which has been irradiated. The pH_{iep} varies between about 2 and 4.

Surface silanols are of two types—free silanols and vicinal (adjacent) silanols which hydrogen bond with each other. It has been shown that the hydrogen bonded groups are almost all eliminated at about 500 °C whereas the isolated hydroxyls remain. The number of hydroxyl sites on silica depends therefore on the surface treatment. Snyder has shown [81] that rehydration of surface siloxane groups (the result of dehydration of vicinal silanol groups) does occur, if slowly, when the surface is exposed to water. Substantial rehydration may take in the order of several months. This may explain the results of several investigators in CZE [82] who report long equilibration times for u_{eo}. Wood [83] has observed that the slow equilibration of ζ potential on glass with electrolyte solutions is easy to understand in terms of slow equilibration of the surface adsorbed ions, but with pure water he attributes it to slow hydration of the surface or gel formation. In fact, there is reason to believe that both factors may be responsible. It is well known that silica dissolves at high pH to form silicic acid. With the pH of buffer solutions used in CZE (7–10 commonly), it is quite possible that both mechanisms are present and result in slow equilibration of the surface. The effect

of basic solutions such as NaOH and KOH which are used to 'clean' the surface of the capillary between electrophoresis runs, may work by cleaning off the partially formed gel layer and adsorbed ions, thus presenting a new surface to the buffer solution. One argument in favour of this conclusion is the fact that reacting the surface silanols with a polymer such as polyethyleneimine [84] produces a capillary in which the electro-osmotic velocity, and therefore the ζ potential, is more stable and reproducible.

The number of silanol groups on the silica surface is in the region of 1–5 OH groups per nm^2. Healy and White [85] have derived a set of expressions which relate the ζ potential to the total number of ionisable sites on the surface. Their work shows that significant reduction in the magnitude of the ζ potential will not occur until the number of hydroxyls is reduced below approximately 1 per nm^2. In fact, Laskowski and Kitchener [86] observed that reaction with trimethylchlorosilane did not change the magnitude of the ζ potential or i.e.p. of the treated silica. It has been found that the maximum concentrations of trimethylsilyl, octadecylsilyl and triphenylmethylsilyl are about 4.5, 3.5 and 1.5 μmol m^{-2} respectively, compared to a bare surface of 8–9 μmol m^{-2} of OH groups [87]. Thus with smaller groups on the surface, it should be possible to use reversed phase particles for electrochromatography without a noticeable drop in the ζ potential or flow rate compared to bare silica.

2.7 Electrophoresis

2.7.1 The Debye-Huckel Equation

In 1923 Debye and Huckel made a major advance in the understanding of ions in solution. They chose one ion, the reference ion, and considered the charge

density and potential around the ion, which was given a discrete charge. The remaining ions and the water were considered as a continuum. The water is a continuous dielectric medium with a dielectric constant taken to be that of bulk water. Within the region or surrounding area of the reference ion there is an excess of counter ions, with an excess charge density ρ. Thus there is a local excess of positive ions around a negative ion and a local excess of negative ions around a positive ion. Overall, the charges balance out and the solution is neutral.

Considering a small volume element dV at a distance a from the reference ion the potential in the volume element is ψ_a with an excess charge density given by ρ. The excess charge density is related to the potential by Poisson's equation, which must be in spherical coordinates as the symmetry of the system is assumed to be spherical. Thus

$$\frac{1}{a^2}\frac{d}{da}\left(a^2\frac{d\psi}{da}\right) = -\frac{\rho}{\epsilon_o\epsilon_r} \tag{2.26}$$

The excess charge density in the volume element dV is equal to the total ion density times the charge on the ions,

$$\rho = \sum n_i z_i e \tag{2.27}$$

where n_i is the number of ion i per unit volume in dV. The number of ions n_i can be related to the number of ion i in the bulk solution by the Boltzmann distribution law

$$n_i = n_i^o \exp(-z_i e\psi/kT) \tag{2.28}$$

and so the excess charge density is given as

$$\rho = \sum n_i^o z_i e \exp(-z_i e\psi/kT) \tag{2.29}$$

Equation 2.29 is equivalent to equation 2.4 used in the derivation of the charge density of the diffuse layer for a 1:1 electrolyte but is a more general form of that equation.

Substitution of equation 2.29 into equation 2.26 presents a difficult differential equation to integrate. The exponential function can be expanded to a Taylor series

$$\exp\left(-\frac{z_i e\psi}{kT}\right) = 1 - \frac{z_i e\psi}{kT} + \frac{1}{2!}\left(\frac{z_i e\psi}{kT}\right)^2 \cdots \tag{2.30}$$

Here again, by utilising the Debye-Huckel approximation that $ze\psi/kT \ll 1$, all terms except the first two in the series can be rejected. Thus

$$\rho = \sum n_i^\circ z_i e\left(1 - \frac{z_i e\psi}{kT}\right) \tag{2.31}$$

$$\rho = \sum n_i^\circ z_i e - \sum \frac{n_i^\circ z_i^2 e^2}{kT}\psi \tag{2.32}$$

$$\rho = -\sum \frac{n_i^\circ z_i^2 e^2}{kT}\psi \tag{2.33}$$

The first term in equation 2.32 is equal to zero due to the overall electroneutrality of the solution. Substituting equation 2.33 into equation 2.26

$$\frac{1}{a^2}\frac{d}{da}\left(a^2\frac{d\psi}{da}\right) = \frac{e^2}{\epsilon_o\epsilon_r kT}\sum n_i^\circ z_i^2\psi \tag{2.34}$$

$$\frac{1}{a^2}\frac{d}{da}\left(a^2\frac{d\psi}{da}\right) = \kappa^2\psi \tag{2.35}$$

The reciprocal double layer thickness of equation 2.11 has been replaced by a more general expression involving the ionic strength of the solution i.e.

$$\kappa^2 = \frac{e^2}{\epsilon_o\epsilon_r kT}\sum n_i^\circ z_i^2 \tag{2.36}$$

To solve equation 2.35, ψ is replaced by ϕ/a giving

$$\frac{d\psi}{da} = \frac{d}{da}\frac{\phi}{a} = -\frac{\phi}{a^2} + \frac{1}{a}\frac{d\phi}{da}$$

$$\begin{aligned}\frac{1}{a^2}\frac{d}{da}\left(a^2\frac{d\psi}{da}\right) &= \frac{1}{a^2}\frac{d}{da}\left(-\phi + a\frac{d\phi}{da}\right) \\ &= \frac{1}{a^2}\left(-\frac{d\phi}{da} + a\frac{d^2\phi}{da^2} + \frac{d\phi}{da}\right) \\ &= \frac{1}{a}\frac{d^2\phi}{da^2}\end{aligned}$$

Equation 2.35 then becomes

$$\frac{1}{a}\frac{d^2\phi}{da^2} = \kappa^2\frac{\phi}{a} \tag{2.37}$$

The differential equation 2.37 is solved by utilising the fact that the differential of an exponential function is given by the exponential function itself multiplied by the constant in the exponent, and so

$$\frac{d^2\exp(\pm\kappa a)}{da^2} = \kappa^2\exp(\pm\kappa a) \tag{2.38}$$

The solution to 2.37 must be of the form

$$\phi = A\exp(\kappa a) + B\exp(-\kappa a) \tag{2.39}$$

and so

$$\psi = \frac{A\exp(\kappa a)}{a} + \frac{B\exp(-\kappa a)}{a} \tag{2.40}$$

As $a \to \infty, \psi \to 0$ which requires that $A = 0$ and

$$\psi = \frac{B\exp(-\kappa a)}{a} \tag{2.41}$$

To evaluate B the behaviour of the ion in a very dilute solution is considered. Since $\kappa \to 0$ as $n_i^o \to 0$, $\exp(-\kappa a) \to 1$ and $\psi = B/a$. If the ion is considered to be a point charge i.e. a is very small compared to $1/\kappa$, then the potential near the ion is simply due to the charge on the ion and

$$\psi = \frac{z_i e}{\epsilon_o \epsilon_r a} \tag{2.42}$$

and so

$$B = \frac{z_i e}{\epsilon_o \epsilon_r} \tag{2.43}$$

$$\psi = \frac{z_i e}{\epsilon_o \epsilon_r} \frac{\exp(-\kappa a)}{a} \tag{2.44}$$

Equation 2.44 therefore shows how the potential of an ion varies with distance a from the reference ion. Combining 2.26, 2.37 and 2.44, the excess charge density as a function of distance from the surface is given as

$$\rho = \kappa^2 z_i e \frac{\exp(-\kappa a)}{a} \tag{2.45}$$

Integration of the space charge density times the volume over a from 0 to ∞ gives a value for the charge on the "ion cloud" surrounding the central ion of

$$q = -z_i e \tag{2.46}$$

The charge on the ion is thus balanced by an equal and opposite charge in the solution. If the excess charge is considered to be contained in a spherical shell, the net charge in the shell varies with a as

$$q = -\int 4\pi z_i e \kappa^2 a \exp(-\kappa a) da$$

$$dq = -z_i e \kappa^2 a \exp(-\kappa a) \tag{2.47}$$

The shell radius which contains maximum charge is obtained by finding dq/da and setting it equal to 0. Using equation 2.47

$$\frac{dq}{da} = -z_i e \kappa^2 (\exp(-\kappa a) - \kappa a \exp(-\kappa a)) = 0 \tag{2.48}$$

Equation 2.48 is only true when $a = 1/\kappa$ and so $1/\kappa$ is termed the thickness or radius of the ion cloud which surrounds an ion.

2.7.2 The von Smoluchowski and Huckel equations

The equation derived for electro-osmotic flow of fluid in stationary channels (equation 2.22) can be applied to the electrophoresis of moving particles in a stationary fluid with

$$u_{ep} = \frac{\epsilon_o \epsilon_r \zeta_p}{\eta} E \tag{2.49}$$

where ζ_p is the potential between the moving particle and the solution at the plane of shear. According to this equation, the electrophoretic velocity is independent of the shape and size of the moving particle. Huckel theory uses Stokes law to equate the linear velocity with the charge on the particle or ion as

$$u = \frac{qE}{6\pi\eta a} \tag{2.50}$$

The ζ potential at the plane of shear is given by

$$\zeta = \frac{q}{4\pi\epsilon_o\epsilon_r a} - \frac{q}{4\pi\epsilon_o\epsilon_r(a + 1/\kappa)} = \frac{q}{4\pi\epsilon_o\epsilon_r a(1 + \kappa a)} \tag{2.51}$$

If κa is small compared to unity then

$$u = \frac{\epsilon_o \epsilon_r \zeta}{1.5\eta} E \tag{2.52}$$

Comparing equations 2.49 and 2.52 there is an obvious discrepancy. Equation 2.49 holds for large values of κa and equation 2.52 holds for small values of κa.

Henry has derived the modified equation

$$\mu = \frac{\epsilon_o \epsilon_r \zeta}{1.5\eta}[1 + \lambda F(\kappa a)] \tag{2.53}$$

in which $\lambda = (k_o - k_1)/(k_o + k_1)$ where k_o is the bulk conductivity of the solution and k_1 is the conductivity of the particles. $F(\kappa a)$ varies between 0 for small values of κa and 1 for large values of κa. For non-conducting particles, $\lambda = 1/2$ and the Henry equation is written in the form

$$\mu = \frac{\epsilon_o \epsilon_r \zeta}{1.5\eta} f(\kappa a) \tag{2.54}$$

$f(\kappa a)$ varies between 1.0 for small κa (Huckel equation) and 1.5 for large κa (von Smoluchowski equation). The Henry equation is based on the same assumptions inherent in the Stern model of the double layer i.e. the Debye-Huckel approximation is made and ϵ_r and η are assumed to be constant throughout the mobile part of the double layer.

The effects of buffer concentration and counter ion valence that were observed to occur with electro-osmosis in reducing the ζ potential and the electro-osmotic velocity would be expected to occur with electrophoresis. Thus increasing the concentration or valence of buffer ions should result in a reduction of the electrophoretic mobility of the analyte ions.

κ can be expected to vary from 10^6 m^{-1} for a 10^{-7} M solution of a 1:1 electrolyte to 10^9 m^{-1} for a 0.1 M solution of the same electrolyte. For electrophoretic analyses concerning ions or molecules, κa would be expected to be small and so the Huckel theory can be applied. As κa increases, concentration and counter ion valence will play a smaller role in the reduction of electrophoretic velocities, as ζ decreases and $f(\kappa a)$ increases with increase in κ. For colloidal particles, where κa is large, equation 2.49 applies, and for colloidal particles of the same material e.g. particles of silica in a silica sol, all particles will move at the same rate through the solution.

Chapter 3

Resolution and Band Broadening

3.1 Dispersion

The ultimate goal of a separation process of any kind is the complete separation or resolution of the constituents of a sample mixture. Resolution depends on two factors, the selectivity of the system which acts to increase the resolution, and entropy driven processes which act in the reverse direction and tend to increase the disorder of the system. In chromatographic processes, selectivity depends on differential partitioning between the moving phase and stationary phase. Selectivity in electrophoresis depends on differing electrophoretic mobilities of the sample.

The entropy driven processes which decrease the resolution are any processes which increase the width of the initial sample zone, and are termed band broadening processes. The column efficiency, often designated as the height equivalent to a theoretical plate (HETP or H) provides a measure of how peaks broaden as

they pass through the column. The plate theory of chromatography was developed by Martin and Synge [88] by analogy with fractional distillation and applied initially to chromatography and later to electrophoresis. The theoretical plate has dimensions of length and can be considered as the thickness of a layer such that the composition of eluent emerging from the layer is in equilibrium with the eluent composition which would exist if the layer were isolated and allowed to reach equilibrium. The HETP or H is given by

$$H = \sigma_{tot}^2 / L \tag{3.1}$$

where σ_{tot}^2 is the variance of the peak due to the dispersion forces present, and L is the length of the column over which the separation is taking place. Equation 3.1 applies only where dispersive forces are constant over the column length, which is generally assumed to be the case.

The efficiency N or number of theoretical plates to which a column is equivalent is given by

$$N = \frac{L}{H} = \frac{L^2}{\sigma_{tot}^2} \tag{3.2}$$

Giddings [89] has referred to separation as the art and science of maximising the ratio of separative transport to dissipative transport. In systems where longitudinal or axial diffusion is the only means of dispersion, the variance is given by the Einstein equation as

$$\sigma^2 = 2Dt \tag{3.3}$$

where D is the diffusion coefficient and t is the time for separation. H and N therefore become

$$H = \frac{2Dt}{L} = \frac{2D}{u} \tag{3.4}$$

$$N = \frac{L^2}{2Dt} = \frac{Lu}{2D} \tag{3.5}$$

where u is the linear velocity of the sample.

Lu can be written as

$$Lu = -\frac{1}{f}\frac{d\mu^{ext}}{dL}L = -\frac{\Delta\mu^{ext}}{f} \tag{3.6}$$

where $-d\mu^{ext}/dL$ is the driving force behind the separation, f is the friction coefficient, and $\Delta\mu^{ext}$ is the chemical potential drop experienced by the species migrating over a distance L.

The Einstein equation relates D to f and T by

$$D = RT/f \tag{3.7}$$

Inserting 3.6 and 3.7 into 3.5 yields

$$N = -\frac{\Delta\mu^{ext}}{2RT} \tag{3.8}$$

N can be seen to be a function of two energies. $-\Delta\mu^{ext}$ is the energy that drives the separation and RT is thermal energy, acting against the separation. When other dispersive forces are at work, 3.8 becomes

$$N = -\frac{\Delta\mu^{ext}}{2\epsilon RT} \tag{3.9}$$

where ϵ is greater than or equal to unity, and accounts for the loss in separation as a result of the extra dispersive processes.

3.1.1 Dispersion in Open Tubes

In open tubular capilleries, in which there is no interaction of the solute with the walls of the capillaries or a support, dispersion of the peak depends on the type of flow present. With pressure driven flow, the flow variation across the tube disperses the solute. This is counteracted by radial molecular diffusion. The total plate height combining the two dispersive forces is given by the Taylor equation [90]

$$H = \frac{2D}{u} + \frac{ud_c^2}{96D} \tag{3.10}$$

The plate height is thus dependent on the square of the column diameter. With pressure driven flow, the plate height goes through a minimum as u is increased. This occurs at $u = 14D/d_c$ with $H_{min} = 0.29d_c$. In capillary electrophoresis, the overall bulk flow of the fluid is due to electro-osmosis with a plug like profile. With no other dispersive processes present, N and H are given by equations 3.4 and 3.5. This had been assumed by Jorgenson and Lukacs in their first papers on CZE in 1981 [15, 17, 18].

It is immediately obvious with reference to equations 3.10 and 3.4 that electro-osmotic flow has an advantage over pressure driven flow in chromatography, and it would appear that any column diameter can be used, with H decreasing or N increasing as u increases. However, equations 3.10 and 3.4 have been derived for unretained solutes. For chromatographic separations, some interaction with a solid support is necessary for separation to take place. The phase capacity ratio k' is a measure of the degree of retention of a solute and is defined by

$$k' = \frac{t_r - t_o}{t_o} \tag{3.11}$$

where t_o and t_r are the retention times of an unretained and retained solute respectively.

With retention, an additional dispersive force, due to mass transfer is introduced. The equation for pressure driven flow has been derived by Golay [91] as

$$H = \frac{2D}{u} + \frac{1 + 6k' + 11k'^2}{96(1 + k')^2} \frac{d_c^2 u}{D} \tag{3.12}$$

For electro-osmotic driven flow the equivalent equation is due to Aris [92]

$$H = \frac{2D}{u} + \frac{k'^2}{16(1 + k')^2} \frac{d_c^2 u}{D} \tag{3.13}$$

Comparing the two equations it is apparent that while electro-drive does produce lower plate heights, the difference between the two types of flow decreases

as k' increases. As $k' \rightarrow \infty$, the mass transfer term in the Golay equation tends to $11d_c^2u/96D$ while in the Aris equation it tends to $d_c^2u/16D$. There is a net improvement of 6/11 when considering the mass transfer terms of the two equations at the same velocity [77]. As a result , while there *is* an improvement with using electro-drive, the actual plate height achieved is strongly dependent on k' and d_c^2. In addition the plate height goes through a minimum as u is increased. For electro-drive

$$H_{min} = 0.707d_c\left(\frac{k'}{1+k'}\right) \tag{3.14}$$

and occurs at

$$u_{min} = 5.66\frac{D}{d_c}\frac{1+k'}{k'} \tag{3.15}$$

For pressure drive

$$H_{min} = 0.289d_c\frac{\sqrt{1+6k'+11k'^2}}{1+k'} \tag{3.16}$$

and occurs at

$$u_{min} = 13.86\frac{D}{d_c}\frac{1+k'}{\sqrt{1+6k'+11k'^2}} \tag{3.17}$$

Table 3.1 illustrates the improvement of electro-drive over pressure driven flow for a range of k' from 0.1 to 100. It is apparent that at a constant column diameter and diffusion coefficient of sample, H_{min} is always lower for electro-drive and occurs at a faster velocity (and so faster analysis times). As $k' \rightarrow \infty, u_{min}(E) \rightarrow 1.354u_{min}(P)$ and $H_{min}(E) \rightarrow 0.738H_{min}(P)$ where P and E represent pressure driven and electro-drive systems respectively. While major improvement is not possible at high k' values, the improvement at k' values between 0 and 1 is substantial. The optimum column diameter for OTLC with pressure driven flow is 2 μm. If time of analysis and H are not crucial, then use of electro-drive in preference to pressure drive will allow use of a larger diameter capillary for the same u and k', thus leading to an improved sensitivity.

	Pressure drive		Electro-drive	
k'	$u_{min}d_c/(D)$	H_{min}/d_c	$u_{min}d_c/(D)$	H_{min}/d_c
0.1	11.66	0.344	62.22	0.064
0.5	8.00	0.501	16.97	0.236
1.0	6.53	0.613	11.31	0.354
5.0	4.75	0.843	6.79	0.589
10.0	4.47	0.895	6.22	0.643
50.0	4.24	0.945	5.77	0.693
100.0	4.21	0.952	5.71	0.700

Table 3.1. Comparison of minimum plate height and velocity for electro-drive and pressure drive as a function of capacity factor.

3.1.2 Dispersion in Packed Columns

With packed columns, three different processes have been identified as causing peak broadening [87].

1. As in OTLC, longitudinal or axial molecular diffusion is one of the modes of dispersion.

2. Dispersion is also caused by the tortuous nature of the flow through a packed bed. In a packed bed there will be a variation in channel diameter due to irregularities in the packing. With pressure driven flow, the mean velocity will therefore vary from channel to channel. Within a channel, the velocity depends on the radial position, leading to further dispersion of the peak.

3. Dispersion is caused by slow equilibration of the solute between the stationary and mobile phases.

The combined effects of the above three processes are included in the Knox equation

$$h = B/\nu + A\nu^{1/3} + C\nu \tag{3.18}$$

where h and ν are the reduced plate height and reduced velocity respectively

and are given by

$$h = H/d_p \tag{3.19}$$

$$\nu = ud_p/D \tag{3.20}$$

where d_p is the particle size and A, B and C are constants. Use of reduced parameters allows direct comparison of columns containing different particle sizes. Inserting 3.19 and 3.20 into 3.18 and rearranging

$$H = \frac{BD}{u} + \frac{Ad_p^{4/3}u^{1/3}}{D^{1/3}} + \frac{Cd_p^2u}{D} \tag{3.21}$$

The plate height is dependent on the particle diameter. Use of smaller particles will thus result in lower plate heights. With pressure driven flow, as the velocity is proportional to d_p^2, the pressures required to pump fluid through beds of small particles are very high. With electro-osmotic flow, as pointed out in the last chapter, the fluid flow is essentially independent of channel diameter, and so use of small particles should not present any difficulties. Grant [73] has shown that the electro-osmotic velocity through beds of particles from 50 μm to 1.5 μm is independent of the particle diameter as expected.

For a well packed column, $A < 1$, $B \sim 2$ and $c < 0.1$. With electro-osmotic flow, it would be expected that due to the flat velocity profile, and the lack of dependence on d_p, that the A term in equations 3.18 and 3.21 would be negligible or absent. This has been shown to be the case by Grant, comparing pressure driven and electrodriven chromatograpy on 5 μm Hypersil. His results show that in all cases, at a given velocity, electro-drive produces lower plate heights than pressure driven flow.

Electro-drive is therefore to be preferred over pressure drive for two reasons

1. Virtual elimination of the eddy diffusion/flow tortuosity term in the Knox equation.

2. Use of smaller diameter particles allowed.

Using equation 3.18 and substituting values for B and C where $B = 2$ and $C = 0.1$ and assuming $A = 0$ the plate height equation for electrochromatography becomes

$$H = \frac{2D}{u} + \frac{0.1 d_p^2 u}{D} \tag{3.22}$$

If equation 3.22 is taken to be valid for electrochromatography, then it is obvious that a minimum plate height (H_{min}) exists at a specific velocity u_{min} where

$$H_{min} = \frac{2}{\sqrt{5}} d_p \tag{3.23}$$

$$u_{min} = 2\sqrt{5}\frac{D}{d_p} \tag{3.24}$$

$h_{min} = H_{min}/d_p$ is constant for any particle size and is equal to 0.89. H_{min} is directly related to d_p and u_{min} is inversely proportional to d_p and is also dependent on the diffusion coefficient. Table 3.2 gives some values of H_{min} and u_{min} for various values of d_p. The trend is obvious, with lower particle diameters producing lower plate heights at faster velocities. Table 3.2 also shows the number of plates expected per metre (N_{max}) for each particle diameter.

A column packed with 1 μm particles could be expected to give in excess of 10^6 plates per metre if operated under optimum conditions. With a diffusion coefficient of 10^{-9} m^2s^{-1}, the number of theoretical plates expected from CZE operated at the same linear velocity is also shown.

Comparing N_{CZE} and N_{max}, it is obvious that the number of plates obtainable from CZE is twice what can be obtained for retained solutes in electrochromatography, operated at optimum velocity. As the number of plates obtainable with CZE increases with velocity (if no other band broadening mechanism is operating) then CZE would be the method of choice for charged compounds. However,

d_p μ m	u_{min} mms^{-1}	H_{min} μ m	N_{max} $\times 10^6$ m^{-1}	N_{CZE} $\times 10^6$ m^{-1}
0.1	44.72	0.09	11.10	22.36
0.5	8.94	0.45	2.22	4.47
1.0	4.47	0.89	1.12	2.24
1.5	2.98	1.34	0.75	1.49
2.0	2.24	1.79	0.56	1.12
3.0	1.49	2.68	0.37	0.74
5.0	0.89	4.47	0.22	0.44
10.0	0.45	8.94	0.12	0.22

Table 3.2. Minimum plate heights and linear velocities for electrochromatography as a function of particle diameter with $D = 10^{-9}$ m^{+2}s^{-1}.

the greater selectivity offered by chromatography for neutral compounds and the possibility of combining separation by both electrophoresis and adsorption, suggests that further development of electrochromatography is desirable.

3.2 Resolution in CZE

At the beginning of this chapter, it was stated that resolution was the ultimate goal of any separation. Complete resolution is said to be attained when the components of a sample are baseline resolved. The resolution of two compounds is defined as the peak separation divided by the mean peak width

$$R_s = \frac{t_{r(1)} - t_{r(2)}}{1/2(w_1 + w_2)} \tag{3.25}$$

where $t_{r(1)}$ and $t_{r(2)}$ are the retention times of the two compounds, and w_1 and w_2 are the peak widths at the base. Complete resolution is achieved when $R_s \geq 1.5$. The resolution can also be expressed as

$$R_s = \frac{N^{1/2}}{4} \frac{\Delta u}{\bar{u}} \tag{3.26}$$

where $\Delta u = u_1 - u_2$ and $\bar{u}$ is the mean velocity of the two samples. Without electro-osmotic flow

$$\frac{\Delta u}{\bar{u}} = \frac{\mu_1 - \mu_2}{\bar{u}} \tag{3.27}$$

but with the addition of electro-osmotic flow

$$\frac{\Delta u}{\bar{u}} = \frac{\mu_1 - \mu_2}{\mu_{eo} + \bar{\mu}} \tag{3.28}$$

Substituting for N from equation 3.31 and for $\Delta u/\bar{\mu}$ from the previous equation

$$\begin{aligned} R_s &= \frac{1}{4}\left[\frac{(\bar{\mu} + \mu_{eo})V}{2D}\right]^{1/2}\left[\frac{\mu_1 - \mu_2}{\bar{\mu} + \mu_{eo}}\right] \\ R_s &= 0.177(\mu_1 - \mu_2)\left[\frac{V}{D(\bar{\mu} + \mu_{eo})}\right]^{1/2} \end{aligned} \tag{3.29}$$

Obvious prerequisites for good resolution are large differences in the electrophoretic mobilities of the samples, small diffusion coefficients and a high applied voltage. While a large electro-osmotic flow may appear to be beneficial with respect to the number of theoretical plates and time of analysis (section 3.3), reference to equation 3.29 shows that strong electro-osmotic flow actually reduces the resolution which is the ultimate aim of the analysis. In fact, the best resolution is attained when $\bar{\mu} = -\mu_{eo}$ but the retention time may be prohibitively high. In capillary electroseparation methods, as in all chromatographic processes, a balance must be struck, in which the aim is to achieve complete separation in as short a time as possible. Dispersive forces act to degrade the resolution. A secondary aim is therefore to minimise these dispersional forces or maximise the number of plates. An understanding of the dispersive forces at work in the system is crucial to allow optimisation of any separation.

3.3 Dispersion in CZE

Concentrating on CZE for the moment, it has been stated that dispersion of the peaks is due primarily to axial diffusion and from equation 3.5

$$N = \frac{uL}{2D}$$

With electro-osmotic flow

$$u = (\mu_{eo} + \mu_{ep})E \tag{3.30}$$

where μ_{eo} and μ_{ep} are the electro-osmotic and electrophoretic mobilities respectively, and E is the electric field strength. Inserting 3.30 into 3.5 and replacing E with V/L

$$N = \frac{(\mu_{eo} + \mu_{ep})V}{2D} \tag{3.31}$$

It would appear that the number of theoretical plates generated is linearly related to the applied voltage. Since the time for separation is

$$t = \frac{L}{u} = \frac{L^2}{(\nu_{eo} + \mu_{ep})V} \tag{3.32}$$

the equations suggest that high voltages applied to short columns would give the highest efficiencies in the shortest time. This is true to a certain extent but is limited by the power and heat generated.

There is one major difference between chromatography and electrophoresis with regard to separation efficiency. In chromatography, detection is generally 'off-column' and all peaks move at the same rate through the detection zone, at a velocity equal to the flow velocity of the mobile phase, and the peak efficiencies for each peak in a chromatogram are a direct indication of the degree of dispersion for each peak. With capillary electroseparation techniques, detection is 'on-column' and peaks move at different rates through the detection zone. The peak widths

measured are therefore not a true indication of the dispersion of each peak. The peak widths should be multiplied by the zone velocity before direct comparison from peak to peak within an electropherogram can be made [94].

With free solution electrophoresis, it had been initially assumed that axial diffusion was the only dispersive method present in the system. It was gradually realised that while plate numbers per separation were high in comparison to HPLC, and approaching those of capillary GC, the plate numbers realised were in general a fraction of those expected on the basis of molecular diffusion alone. Many papers dealing with dispersion in CZE have been published and the main sources of dispersion identified to date are now described. In equations 3.1 and 3.2, H and N were defined as

$$H = \sigma_{tot}^2/L$$
$$N = L^2/\sigma_{tot}^2$$

The variances σ_i^2 due to a number of dispersing forces are additive, and so σ_{tot}^2 is given by

$$\sigma_{tot}^2 = \sum \sigma_i^2 \tag{3.33}$$

Therefore, H is seen to be a result of the addition of each variance per unit length of column. As expected, additional dispersive forces increase the plate height and reduce the number of theoretical plates obtained.

Smith *et al* [112] have described the band broadening processes as being of two kinds—time dependent and time independent. Given that the total variance is the sum of the individual variances then

$$\sigma_{tot}^2 = \sigma_{ti}^2 + \sigma_{td}^2 \tag{3.34}$$

where σ_{ti}^2 is the variance due to time independent processes and σ_{td}^2 that due to time dependent processes. By measuring the total variance of a peak and plotting

against the time the intercept, when $t = 0$, will give the total time independent variance. If no other time dependent dispersive processes are present, the slope of the plot will allow calculation of the effective diffusion coefficient from the Einstein equation.

3.3.1 Injection Length

The variance due to the length of the injection zone l_{inj} has been given as [93]

$$\sigma_{inj}^2 = l_{inj}^2/12 \tag{3.35}$$

and so

$$H_{inj} = l_{inj}^2/12L \tag{3.36}$$

where L is the length of the column over which separation takes place. The length of the injection zone can therefore have a large effect on the expected plate height. With a diffusion coefficient of 10^{-9} m^2s^{-1} eluting in a time of 600 s over a 1 m column, $H_{th} = 1.2$ μm or $N = 833,000$ plates, assuming no effect of injection. With a 1 mm sample slug H_{th} increases to 1.28 μm and N decreases to 781,000 plates. If the sample slug is 2 mm in length, H_{th} increases to 1.53 μm, decreasing N to 654,000 plates, 79% of that expected. The diffusion coefficient assumed is quite high, and applies in general only to small molecules. With the larger molecules e.g. peptides and proteins often separated by CZE, the effect of injection length on the percentage of plates attained as compared to axial diffusion alone is more critical. Early papers on CZE in which the performance is particularily poor can often be attributed to the long injection lengths employed. Wallingford and Ewing [96] reported using an injection volume of 430 pl which yields an injection zone length of 3.5 mm. N varies linearly with voltage only for small injection lengths. Similarily voltage affects R_s only for small injection

volumes. In practice, l_{inj} of 0.5–1 mm are as small as can be realised, (although Zare claims to use 0.2 mm [94]) owing as much to detector insensitivity as to difficulty in injecting small amounts.

With electrokinetic injection, the amount injected can be controlled by varying the applied voltage or the time of injection. Sepaniak *et al* [95] have studied the effects of both. Not surprisingly, they found that for MECC, increasing the voltage from 5 to 30 kV led to a decrease in N for a caffeine sample from 95,000 to 1,800 plates. Similarily, increasing the injection time from 10 to 60 s while holding the voltage constant resulted in a large decrease in N from 240,000 to 26,000 plates. In addition, the peak shape observed deviated from the expected Gaussian peak shape to a trapezoidal shape.

Zare [94] has shown that with small injection lengths, the peak width measured is effectively independent of the injection length, but that this effect is dependent on the time of analysis i.e. whether the time is long enough for diffusion to become important. Measurement of the peak width at short injection lengths can therefore allow calculation of the diffusion coefficient of the sample, as a plot of the peak width versus injection length will give a value for $A(2Dt)^{1/2}$ at the intercept at zero injection length, where A depends on whether the peak width at full width half height (FWHH) or at the base or at 0.607 of the full height is taken, and assuming no other band broadening mechanisms are present. Zare estimates that the minimum injection length is 0.2 mm.

Grushka and McCormick [97] have expressed the injection length as

$$l_{inj} = (24DGt)^{1/2} \tag{3.37}$$

where G is the acceptable increase in H relative to the theoretical minimum HETP due to axial diffusion alone. Similar equations have been derived by Otsuka *et al* [98].

Grushka and McCormick also identify an additional source of dispersion due to sample injection. When the capillary is inserted into the sample vial, a volume of sample penetrates the capillary, even when conditions are such that hydrostatic flow is from the capillary back into the sample vial. The length of this extraneous sample zone can be as large as 700 μm, and can result in larger overall zone lengths than is acceptable. Density differences between the sample and buffer solutions play a major role in this extraneous injection.

3.3.2 Detection Length

As for sample injection, the additional variance observed as a result of the length of the detection zone is given by

$$\sigma_{det}^2 = l_{det}^2/12 \tag{3.38}$$

l_{det} has the same effect on the peak efficiency as l_{inj}. Combined injection and detection zones of 1 mm each in length will increase H from 1.28 μm to 1.53 μm for $D = 10^{-9}$ m^{2}s^{-1} and $t = 600$ s with $L = 1$m.

In general, l_{det} is less than 0.5 mm, and with the ABI Model 270A instrument l_{det} is as low as 0.2 mm. With LIF and optical fibres, the detection zone length has been reported to be 75 μm, and with conductivity detection Zare [99] has reported a detection volume of 30 pl which corresponds to a detection zone length of less than 20 μm.

With very small diffusion coefficients and high applied voltages (or large velocities) the length of injection and detection zones are limiting factors in the number of plates possible. The faster the analysis and the smaller the diffusion coefficient, the greater the effect or, alternatively, the smaller these must be to limit the percentage loss of plates due to them.

Additional band broadening occurs as a result of the detector time constant [98]. The time variance generated within the column is

$$\sigma^2_{t,col} = \sigma^2_{col}/u^2 \tag{3.39}$$

and the time constant τ is given by

$$\tau = \sigma_{t,det} \tag{3.40}$$

As in the equation derived by Grushka for injection zone length, the maximum allowed time constant is given by

$$\tau = \sqrt{2DGt}/u \tag{3.41}$$

$$\tau = t_r\sqrt{G/N} \tag{3.42}$$

where again G is the acceptable increase in H relative to the theoretical minimum HETP. For a separation with 500,000 plates, t_r = 600 s and an acceptable increase of 10%, τ = 0.275 s. The time constant allowed increases with retention time and diffusion coefficient as do the allowed injection and detection zone lengths. Variance due to injection and detection has been termed extra-column band broadening [98].

3.3.3 Voltage Switching

Smith *et al* [112] have identified another source of time independent dispersion, due to the switching on and off of the voltage. With electrokinetic injection, this will occur at least once during a run. The effect will be dependent on the number of times the voltage is switched on and off during the run. Their results indicate that this effect is negligible when compared to the effects of injection and detection length, and that the voltage can be manipulated during a run without affecting the efficiency.

3.3.4 Analyte adsorption

Proteins have small diffusion coefficients, $5 \times 10^{-10} - 10^{-10}$ m^2s^{-1}, as a result of their size and so were expected to give in the order of millions of theoretical plates. While the plate numbers observed experimentally were relatively high, it was noticed that they were not as high as expected, and in many cases the peaks deviated from the expected Gaussian peak shape. These factors were attributed to protein adsorption on the capillary wall, which automatically results in the inclusion of a mass transfer term , as discussed for OTLC, and a lowering of the number of plates expected. In many cases, the proteins were in buffer solutions at a pH below their isoelectric points and bore some positive charge, and were thus attracted to the negatively charged capillary wall. Lauer and McManigill [42] suggested that operating at pH's above the isoelectric points of all the proteins in a given sample should eliminate the effect, which it did to a certain extent. However, it has been observed that even above the i.e.p., proteins may contain areas of localised positive or negative charge. These localised areas of positive charge are attracted to the walls and result in protein adsorption. To eliminate this effect, Jorgenson and Green [100] suggested using a high ionic strength buffer. Competitive adsorption between the large number of positive buffer ions and the much smaller number of protein molecules results in elimination of protein adsorption. As expected from double layer theory, the effectiveness of the ions increases in the order $Li^+ < Na^+ \sim K^+ < Cs^+$. Due to the high optical absorbance of Cs^+, K^+ or Na^+ are the most useful with uv detection. The disadvantage of the method is that the high concentration of buffer (> 0.3 M) results in high power levels and so necessitates the use of lower applied voltages to prevent excessive heat generation. In addition, the high ionic strength and positive ion adsorption in the compact layer reduce the ζ potential,

reducing the electro-osmotic flow and increasing analysis times.

An alternative method to eliminate protein adsorption is to coat the capillary with a hydrophilic non-ionic phase such as glycerol propylsilyl [101]. Alternatively the wall can be coated with an ionisable phase, which causes a change in the ζ potential of the double layer and results in a different electro-osmotic flow [102].

3.3.5 Migrational Dispersion

Migrational dispersion is the term used by Mikkers *et al* [103] to describe the non-Gaussian non-symmetric peaks obtained when the conductivity in the sample zone is very different to that of the buffer. These effects occur as a direct result of Ohm's law and the Kohlrausch regulating functions. As the current I must be the same at all points in the capillary, zones with different conductivities will have diferent potential gradients across them. In the case where the sample zone has a higher conductivity than the bulk solution, the electric field will be lower across the sample zone,

$$E_s k_s = E_b k_b \Rightarrow E_s = \frac{k_b}{k_s} E_b \tag{3.43}$$

where k_s and k_b are the conductivities of the sample and bulk buffer solutions respectively, and E_s and E_b are the potential drops across the respective zones. The sample zone will move at a slower velocity than the bulk solution. The net result is a diffuse leading edge with a sharp trailing edge. The opposite effect is observed when the sample zone has a lower conductivity than the bulk solution. In this case, the peak has a sharp front end with a diffuse trailing edge.

The effect can be understood in terms of the mobility of the sample constituent. If a sample ion lags behind the sample zone, it enters a region of higher field strength, increases its velocity and moves back into the sample zone, giving

the distinctive sharp trailing edge. In contrast, if a sample molecule gets into the region of high field strength at the front end of the zone, it too begins to move faster, and becomes separated from the rest of the sample molecules. Thus the front edge is diffuse. A similar mechanism explains the reverse type peak shape observed for the lower conductivity or mobility case.

Thormann *et al* [104] have concluded that for migrational dispersion to be negligible, the buffer/sample concentration should be in the ratio of 100/1. Their results were however obtained for a system in which the buffer constituent had a higher mobility than any of the sample ions. As it is the relative conductivities of the zones that are important, and since $k \propto \mu c$ it is apparent that both mobilities and concentration need to be taken into account.

If the conductivity of the sample zone is to be allowed to be only 1% greater than that of the bulk buffer i.e. $k_s = 1.01k_b$, since $k_b \propto \mu_b c_b$ and $k_s \propto \mu_b c_b + \mu_s c_s$ then $\mu_s c_s = \mu_b c_b/100$ where μ_s and μ_b are the mobilities of the sample and buffer ions respectively. From the above equations, a high concentration of sample can be tolerated if the mobility of the sample ion is relatively low or zero. Similarily, to analyse high concentrations of samples with large mobilities, either the buffer mobility can be changed by changing the counter ion e.g. from K^+ to Na^+, or the buffer concentration increased, or a buffer used which dissociates into a larger number of ions of similar mobilities. In essence, the current density will be increased leading to greater power generation and increased temperatures. However, there is plenty of scope for elimination of the above problem, even if other problems are caused in the meantime.

Samples dissolved in low conductivity buffers or water can improve their peak shape as a result of the principles outlined above. Injection of a long injection zone in water results in contraction of the zone as the trailing edge of the zone moves faster than the front edge. The effect has been shown by Mikkers *et al*

[16] and can be used to concentrate dilute samples. The effect is similar to that of 'stacking' in disc electrophoresis.

3.3.6 Thermal Heating

When a current is passed through a solution, the solution heats up. As heat is dissipated at the walls of the containing vessel, a temperature gradient develops between the centre and the walls. This heat has been described as Joule heat or 'self-heating' [105]. In free solution, the temperature gradient results in viscosity, density and conductivity gradients, as these three properties are temperature dependent, and so in turn affect other properties of the system including electrophoretic mobility and diffusion coefficients. One of the main reasons for the widespread use of gels and stabilisers in electrophoresis is to prevent convection flows as a result of density differences in different areas of the system. With the advent of miniaturised electrophoresis systems, it was thought that these temperature gradients may be so small as to be negligible. Many authors carried out theoretical studies on the temperature gradients expected under normal operating conditions. These calculations were mainly carried out in an attempt to explain the low fraction of plates obtained experimentally, as compared to those predicted.

The heat conduction equation to determine the temperature difference across a capillary of cylindrical symmetry is

$$\frac{1}{r}\frac{d}{dr}\left(r\frac{dT}{dr}\right) = -\frac{g}{k_{th}} \tag{3.44}$$

where g is the heat generation rate and k_{th} is the thermal conductivity of the buffer solution. The temperature difference between centre and wall is given by

$$T - T_1 = \frac{gr_1^2}{4k_{th}}\left(1 - \frac{r^2}{r_1^2}\right) \tag{3.45}$$

where T_1 is the temperature at the wall and r_1 is the inner diameter of the capillary. The above assumes that k_{th} is independent of T but in fact, k_{th} increases with T. Coxon and Binder [106] and Brown and Hinckley [107] have derived equations taking into account the increase of k_{th} with T, and have shown that the temperature in the centre of the capillary may be higher than that predicted by equation 3.45, and deviate from the parabolic profile assumed. Grushka and Jones [108] are in broad agreement with these predictions at high powers, but say that the true temperature profile is almost identical to a parabolic one at powers below 5 W m^{-1}, the maximum likely to be used in CZE systems.

Parabolic temperature gradients may be expected to cause additional band dispersion as follows.

1. Effect on viscosity and electrophoretic mobility. A radial temperature gradient will result in a corresponding radial viscosity gradient. The electro-osmotic velocity in the bulk solution will not be affected, as electro-osmotic flow is generated in the double layer which is normally too narrow to develop a temperature gradient. As the electrophoretic velocity is inversely dependent on viscosity, (equation 1.5), a variation in electrophoretic mobility of the sample ions with radial position occurs. The original equations were derived by Virtanen [109] and have been derived independently by a number of researchers. The formula derived by Knox and Grant [4] for the contribution to the plate height H_{th} due to the electrophoretic velocity gradient is

$$H_{th} = 7 \times 10^{-9} \frac{\epsilon_o \epsilon_r \zeta \lambda^2 d_c^6 E^5 c^2}{D \eta k_{th}^2} \tag{3.46}$$

where λ is the molar conductivity of the solution. Inserting typical values for the constants, and with the requirement that $H_{th} < 0.1H$, Knox [105] has given the operating conditions below which H_{th} should be negligible as

$$(d_c/\mu m)^3 (E/kV\ m^{-1})^3 (c/mol\ l^{-1}) < 3.3 \times 10^9 \tag{3.47}$$

Grushka *et al* [110] quoted the thermal contribution to the plate height as

$$H_{th} = \frac{r^6 E^4 c^2 B^2 \lambda^2 u_{eo}}{24D(8k_{th}T_1^2 - E^2\lambda c r^2 B)^2} \tag{3.48}$$

where B is the buffer related constant in the viscosity equation. Equation 3.48 is a more general form (with less simplifying assumptions) than 3.46, but is equivalent to it when $E^2\lambda c r^2 B \ll 8k_{th}T_1^2$.

Davis [111] has calculated the temperature distribution and contribution to the plate height using a more accurate model for the variation of viscosity with temperature than the Andrade equation used by Grushka *et al* in their equations. According to his results, the errors introduced by use of the Andrade equation may result in calculation of H_{th} that are a factor of two too low.

With MECC [113], the analyte partition coefficient P (where P is the thermodynamic distribution of analyte between mobile and micellar phases) decreases with increasing temperature. For neutral molecules, the net effect will be that of a parabolic velocity gradient. For charged molecules, this effect will be superimposed on the variation of electrophoretic mobility with temperature. The situation is further complicated by the expected variation in the electrophoretic mobility of the micelle. Depending on the charges of the analyte ion, variation of P may result in additional dispersion or a partial cancelation of the dispersion as a result of the variation in electrophoretic mobility.

2. Radial variation of diffusion coefficient. The diffusion coefficient is known to be temperature dependent and so its variation with radial position might be expected to contribute to the plate height. Davis [111] has carried out an extensive mathematical treatment of this scenario and concluded that the effect of variation of the diffusion coefficient contributes little to the plate height when the temperature difference between the centre and walls of the capillary is less than 5 °C.

3. Free convection. As previously mentioned, the main reason for the introduction of gels in electrophoresis was to prevent the convection currents which arise as a result of temperature and density gradients within the separating medium and which were destroying separations and reducing the number of plates obtained. Convection may be eliminated by the use of additional force fields, by operating in a micro-gravity environment [16] or by use of the anti-convective wall effect. Holman [114] says that free convection is negligible and heat transfer is by pure conduction when

$$\frac{g\beta d_c^3 \Delta T}{\nu^2} < 1700 \tag{3.49}$$

where β is the reciprocal of the average temperature, d_c is the column inner diameter, g is the acceleration due to gravity and ν is the kinematic viscosity of the buffer solution.

For $\beta = 1/293$ K^{-1}, $\Delta T = 10$ K, $d_c = 200$ μm and $\nu = 1.002 \times 10^{-6}$ m^{2}s^{-1} the above term is equal to 2.7. Convection currents will therefore not be expected to be present in capillary electroseparation systems. The above dimensionless number is known as the Grashof number and will crop up again later in chapter 7.

3.3.7 Poiseuille Flow

Joule heating has been seen to produce a (roughly) parabolic velocity profile, which will result in increased dispersion of the peak. The superimposition of a parabolic velocity gradient due to a pressure gradient within the capillary may also be expected to contribute to zone broadening. The most likely way for this to occur is through the liquids in the buffer reservoirs being at unequal levels. The average velocity in a capillary due to a pressure gradient is given by the

Poiseuille equation

$$u_p = \frac{\Delta P d_c^2}{32\eta L} \tag{3.50}$$

where ΔP is the pressure gradient and L the length of the capillary. When the pressure gradient is as a result of differing reservoir levels (assumed at atmospheric pressure)

$$\Delta P = \rho g h \tag{3.51}$$

where h is the difference in levels and ρ is the density of the buffer solution. Combing the two equations

$$u_p = \frac{\rho g h d_c^2}{32\eta L} \tag{3.52}$$

In CZE, this average velocity profile is superimposed on the flat electro-osmotic profile to give the overall average velocity

$$u_{ave} = u_p + u_{eo} \tag{3.53}$$

A parabolic flow profile has a maximum velocity at the centre and zero velocity at the walls of the capillary. The difference in velocity between the overall average velocity $(u_{eo} + u_p)$ and the maximum velocity is given by Δu and is equal to u_p.

Making use of the Taylor equation in a similar fashion to Knox and Grant [4] in their study of thermal effects

$$\frac{\sigma^2}{L} = \frac{d_c^2}{96D}\frac{\Delta u^2}{u} \tag{3.54}$$

Using $H = \sigma^2/L$ and substituting for $\Delta u^2/u$

$$H_P = \frac{d_c^2}{96D}\frac{u_p^2}{u_p + u_{eo}} \tag{3.55}$$

In this frame of reference, the plate height due to axial diffusion is given by

$$H = 2D/(u_p + u_{eo}) \tag{3.56}$$

d_c/μ m	Diffusion Coefficient /m^2s^{-1}		
	10^{-9}	5×10^{-10}	10^{-10}
50	114.5	57.3	11.5
75	33.9	17.0	3.4
100	14.3	7.2	1.4
125	7.3	3.7	0.7
150	4.2	2.1	0.4

Table 3.3. Allowed buffer level difference (mm) as a function of diffusion coefficient and column diameter

If the condition is imposed that $H_P < 0.1H$ then

$$\frac{d_c^2}{96D}\frac{u_p^2}{u_p + u_{eo}} < 0.1\frac{2D}{u_p + u_{eo}} \tag{3.57}$$

Substituting for u_p and rearranging

$$\frac{d_c^3 h}{L} < 140.22\frac{\eta D}{\rho g} \tag{3.58}$$

Substituting typical values of $\eta = 1.002 \times 10^{-3}$ kg $m^{-1}s^{-1}$, $\rho = 1000$ kg m^{-3} and $g = 9.81$ m s^{-2}

$$d_c^3 h/L < 1.432 \times 10^{-5} D \tag{3.59}$$

Whether or not Poiseuille flow adds to the overall zone broadening is strongly dependent on d_c and to a lesser extent on h, L and D. Table 3.3 illustrates allowed differences in h when $L = 1$ m and $D = 10^{-9}$ or 5×10^{-10} or 10^{-10} m^2s^{-1}. Under these conditions, a 100 μm i.d. column can tolerate differences in the relative levels of the buffer reservoirs of 7 mm when $D = 5 \times 10^{-10}$ m^2s^{-1}, but the difference in levels for a 150 μm capillary must be less than 2 mm, quite a stringent requirement.

3.4 Conclusions

Apart from band broadening due to axial diffusion, the main causes of band broadening in the majority of capillary electroseparation systems are due to sample injection, detection, migrational dispersion, thermal gradients, solute adsorption and Poiseuille flow. The effect due to solute adsorption is difficult to quantify. In general terms, if it is present, then it is likely to be the largest contributor to zone broadening and all other mechanisms become insignificant in comparison. Limiting equations have been derived for the other effects. In each case, the equation or condition has assumed that the particular effect is the only one affecting the separation, and has based the conditional equation that the plate height due to it contributes less than 10% to the plate height due to axial diffusion alone. In a normal system, all effects will potentially be operating at once. While the conditions given for each broadening mechanism may appear to reasonable (i.e. easily achieved), it should be remembered that the variances are additive. Therefore if five band broadening mechanisms are operative, then the total variance due to them must not be allowed to be greater than 10% of the plate height from axial diffusion alone. Some of the requirements may be conflicting. Thus in order to minimise migrational dispersion, the conductivity or concentration of the buffer must be as high as possible. Increasing either of these parameters increases the power and so increases the plate height due to thermal effects. Similarily increasing the injection length to increase sensitivity may reduce the leeway in the precision of the levels of the buffer reservoirs. In order to achieve the best possible separation efficiency, a balance must be struck between any conflicting requirements. Even so, the requirements to achieve high plate numbers are not extreme and it would be expected that, with due consideration of the factors outlined in this chapter, it should be possible to routinely

achieve high plate numbers.

Chapter 4

Experimental Details

4.1 Instrumentation

The instrumentation necessary to carry out CZE and the other capillary electroseparation techniques is very simple and has been described briefly in Chapter 1. The main requirements are a high voltage power supply, a suitably modified detector to allow "on-column" detection, a recording device, buffer reservoirs and an isolation cage with an interlock to prevent the operator coming in contact with the high voltage end. The work detailed in this and the following chapters has been carried out on three different systems which are now described.

4.1.1 Home-made system (1)

The electrochromatographic separations described in chapter 5 were carried out on a home-made system originally built and described by Grant [73]. It consisted of the following:

1. A Brandenburg (U.K.) Model 2829P High Voltage power supply capable of delivering a positive high voltage up to 100 kV with a maximum current output of 1 mA.

2. A Perkin Elmer (Beaconsfield, U.K.) Model LS4 fluorimeter originally designed for use in HPLC. The detector had been modified for use as an electrochromatography detector by removing the original detector cell and supports and replacing them by two stainless steel tubes lined with Teflon tubing, the ends of which were separated by approximately 1 cm. The separation capillary is fed through the Teflon tubing until the detection zone is midway between the ends of the tubing. Light is focussed onto the detection zone by means of a parabolic mirror, and the fluorescence collected at right angles by another parabolic mirror. Once the separation capillary is in place, the mirrors can be adjusted to give the maximum signal. The detector can operate with excitation wavelengths in the range 230–700 nm, while emission can be collected from 250–800 nm. The detector was mounted on its side and supported on a moving carriage. This was to allow easy movement of the detector to permit the distance between injector and detection zone to be easily varied. The system permitted the use of separation capillaries in the range 500–1500 mm.

3. The high voltage end is surrounded by a Faraday cage made from angle iron and covered with a wire mesh. The floor of the cage was fitted with a shunt lock and microswitch which, when opened, cut off the high voltage immediately, thus preventing operater contact with the high voltage.

The injection components were supported on a PVC table in the centre of the cage. The relative positions of the injection end and the detection zone were such as to allow the use of rigid glass capillaries. The injection end was comprised of a plexiglass box into which was fitted the injection port and the electrode. The box was filled with electrolyte which provided the electrical contact between the electrode and column. The injection system consisted of stainless steel tubing with three ports and a three way valve. The column was inserted into one port and held in place with a Teflon ferrule and Swagelok nut. The second port

contained a needle port for injection and the third port led to a waste container. The total volume of this arrangement was about 250 μl. To inject sample the tubing was filled with the sample solution. The valve was closed, thus cutting off the waste container, and a small voltage (up to 5 kV) was applied for up to 30 s. A sample slug was thus deposited on the column. The valve was then reopened and the tubing washed out with the running eluent. The valve was then closed and the running voltage applied.

4.1.2 Home-made system (2)

The initial CZE separations described at the end of this chapter, and the preliminary work on heating effects without forced convective cooling of the capillary, described in chapter 6, were carried out in a home-made system built by Applied Biosystems Inc. (Foster City, C.A., U.S.A.), which became the prototype for their first commercial system. It consisted of the following:

1. Hippotronics (Brewster, N.J., U.S.A.) High Voltage power supply, Model 830B/830-5, which delivered up to 30 kV with a maximum current output of 5 mA. The power supply was fitted with an interlock which cut off the applied voltage when opened, thus preventing accidental contact with the high voltage end. Polarity was reversed by switching the high voltage and return cable in the back of the instrument and reversing the polarity of the meters. The voltage was dialled up from zero at the beginning of each run. This presented a disadvantage for injection. Due to the short time of injection (up to 20 s) the time to reach the required voltage may have had an effect on the actual amount injected. While this did not directly affect the studies that were done here, it would have presented difficulties if quantitation had been required, due to the lack of reproducibility expected.

2. The detector used was a Spectroflow 773 (Kratos Analytical, N.J., U.S.A.) UV variable wavelength detector, which allowed operation at wavelengths from 190–700 nm. The separations and results in this thesis were obtained at wavelengths between 200 and 230 nm. The detector was operated at the lowest rise time allowed of 0.1 s (equivalent to a time constant of 0.045 s), and at a sensitivity of 0.01 AU. The original detector cell had been modified with sapphire optics to allow better focussing of the beam on the column. The body of the detector had been modified to allow the capillary to pass through the detector area and was operated on its side. The length of the detection zone was 0.2 mm.

3. The high voltage end of the system was enclosed in a plexiglass box fitted with an interlock. The box contained a carousel buffer and sample vial container, which had spaces for 1 buffer reservoir and 3 sample vials. A plastic box containing a heating element sat on top of the plexiglass box. The high voltage electrode passed through the upper box and down into the plexiglass box into the buffer reservoir or sample vial. The capillary or separation column dipped into the same reservoir, the bulk of the column was coiled in the top box and passed out through a hole in the side of the box, through the detector and into the cathode reservoir. The top box contained a heating element and a fan which allowed operation at temperatures above ambient, and/or cooling of the column. These were not used in these studies as they contributed excessive noise to the detector and it was not possible to operate the heating element without the fan. The system was therefore operated at ambient or laboratory temperature, which was about 20 °C.

To inject sample, the carousel was lowered and rotated until the sample vial was underneath the electrode and capillary, and then lifted until both were inserted into the vial. The interlock was closed, and a small voltage (2 kV) applied for enough time to give a 1 mm slug of the fastest moving component on the

column. This time was estimated from an initial faster run at 20–30 kV. The carousel was lowered and rotated to bring the buffer solution to the correct position and then raised to bring the levels of the buffers to the same height in both reservoirs. This was confirmed by the use of a travelling microscope. The interlock was closed again, and the running voltage dialled up.

Electrokinetic injection was always used in these studies. Hydrodynamic or pressure injection is less convenient when using columns of different diameters, as the amount injected depends on the square of the column diameter (Poiseuille equation). As the amount injected elecrokinetically is independent of the column diameter (von Smoluchowski equation) it is more easily regulated and the actual amount injected can be estimated from a run at the same voltage, or a higher voltage if no heating of the solution takes place (Chapter 6). Bias in injection due to the variable electrophoretic mobilities has been recognised [116] but can be easily calculated from the relative retention times of the analytes.

The current in the system was obtained by measuring the voltage across a load resistor of 10^4 Ω.

4.1.3 Commercial system

The studies with forced convective cooling were carried out using the Applied Biosystems Instrument Model 270A. This system derives from the home-made system just described but was automated, and so less error in sample injection was to be expected. The temperature of the chamber which contained the bulk of the capillary could be set in a range from about 5 °C above ambient to a maximum of 60 °C. In general a temperature of 30 °C was used. The capillary chamber was cooled by a fan. The system allowed both vacuum and electrokinetic injection but electrokinetic injection was invariably used. With this system, the

only injection voltage permitted was 5 kV. The injection times were therefore varied accordingly to permit a maximum of a 1 mm slug of the fastest moving sample component on the column.

4.2 Capillaries

The capillaries used were of polyimide coated fused silica. The initial experiments used SGE (Australia) fused silica, but later experiments used Polymicro (Arizona, U.S.A.) fused silica which was found to give better and more reproducible results. The fused silica was purchased in lengths of 10 m and cut to the required length ($0.5 - 2$m). After cutting, a portion of the coating (2-5 mm) was removed from either end of the capillary by burning in a small flame. This was to prevent sample from sticking onto the coating and contaminating the buffer solution or affecting the peak efficiency, and to prevent an uneven injection end due to the jagged edges of the coating. The polyimide coating is not transparent to uv radiation and so a window for detection was made about 20 cm from the outlet end of the capillary by burning off a portion of the coating. The disadvantage of forming these windows is that, particularily with columns with small outer diameters, it produces a brittle section which is easily broken and needs to be handled with great care. The new transparent coatings now available overcome this disadvantage and allow detection at any point along the column.

Before use the columns were conditioned with 0.1 M NaOH for 20 minutes and then filled with the buffer solution. With the manual system, flushing of the column was not carried out regularily as it was time consuming and difficult to regulate. Flushing was carried out only when it was noticed that the peaks were noticeably assymetric or broader, which appeared to happen suddenly. When this

occurred, the column was immediately flushed with 0.1 M NaOH for 2-5 minutes and re-equilibrated with buffer. In many instances, it was sufficient to flush with the running buffer to bring the column back to its previous performance. As a rule of thumb, column flushing is probably only necessary every 8 to 10 runs to prevent deterioration of performance (but for reproducibility of retention times column flushing must be more frequent.)

4.3 Preparation of Samples and Buffers

The buffers used were Na_2HPO_4, NaH_2PO_4, $Na_2B_4O_7$, and NaOH at various concentrations. The salts were all of SLR grade and were initially made up to 0.1 M (0.08 M for $Na_2B_4O_7$) in double distilled water. These stock solutions were diluted down to the required concentrations, and were usually used without adjustment of the pH, which was done with NaOH or HCl solutions if deemed necessary.

Stock solutions of the samples ($10^{-2} - 10^{-4}$) M were made up in double distilled water and were diluted down to the required concentration with the addition of sufficient stock buffer solution and water to give the same concentration of buffer in the sample solution as in the running buffer. The concentration of sample was at least 150 times less than the concentration of buffer to prevent electromigrational dispersion. Sample solutions were filtered through a 0.22 μm syringe filter and ultrasonicated before use. Buffer solutions were initially treated in the same way, but experiments revealed that ultrasonication did not appear to improve the results or noise level of the detector, and so buffer solutions were henceforth only filtered.

4.4 Collection and Analysis of Results

The detector was connected to a BBC Model B micro-computer for collection of electropherograms. The output was passed through a voltage amplifier which amplified the signal from 1 V per AU from the output port of the detector to whatever magnitude was necessary to give a reasonable signal. The gain was usually set at 100. The program used for data collection was one developed by I.H. Grant [73] which took as input relevant variables such as the effective length of the column (i.e. the length to the detector) and, for packed capillaries, the particle diameter to allow later calculation of plate numbers and heights. Data collection was started manually. The program was modified to allow collection of multiple runs with the ABI 270A commercial system. Memory space was limited to 16K so the frequency of data collection was determined by the expected retention times. For retention times less than 10 minutes, a frequency of 16 Hz was used. Between 10 and 27 minutes, 10 Hz was used and for retention times greater than 27 minutes, 5 Hz was used. Results were only taken for reasonably symmetrical peaks where the peak symmetry at 10% of the full height was between 0.9 and 1.1.

The data collection program calculated a variety of relevant parameters and printed them out. The program calculated the number of plates by two methods, the method of second moments and at full width half height. The value from the calculation at full width half height was used, as it was less susceptible to the positioning of the defining points of the peak.

4.5 CZE Experiments

At first, there were a lot of problems with the technique. Columns were giving 30,000 plates instead of the 300,000 expected. These problems were due to a combination of factors—lack of detector sensitivity resulting in sample overloading, unequal buffer levels leading to band broadening as a result of Poiseuille flow and poor performance as a result of insufficient pretreatment and equilibration of the column. The lack of reproducibility from column to column also caused problems. Phosphate buffers in particular gave the worst results, even though the majority of papers in the literature at that stage (1988) were using phosphate buffers of one kind or another. Eventually however, the problems were solved and the power of capillary electrophoresis became obvious. Some sample electropherograms obtained at that stage are shown in figures 4.1 to 4.6.

Figure 4.1 illustrates the separation of a group of naththalene compounds in 0.02 M NaOH. The compounds range from a neutral one (naphthylamine) to 2,7-naphthalene disulphonic acid, which has two negative charges. The power of the technique can be seen in the complete resolution of the two geometric isomers, 1- and 2-naphthol whose pKa's are 9.34 and 9.51 respectively. The average plate number of the separation is 300,000.

Figure 4.2 is a separation of some dansyl amino acids in a 0.01 M $Na_2B_4O_7$ buffer, each amino acid differing from the next by one CH_3 group, a difference in mass of about 4%. While complete resolution has not been achieved for all components in the mixture, it is obvious that with optimisation e.g. reducing the electro-osmotic flow, complete separation could be attained. The average plate number for the separation is over 500,000 plates.

Figure 4.3 shows an expanded view of the peak due to dansyl glycine from figure 4.2. The peak is very obviously symmetrical (peak symmetry is 1.00 at

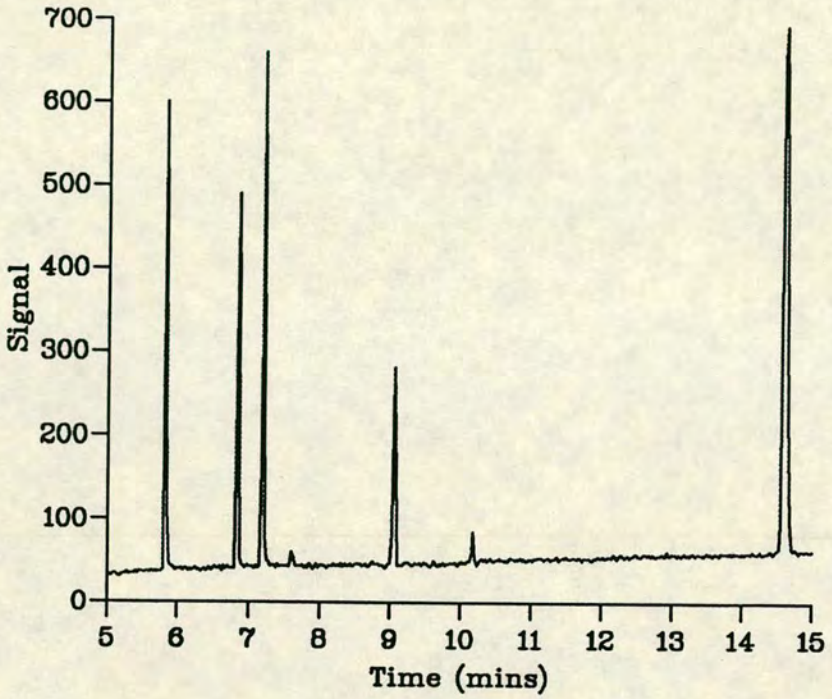

Figure 4.1. Separation of naphthalene derivitives. Column 50 μm i.d., 1000 mm long, 790 mm to detection zone. Buffer 0.02 M NaOH. Applied Voltage 30 kV. Detection 230 nm uv. Peaks in order of appearance : 2-naphthylamine, 2-naphthol, 1-naphthol, 2-naphthalene sulphonic acid, 2,7-naphthalene disulphonic acid.

10% of full height) and Gaussian in shape. With a retention time of 564 s, this peak shows an efficiency of 680,000 plates over an effective column length of 780 mm.

In illustrating the versatility of the technique, figures 4.4, 4.5 and 4.6 show samples of some common beverages, apple juice, coffee and a low alcohol wine. The samples were run in 0.04 M $Na_2B_4O_7$ buffer, and sample preparation consisted simply of diluting the beverage to half with 0.08 M $Na_2B_4O_7$ buffer to give the same concentration of the running buffer. The peaks have not been identified, but the resolution and simplicity of the technique is obvious.

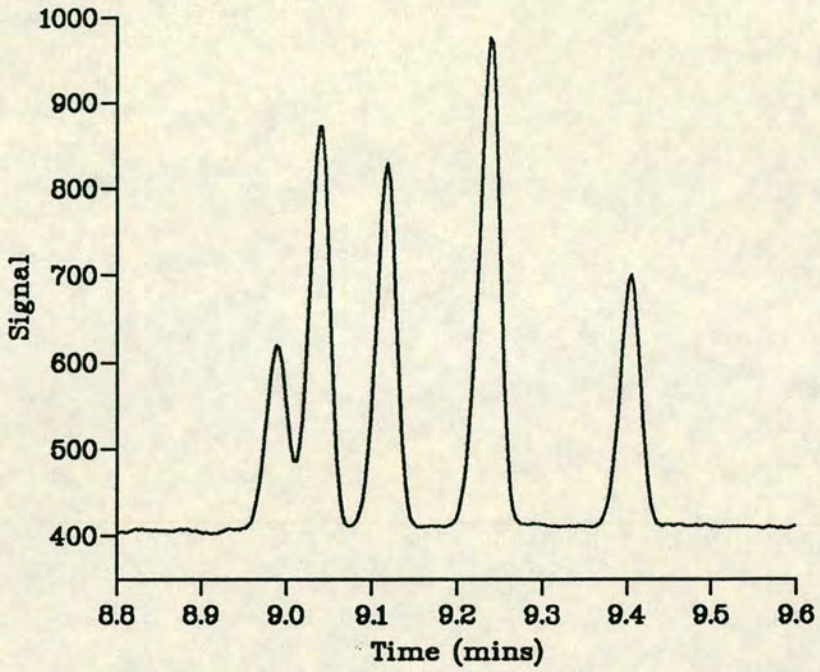

Figure 4.2. Separation of dansyl-amino acids. Column 50 μm i.d., 990 mm long, 780 mm to detection zone. Buffer 0.01 M $Na_2B_4O_7$. Applied voltage 30 kV. Detection 217 nm uv. Peaks in order of appearance : dns-leucine, dns-norvaline, dns-alphabutyric acid, dns-alanine, dns-glycine.

4.6 Measurement of the Diffusion Coefficients

The diffusion coefficient of 2-naphthalene sulphonic acid was measured at a variety of temperatures after the method of Walbroehl and Jorgenson [117]. A 4.9×10^{-5} M sample solution was made up in 0.0099 M NaH_2PO_4, a low concentration buffer in which no heating of the solution is assumed to take place. A straight run of the sample gave a retention time of 1630 s at 10 kV m^{-1}. Sample was injected and run for 900 s at 10 kV. The voltage was switched off, and the sample allowed to diffuse in the capillary for a set period of time (from 15 to 400 minutes), the voltage switched on again, and the peak eluted. In between each 'stopped flow' step, a straight run was carried out to enable confirmation

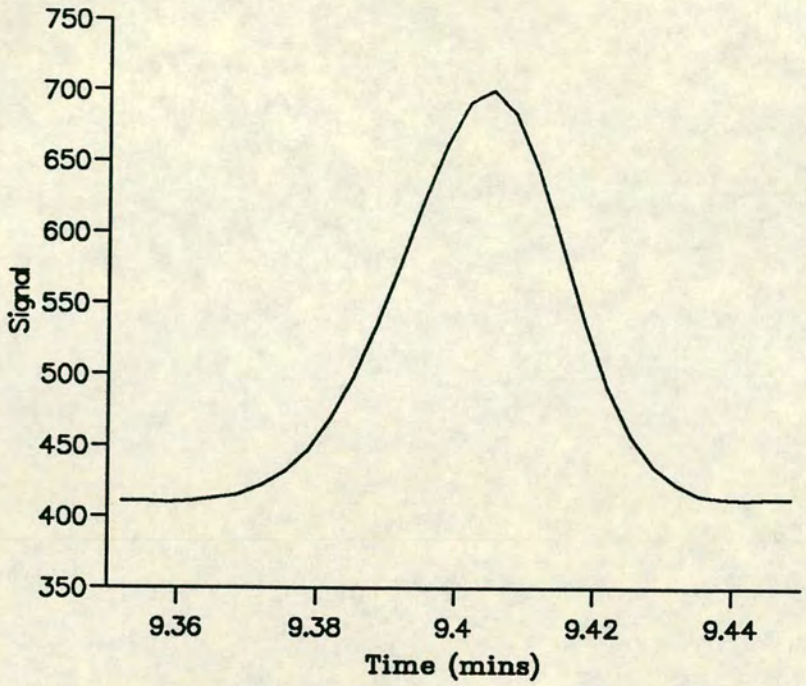

Figure 4.3. Expanded glycine peak from figure 4.2 to illustrate symmetry of the peak.

of the eluting velocity (which may change with time) and so calculation of the variance in units of m^2. From a plot of the variance versus time, the slope was calculated from which the diffusion coefficient was calculated according to the Einstein equation (Chapter 3). A sample plot is shown in figure 4.7 for the calculation of the diffusion coefficient of 2-naphthalene sulphonic acid at 30 °C. This process was repeated for a number of temperatures ranging from 20 °C to 60 °C.

4.7 Measurement of the Buffer Conductivity

The conductivity of some of the solutions used as buffers in these experiments were measured at a variety of temperatures using a Kohlrausch type conductivity cell. The conductivity cell was washed out with conductivity water until a reading

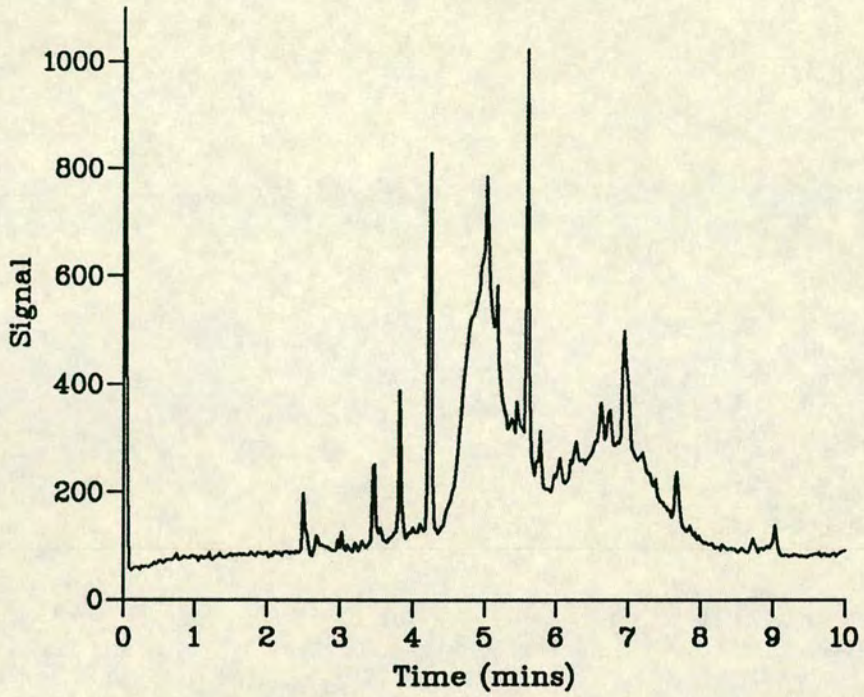

Figure 4.4. Apple Juice sample. Column 50 μm i.d., 770 mm long, 570 mm to detection zone. Buffer 0.04 M $Na_2B_4O_7$. Applied voltage 20 kV. Detection 200 nm uv.

of less than $5 \times 10^{-6}\ \Omega^{-1}$ was obtained between each change to a different buffer. The buffers were made up in conductivity water and clamped in a lidded glass jar in a thermostatted water bath. 0.100 M KCl was used to determined the cell constant. At 25 °C the electrolytic conductivity κ of 0.100 M KCl is 1.286 $\Omega^{-1}m^{-1}$. The cell constant CC is therefore given by

$$CC = \kappa / c_o \tag{4.1}$$

where c_o is the measured conductivity of the sample solution. The electrolytic conductivity at any temperature for any buffer is therefore given by

$$\kappa = CC \times c_o \tag{4.2}$$

The molar conductivity of the solution λ is related to κ by

$$\lambda = \kappa / c \tag{4.3}$$

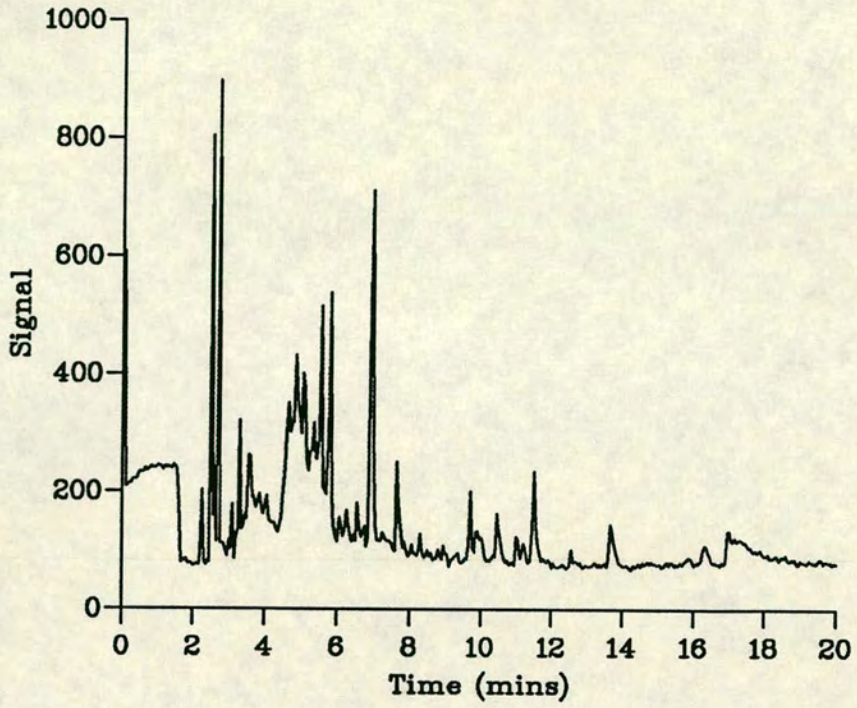

Figure 4.5. Low alcohol wine sample. Conditions as for figure 4.4.

where c is the concentration of the solution in mol m^{-3}.

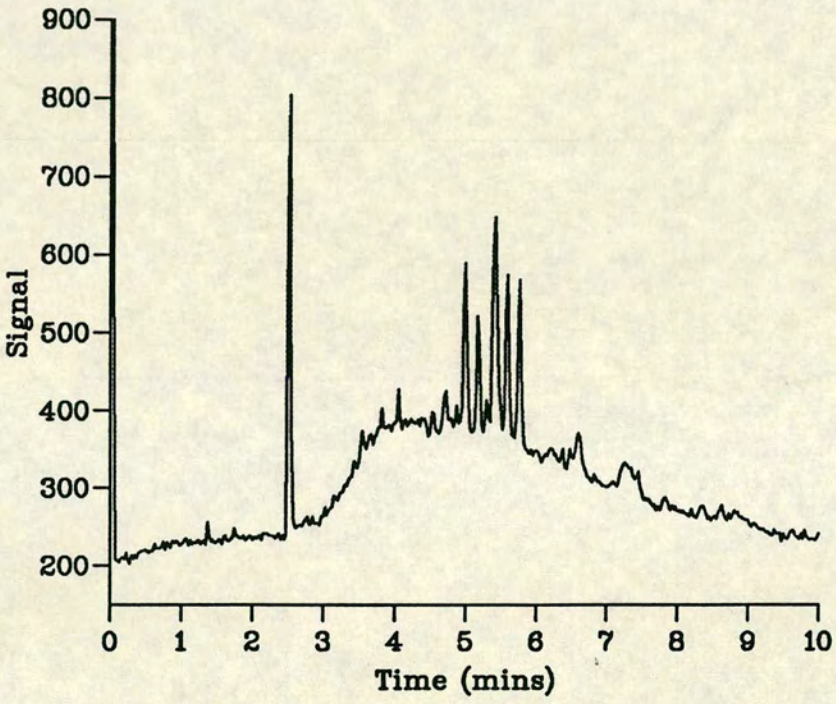

Figure 4.6. Coffee sample. Conditions as for figure 4.4.

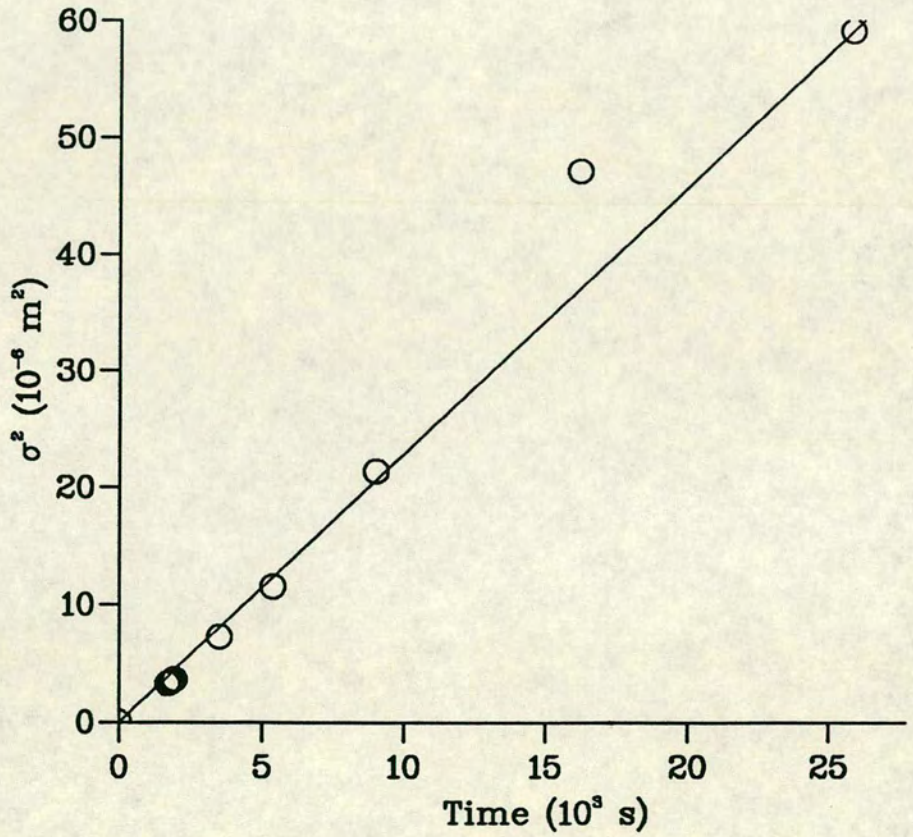

Figure 4.7. σ^2 vs t for 2-naphthalene sulphonic acid at 30 °C

Chapter 5

Electrochromatography

5.1 Column Packing

The advantages of electrochromatography have been outlined in earlier chapters. Grant [73] had presented the first successful results on microbore systems, and shown the potential of electrochromatography with a separation on polyaromatic hydrocarbons on 5 μm ODS Hypersil. He had also shown the improvement in performance by using electro-osmotic flow as compared to pressure driven flow, and that the flow rate was independent of particle diameter, subject to the limitation of the Rice-Whitehead theory. One of the aims of this thesis was to extend his results to columns packed with micron and sub-micron particles and to extend the range of separations.

Three methods of packing the columns have been identified and attempted.

5.1.1 Drawn Packed Capillaries

This method was developed by Novotny [118] and Tsuda [119] for use in microbore LC. A heavy walled pyrex tube is prepacked with the packing material and then drawn down to the desired diameter using a glass drawing machine. Some

of the particles become partially embedded in the capillary wall, thus holding the bed in place without the need for retaining frits. These columns are reputed to have high permeabilities. Grant successfully produced drawn packed capillaries with 5 μm and 3 μm particles which showed very high efficiencies or low reduced plate heights. In order that the packing material is retained without a frit, the column diameter must be less than 10 times the diameter of the packing material. This would have necessitated the production of capillaries of 10 μm or less with the micron and sub-micron particles which it was hoped to use. The difficulties in production, handling and detection with such small capillaries suggested that efforts should be concentrated elsewhere.

5.1.2 Slurry Packed Capillaries

This method of packing is the most common method used in the packing of columns for HPLC and has been adapted for use in packing microbore columns.

The columns used are of fused silica, as for CZE, of 50–100 μm i.d.. A retaining frit is produced in one end by the following method. Some of the packing material is mixed to form a nearly dry paste with water glass diluted to 25% with water. The end of the capillary is repeatedly dipped into the paste until 200–1000 μm has been forced into the capillary. This end is then heated in a low flame until the silica particles fuse and form a porous frit. The frit is tested before use by forcing eluent through at 4,000–6,000 p.s.i.. If it holds, then it will generally hold for packing.

The packing material is made up into a slurry in an acetonitrile or acetonitrile/water mixture, about 2.5 mg cm^{-3}, and ultrasonicated for 10 minutes to ensure even dispersion of the packing material. The reservoir consisted of a stainless steel HPLC column, 10 cm long, 4.6 mm i.d.. The slurry was injected

into the column using a syringe until the reservoir was full, excluding all air bubbles. The capillary to be packed was attached to one end of the reservoir using Swagelok fittings and Teflon ferrules. The other end of the reservoir was connected to a high pressure packing pump (Shandon Scientific, Runcorn, U.K.). The capillary and reservoir were placed vertically in a cylindrical water bath (3.5 cm in diameter, 1.2 m high) which was sitting in an ultrasonic bath. The pressure was increased gradually from zero to the final packing pressure (6,000-9,000 p.s.i.) over about 5 minutes with ultrasonication. With 5 μm particles, packing took in the order of 10-40 minutes, depending on the slurry concentration and column diameter. Once packing was complete, the ultrasonic bath and pressure were switched off and the column left for the pressure to dissipate gradually over a number of hours or overnight.

The column must be removed from the packing pump to the electrochromatography system without any drying of the capillary being allowed to occur, otherwise electro-osmotic flow is not possible.

In the work described by Grant only one end of the capillary had been plugged, the injection end (the end at the anode). He did not report any problems with this. In our work, however, no matter which end the plug was at, on application of the voltage, packing material began to pour out of the capillary. This happened for all packing materials and eluents tested, and whether the outlet was horizontal or vertical. It was obvious that the other end would need to be plugged.

The best way to plug the other end was as follows. Once the column had been packed, it was removed from the packing pump and the unplugged end allowed to dry out a little. This end was then placed in a vial of 25% water glass and left until some of the water glass had been sucked into the packing material by capillary action. The capillary was removed from the vial and the packing

material fused to form a plug by the application of a small flame. The column was then refilled with the running eluent under pressure and tested.

The packed columns produced were tested with an eluent of 70:30 acetonitrile:water containing 0.002–0.006 M Na_2HPO_4. The sample was a 10^{-4}–10^{-5} M solution of fluorene in the eluent. Reproducibility and efficiency were measured by using fronts, both leading and trailing, or peaks.

With 5 μm Hypersil, it was possible to achieve reduced plate heights of 2 for an unretained solute with up to 42 kVm^{-1} applied to a 100 μm i.d. column in about 15 minutes. These results were never reproducible. In general, the retention times decreased and the reduced plate heights increased with time. On observation of the columns, gaps were evident in the packing material. The gaps were of the order of 0.1–1 cm in length and varied in position and number from column to column. The gaps were never obvious on examination of the packed capillary under a microscope immediately after packing, at which time the packing material appeared to be well and evenly packed. The gaps developed with time under electro-osmotic flow. When the voltage was removed, the gaps often disappeared or closed up, only to reopen on reapplication of the voltage. The gaps also moved cyclicly up and down the column. On observation of these gaps under a microscope with the voltage applied, the particles always behaved in the same way. The gaps or voids, as they appeared to the naked eye or with a magnifying glass, in fact contained packing material at a much lower density than in the 'packed' areas. At the walls the particles moved in the same direction as the electro-osmotic flow i.e. towards the cathode. In the centre the particles moved in the opposite direction towards the anode. At the interface of the two turbulence was observed in which the particles appeared to move randomly.

The development of the gaps may be explained by uneven packing which produces areas of differing permeabilities. In areas with greater permeability or

looser packing, which may or may not be visible under a microscope, the packing material is relatively freer and can move around. Similarily, the volume flow rate of liquid through the more permeable areas will be greater and, to maintain the overall velocity, there will be or can be a return flow of liquid due to the pressure of electro-osmotic flow down the middle of the channels, similar to the effects of electro-osmosis in closed systems. The forces on the particles in these permeable areas are different to those in the well packed regions, and as a result of the relatively loose packing, the particles may rearrange. Particles at the interface of the well packed and loosely packed area will also be free to move and, as a result, the 'gaps' can move or be regenerated throughout the column length. In the bulk of the column in which the packing material density is high, the particles are attracted to the anode due to their negative charge.

These regions of varying permeability can arise in a number of ways.

1. As a result of the wall effect, the permeability of the column is higher at the walls than in the centre. The volume flow rate will be higher in this region, and if it is higher than the electrophoretic mobility of the particles, and they are free to move, then they will move towards the cathode, thus creating spaces elsewhere in the column.

2. The effects of 'bridging' of particles in the packing of capillaries is well known. When the slurry is forced into the capillary, a point is reached whereby the slurry concentration is increased and the particles touch each other. When a string of particles bridges the whole column diameter and is compressed it becomes quite strong through the bridging effect. These bridges of particles resist further bed compression and do it better as the packing force is increased. When the pressure is removed the bridges of particles are no longer compressed and they collapse. Small gaps are thus created which, under the influence of an applied voltage, may rearrange.

3. The distribution of particle sizes may also have an effect. With 5 μm particles, a range of particle sizes from 4–10 μm may be present. Due to the uneven nature of the packing process and the size distribution of the packing material, gaps or channels of differing sizes may be created. With pressure packing the particles will move in one direction towards the bed. With voltage applied however, the particles may move in either direction, depending on which is stronger, the electrophoretic force or the electro-osmotic force. A smaller particle may therefore move into a space leaving a larger space behind, which in turn can be filled by another particle. Thus it is possible to envision gradual rearrangement of the packing, not possible with pressure alone applied. This type of movement can be seen under the microscope in what appears to be a perfectly packed column.

It is possible therefore to explain the gaps which develop in these columns and how they increase with time, and also to explain why or how the performance of the column gets worse with time. The gaps can be considered or treated as regions of closed capillary operating under electro-osmotic flow. If the electro-osmotic flow velocity in the capillary is given by u_{eo}, then the volume flow rate f is given by the product of the electro-osmotic velocity and the cross sectional area of the liquid, which is in turn a function of the column porosity.

$$f = u_{eo} A \epsilon \tag{5.1}$$

where A is the the area of the column. However, ϵ varies from point to point, being least in the well packed portion and higher in a more loosely packed portion. Consider the column as being in three portions, two packed with porosity ϵ_1 and one in between that is loosely packed with porosity ϵ_2, and $\epsilon_2 > \epsilon_1$ In the densely packed region the eluent flows in with a volume flow rate f_1 and out at f_1 but in the loose region it moves at the higher volume flow rate f_2. To preserve balance

there must be a return flow of eluent down the centre of the loosely packed region due to the electro-osmotic force. This is what causes the movement of particles previously described, where at the walls the electro-osmotic force is greater than the electrophoretic force, and in the centre the pressure driven flow is superimposed on the electrophoretic mobility of the particles.

This return flow can be expected to have disastrous effects on the column efficiency. As the flow profile affects the particles, it will have a similar effect on the sample plug. The flow profile in the loose area is parabolic and will lead to spreading or dispersion of the zones, thereby negating the advantageous effect of the electro-osmotic flow. The larger the gaps, or the more frequent they are, then the greater the effect on the column efficiency. As the gaps increase in length and frequency, so the column efficiency decreases with time.

The negative effects of voids had been observed by Kennedy and Jorgenson [120] for 21 μm and 35 μm i.d. capillaries packed with 5 μm particles for microbore LC in which 'bad' columns had voids or gaps compared to the 'good' columns with no gaps.

5.1.3 Attempts to solve the problem of void formation

As it was postulated that void formation may be due in part to the formation of bridges which collapse when the pressure is removed, 'shock treatment' was attempted on the columns in which the pressure was reduced and then reapplied suddenly. This was repeated a few times, but was unsuccessful. Attempts to reduce the ζ potential and thus prevent repulsion of the particles which may have also contributed to a low density of packing, by adding a high concentration of salt to the slurry solvent, also had no effect.

Porous plugs can also be formed by fusing silica and water in a flame. Once

the column had been packed, water was flushed through the column at the packing pressure. A plug was formed by heating a portion of the column in a flame to fuse the silica while the pressure was still applied, and then breaking the capillary above this point. This did not prevent void formation.

An alternative way to prevent void formation would be to bond all the silica particles together, thus preventing movement of any of them. A variety of methods was tried.

1. Packing in a solution of 25% water glass, as used for making the plugs, and drying out. A number of different ways were tried to fuse the silica and water glass. The packed column and water glass were autoclaved at 200 °C for 4.5 hours, but this produced very brittle columns, although the packing appeared to be stable under 6,000 p.s.i. . The packed column and water glass were refluxed in water for 3–4 hours. This did produce an apparently stable packing, but the reduced plate height was high (3.9) and the detection window produced was very brittle. The column was also dried out by placing it in an oven for a few hours, or by passing quickly over a low flame. In most cases, it was impossible to force eluent through the column after it had been dried out, even at very high pressures and, when it was possible to wet the column, it began to dry out of its own accord once a high voltage had been applied.

2. Precipitation of a solution of colloidal silica in the packing. The columns were packed as before but with the addition of 2% of a colloidal silica solution (Syton X-30) to the slurry. After packing, the columns were dried out either by passing over a low flame or in an oven. A concentration of 5% of colloidal silica was too high and led to blockage of the capillary and inability to refill with eluent. Concentrations of less than 2% were too low and the columns unpacked immediately when pressure was applied to the column. A column packed in 2% colloidal silica at 6,000 p.s.i. was stable with an applied pressure of 6,000 p.s.i.,

with initially good results under electro-osmotic flow with $h = 1.64$ at $\nu = 2.74$ but h increased and the retention time decreased with time. On re-applying pressure the column unpacked immediately. Particle binding was obviously not stable. It was not possible to improve the efficiency or reproducibility any further.

3. Once the column had been packed, water was pumped through until all the acetonitrile had been removed. The column was then heated to fuse all the silica together. As in the previous method, these columns were not stable to electro-osmotic flow.

The three methods just described were all partially successful, but were either irreproducible or unstable. A disadvantage of all three was the necessity for heating, which precludes the use of derivatised materials, necessitating *in situ* derivitisation. This stage was however never reached with these methods. The precipitation of colloidal silica was the most successful of these three methods, and further research may solve the stability problems.

5.2 Electrochromatographic separations

Some electrochromatographic separations were however achieved as follows.

1. A drawn packed capillary (made by Grant) 40 μm i.d., 810 mm long, 630 mm to the detection zone was dynamically derivitised with Tween20 as originally described by Wall *et al* [121]. The packing material was 5 μm Hypersil and the running eluent was 10:45:45 acetonitrile:methanol:water, 0.002 M NaH_2PO_4 with 0.0011 M Tween20 added. The applied voltage was 40 kV and detection was with fluorescence with λ_{ex} at 265 nm and λ_{em} at 330 nm. Figure 5.1 illustrates the separation of naphthalene, methylnaphthalene and fluorene with 40 kV applied. The peaks are symmetrical and give respectively 95,000, 40,000 and 48,000 plates with retention times of 983.6, 1013.1 and 1043.4 s. The retention time of an

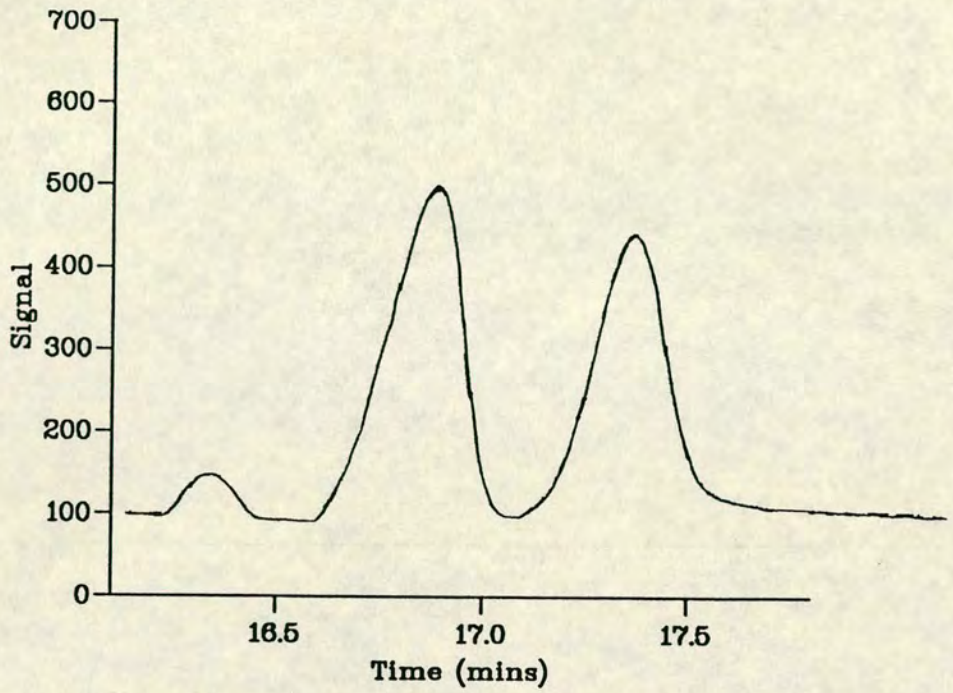

Figure 5.1. Separation of polyaromatic hydrocarbons on a drawn packed capillary packed with Hypersil and dynamically derivitised with Tween20. Details in text. Peaks in order of appearance: naphthalene, 2-methylnaphthalene, fluorene.

unretained peak t_o was obtained by filling the column with fluorene and then injecting some pure eluent. A negative peak at 882 s corresponded to t_o and allowed calculation of k' for each compound. The values of k' obtained were 0.115, 0.149 and 0.183 for naphthalene, methylnaphthalene and fluorene. From equation 3.22, with $D = 3 \times 10^{-10}$ m^2s^{-1}, a peak efficiency of 100,000 plates is expected which compares well with the 95,000 plates obtained for the naphthalene peak, while the other two peaks yield 40% and 48% respectively of the plates expected.

2. The second separation (figure 5.2) is of a number of polyaromatic hydrocarbons obtained on a 100 μm i.d., 627 mm long column, 457 mm to the detection zone packed with 5 μm MOS (Shandon). 30 kV was applied to the column. The column was packed in acetonitrile at 6,000 p.s.i. and plugged at the other end

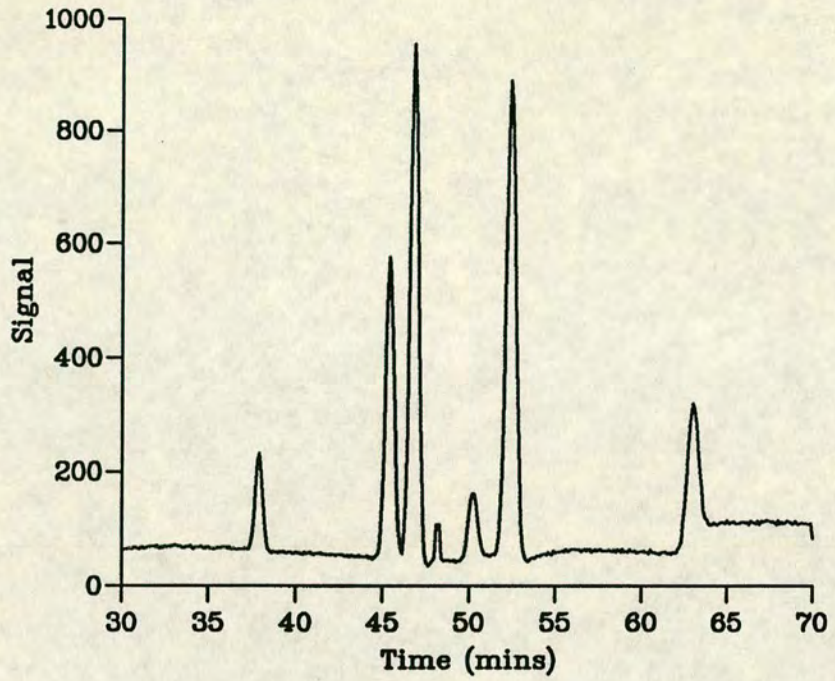

Figure 5.2. Separation of hydrocarbons on a 5 μm MOS column. Details in text. Peaks in order of appearance: naphthalene, 2-methylnaphthalene, fluorene, phenanthrene, anthracene, pyrene.

by allowing the column to dry out, dipping in 25% water glass and fusing as described. Complete separation of the 6 polyaromatics was achieved in less than 70 minutes. The reduced plate heights varied from 2.3 to 2.6. The running eluent was 70:30 acetonitrile:water, 0.005 M NaH_2PO_4. Detection was by fluorescence with λ_{ex} = 265 nm and λ_{em} = 330 nm until the fluorene peak was eluted, after which the wavelengths were changed to λ_{ex} = 238 nm and λ_{em} = 390 nm.

3. Figure 5.3 illustrates the separation of some coumarins with the same column and eluent as used for figure 5.2. Detection was by fluorescence with λ_{ex} = 308 nm and λ_{em} = 480 nm at a running voltage of 40 kV. The reduced plate heights were 2.46, 1.92 and 2.34 respectively for the three peaks.

4. Figure 5.4 is a separation achieved on 1.5 μm RP18 non-porous silica, in

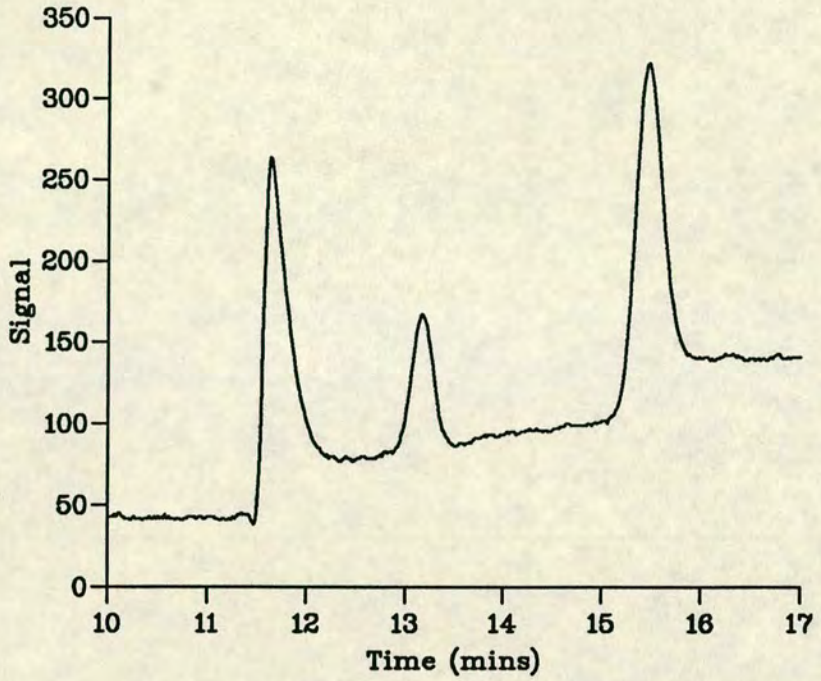

Figure 5.3. Separation of coumarins on a 5 μm MOS column. Details in text. Peaks in order of appearance: C47, C500, C102.

a 50 μm i.d. column. The column was prepared as for column 2 above and was 700 mm in length and 500 mm to the detection zone. The running buffer was 70:30 acetonitrile:water, 0.005 M NaH_2PO_4 with an applied voltage of 30 kV. Detection was by flourescence as for figure 5.2. Due to the non-porous packing material, the flow rate is fast compared to 5.2 above and the selectivity is poor. While the peaks show 90,000–100,000 plates per metre, the reduced plate heights are high (6.2–7.4) and so this separation does not show the expected potential of electrochromatography with small particles.

5. Figure 5.5 is a separation of polyaromatic hydrocarbons on a 5-15 μm ODS material. The column was packed in acetonitrile at 6,000 p.s.i. and the end plugged as for column 2 above. The column was 100 μm i.d., 750 mm long and 600 mm to the detector. Detection was by fluorescence with λ_{ex} at 265 nm

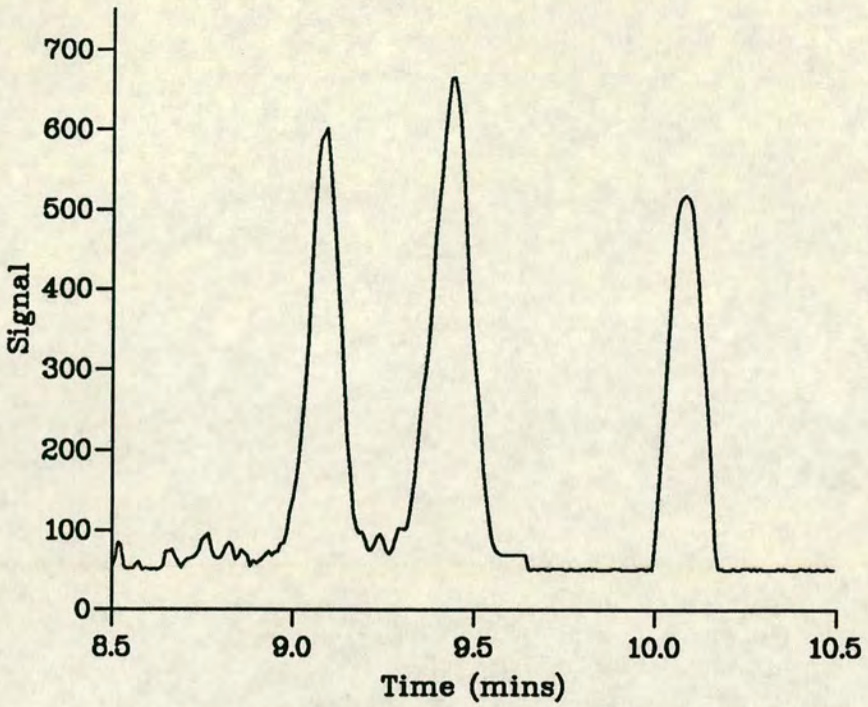

Figure 5.4. Separation of polyaromatic hydrocarbons on a 1.5 μm non-porous material. Details in text. Peaks in order of appearance: naphthalene, fluorene, pyrene.

and λ_{em} at 330 nm. The running eluent was 70:30 acetonitrile:water, 0.005 M Na_2HPO_4. The column was filled with the running eluent at 1,500 p.s.i. and operated at 40 kV. The peaks were symmetrical and the column had a reduced plate height of 1.32 if the average particle size is considered to be 10 μm.

5.3 Electrokinetic packing

Pretorius had suggested in 1974 [74] the packing of capillaries by electrokinetic means. With the lack of success with slurry packed capillaries, it was hoped that electrokinetic packing would provide the solution. In addition, it was hoped that electrokinetic packing would provide a relatively easy way of packing micron and sub-micron particles, which is slow and difficult ordinarily under pressure.

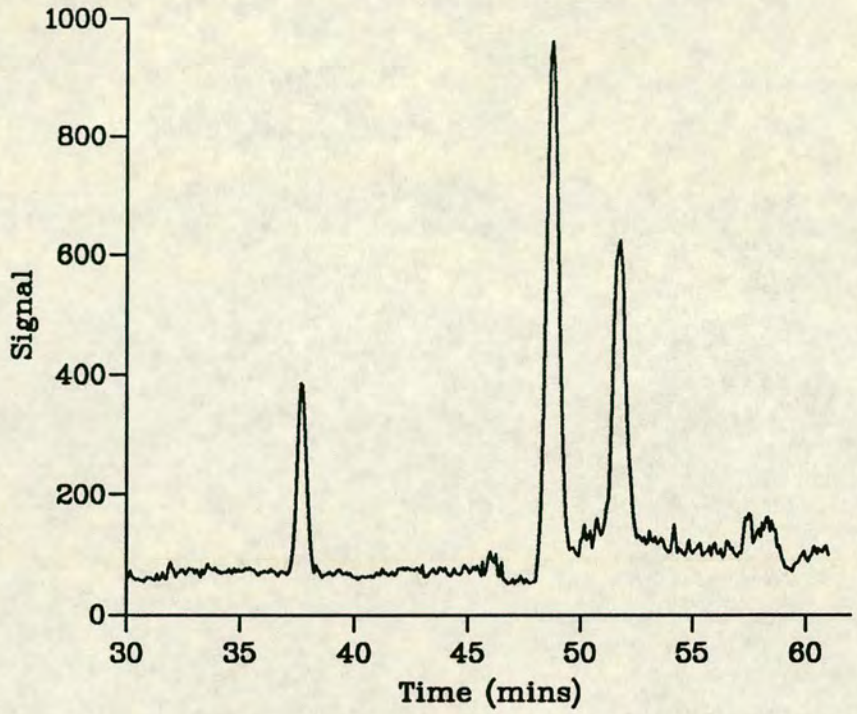

Figure 5.5. Separation of polyaromatic hydrocarbons on a 5–15 μm ODS material. Details in text. Peaks in order of appearance: naphthalene, 2-methylnaphthalene and fluorene.

Pretorius had filled the glass column with a slurry of the packing material (a microparticulate silica) and reversed the field so that the particles were sedimented by electrophoresis. The packing density obtained was comparable to that obtained by centrifugation.

When a voltage is applied across a slurry of silica particles the particles move towards the cathode. This is due to the fact that the electro-osmotic mobility is greater than the electrophoretic mobility of the particles.

The column to be packed was plugged at one end as described in the section on slurry packed capillaries and filled with eluent. One end was placed in a reservoir of liquid and the other end into the slurry reservoir, preventing any bubbles getting into the capillary. The slurry reservoir was then filled with slurry

and the voltage applied, with a high negative voltage at the plug end. The slurry moved quickly to the bottom of the capillary. The slurry would appear to bounce off the plug, and then retreat back up the capillary. In some cases it came back down again and stayed, in other cases the voltage had to be reduced before the slurry would descend to the plug.

The slurry solvents were varied quite a bit from pure solvents (methanol, acetonitrile and water) to mixtures of these, with salts and organic modifier (isopropyl alcohol), ammonia and CTAB added. The most effective packing appeared to occur with pure acetonitrile or pure methanol. The columns appeared to pack with these two, using 5μm Hypersil, but there were a lot of problems. In some cases, the column would appear to be packing well, but would then start to dry out at some stage. It was impossible to prevent this, even by applying a positive pressure to the slurry reservoir in addition to the high voltage. Eventually, some packed columns were obtained which under the microscope appeared well packed. On application of up to 6,000 p.s.i. to the columns, the packing material invariable compressed by up to 5 cm. Observing the columns under the microscope while packing, a packed portion would appear to be static. On observation for a few minutes, the particles in this region would start to move, until eventually all the particles were moving towards the cathode at the wall and towards the anode in the centre. Further observation of this portion would see the disturbance move up or down the column and the region become still again.

It was never possible to obtain a densely packed capillary without drying out occurring. The reason for this is similar to that used in explaining the movement of voids in slurry packed capillaries. The slurry is moving at the electro-osmotic flow rate of the open tube. When it meets the plug or a packed portion the overall volume flow rate is much reduced and so a reverse or return flow is inevitable.

Depending on the relative flow in the packed and open (or unpacked) portions and on the density of the slurry, some packing may, and does, occur. Complicating this is the fact that once the particles are no longer under the influence of a strong electro-osmotic flow, they have a tendency to move in the opposite direction due to their electrophoretic attraction for the anode (or repulsion from the anode). This tends to enforce the 'unpacking' or loose packing, and prevents good or dense packing of the capillary.

5.4 Conclusions on electrochromatography

In common with Jorgenson and Lukacs [18], this technique was found to be difficult. Columns produced were no improvement on those produced or run under pressure driven flow and rarely achieved the performance of those reported by Grant. On the odd occasion when a low reduced plate height was achieved, it was never reproducible. While electrochromatography undoubtedly presents great advantages for the chromatographer over microbore LC and HPLC, the disadvantages of the high pressures required to pack small particles into columns, which has prevented their use in HPLC, may be the obstacle preventing successful packing of these columns for use in electrochromatography. While packing these columns electrokinetically appeared to present the solution to this, successful results were not achieved. Further research obviously needs to be done on this technique.

Chapter 6

Temperature in CZE (1)

6.1 Introduction

Theory predicts (chapter 3) that both the velocity of the solute, whether charged or uncharged, and the number of plates generated should be directly proportional to the magnitude of the applied voltage. Figure 6.1 is a plot of the electro-osmotic flow velocity u_{eo} against the applied field E for four different buffer concentrations of $Na_2B_4O_7$ under otherwise identical conditions, with the system operated at ambient temperature (20 °C) with no cooling. Figure 6.1 illustrates that while u_{eo} versus E is linear for the lowest concentration of buffer used (0.004 M), the remaining plots are distinctly curved with the degree of curvature increasing as the concentration of buffer is increased. With low potentials applied, the electro-osmotic velocity at a given voltage decreases as the buffer concentration increases. This is to be expected from double layer theory as the thickness of the double layer δ, and therefore the ζ potential, decreases with concentration of the buffer.

Figure 6.2 plots the electro-osmotic flow velocity against the applied field for four column diameters with 0.02 M $Na_2B_4O_7$ buffer with all other conditions

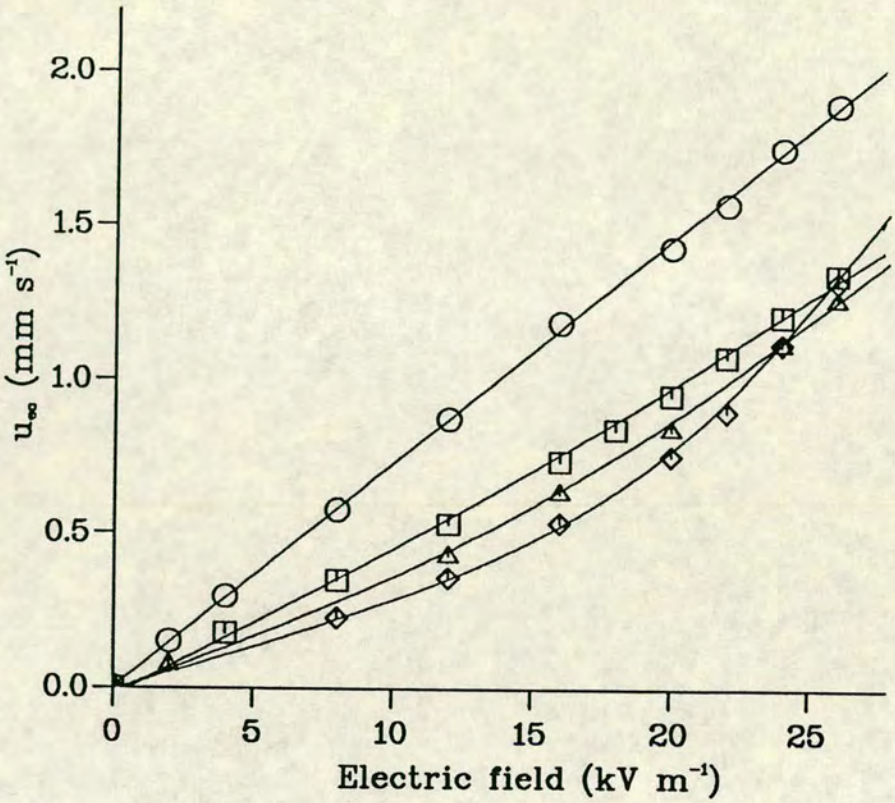

Figure 6.1. u_{eo} vs E as buffer concentration is varied. Column 50 μm i.d.. Buffer $Na_2B_4O_7$: o 0.004 M, □ 0.02 M, △ 0.05 M, ◇ 0.083 M

identical to those for figure 6.1. Figure 6.2 illustrates that the effect of column diameter on the velocity is similar to the effect of buffer concentration i.e. the plots show distinct curvature and the degree of curvature increases with column diameter. The plots suggest that the larger the diameter, the greater the velocity. This is in contrast to theory which suggests that the velocity should be independent of column diameter.

Figures 6.3 and 6.4 show the effect of buffer concentration and diameter on the relationship of N and u_{eo}. Figures 6.5 and 6.6 show plots of the velocity and plate number for a charged compound (dns-leucine) under identical conditions.

The plots are reasonably linear at the lower potentials but level off at the

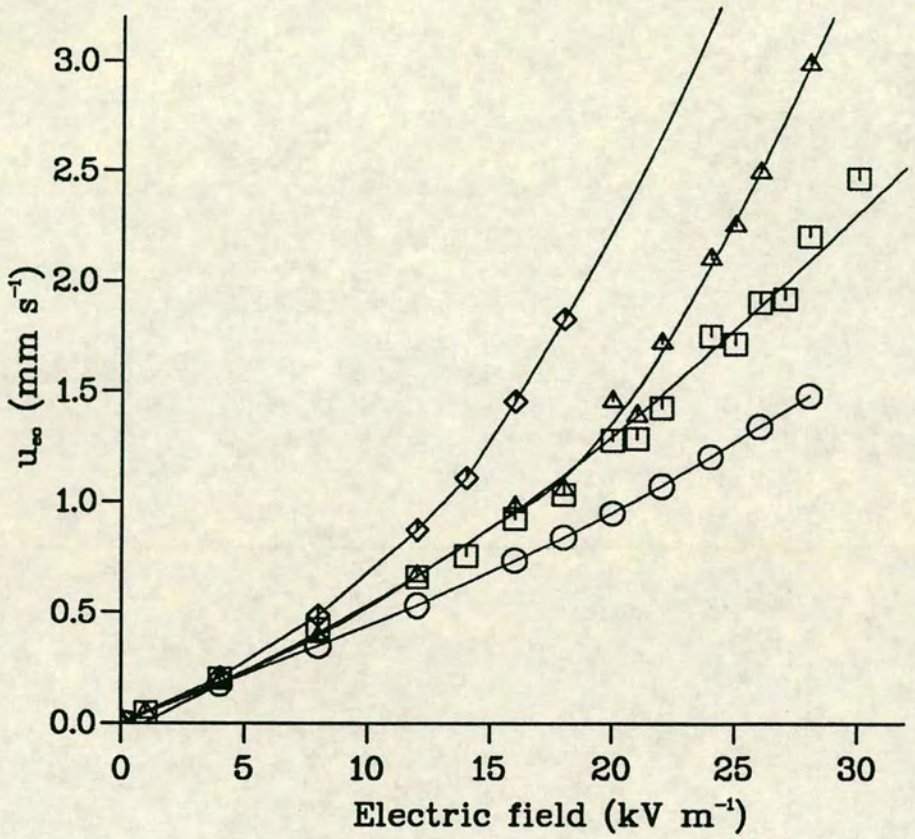

Figure 6.2. u_{eo} vs E as column diameter is varied. Buffer 0.02 M $Na_2B_4O_7$. Column diameters: o 50 μm, □ 75 μm, △ 100 μm, ◇ 150 μm

higher potentials. Levelling off of the plots occurs at lower voltages as the buffer concentration and column diameter are increased. Similar effects are observed for both charged and uncharged solutes.

Linearity of current and applied potential is expected from Ohm's Law:

$$I = \pi r^2 k_e E \tag{6.1}$$

where r is the capillary radius and k_e the conductance of the buffer. Since

$$k_e = \lambda c \tag{6.2}$$

where λ and c are the molar conductivity and concentration of the buffer respectively, the conductance and therefore the current, are directly dependent on the

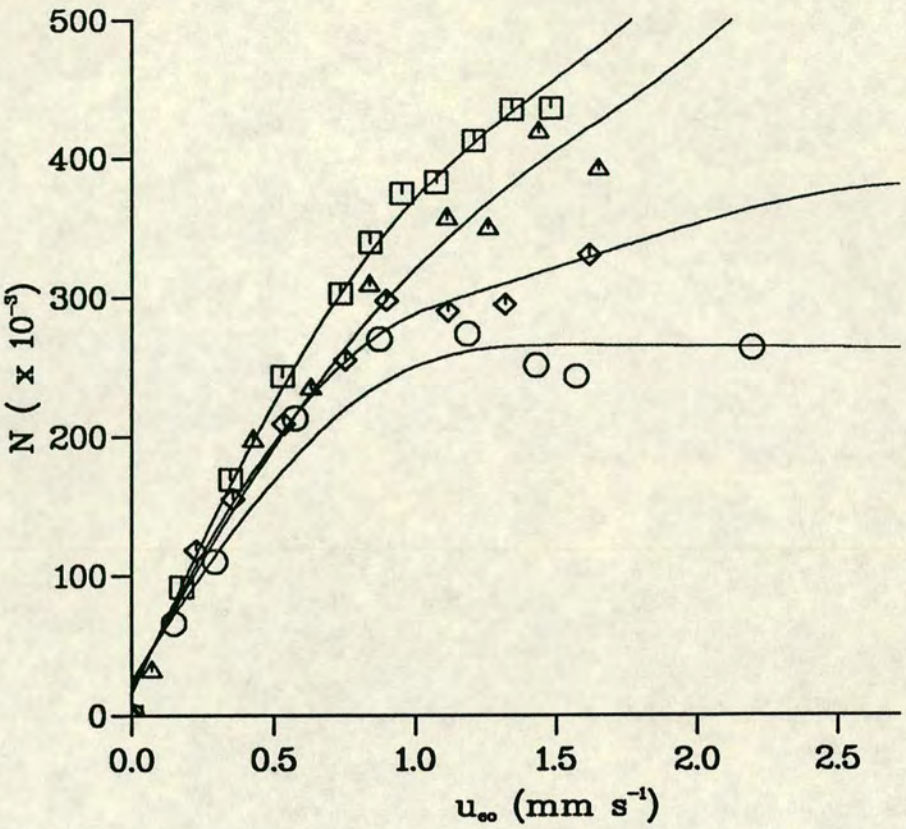

Figure 6.3. Effect of buffer concentration on N vs u_{eo}. Column 50 μm i.d.. Buffer $Na_2B_4O_7$: o 0.004 M, □ 0.02 M, △ 0.05 M, ◇ 0.083 M

buffer concentration. While it would be more correct to plot I/c against E when considering the effect of buffer concentration, the data points all lie in the same region, and curvature of the individual plots is difficult to visualise. Similarily, as the current is directly proportional to r^2, it would be more correct to plot $I/\pi r^2$ against E when considering the effects of column diameter. For visualisation purposes and since it is the linearity or relative curvature of the plot that is of interest, the current and not the current density has always been plotted.

The effect of buffer concentration and column diameter on the linearity of current against applied voltage is illustrated in figures 6.7 and 6.8 respectively. As before, linearity is achieved at the lowest buffer concentration and column

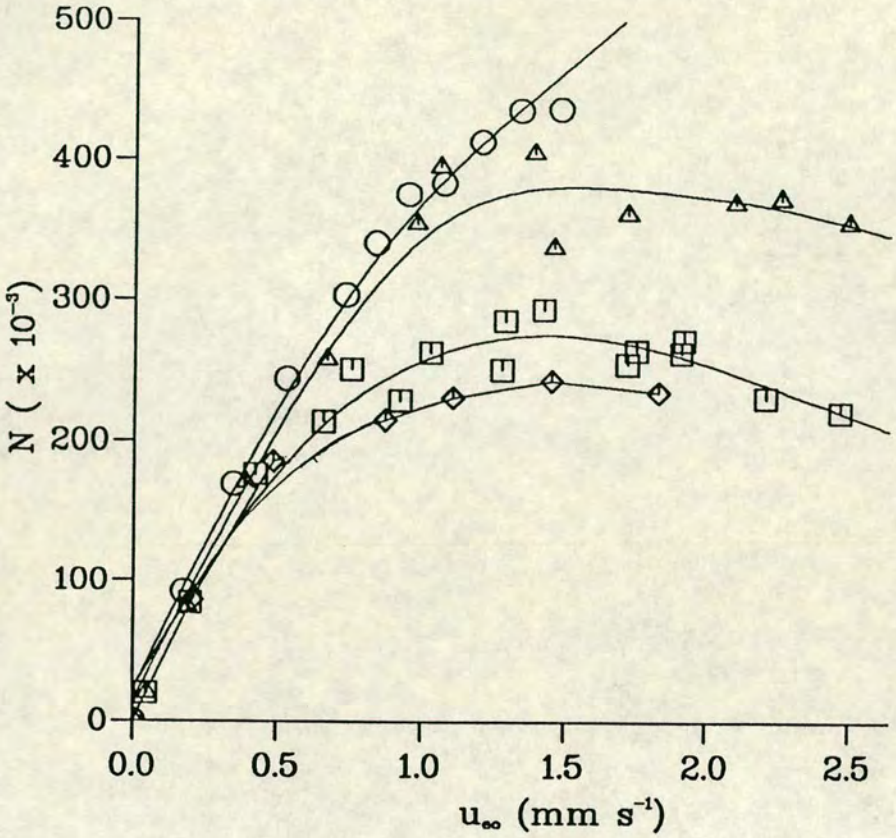

Figure 6.4. Effect of column diameter on N vs u_{eo}. Buffer 0.02 M $Na_2B_4O_7$. Column diameter: o 50 μm, □ 75 μm, △ 100 μm, ◇ 150 μm

diameter with the deviation from linearity increasing with both concentration of buffer and column diameter.

The preceding figures have shown that the original equations predicting velocities and performance in capillary electrophoresis are good for a limited number of cases. Previous researchers [15] have attributed any deviation from theory in experimental results to Joule heating. Knox and Grant [4] have calculated that it should be possible to use capillaries up to 200 μm i.d. with up to 50 kV m^{-1} applied with buffer concentrations up to 0.01 M before any noticeable loss in efficiency would occur. It is obvious from the results just presented that this is an over optimistic calculation. Care was taken in all these experiments to

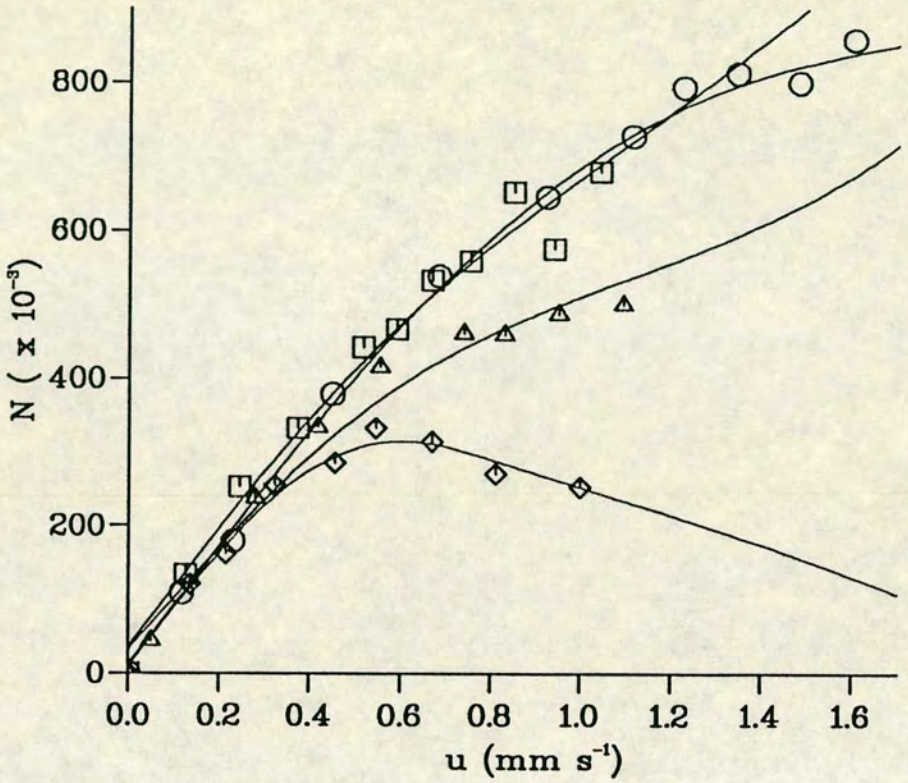

Figure 6.5. Effect of buffer concentration on N vs u for a charged compound (dns-leucine). Column 50 μm i.d.. Buffer $Na_2B_4O_7$: o 0.004 M, □ 0.02 M, △ 0.05 M, ◇ 0.083 M

limit the band broadening due to all sources discussed in chapter 3. It is therefore apparent that some other factor, not previously considered by investigators, is responsible for the excessive band broadening observed.

The power dissipated in the system can be quite high—up to 3 W m^{-1} in these experiments. As a result, it is expected that there would be a corresponding temperature rise in the capillary. The deviation of current and electro-osmotic velocities from linearity with the applied voltage has been explained as a result of heating in the system [131]. To date however, no satisfactory explanation for the levelling off of the number of plates achieved has been proposed. It would

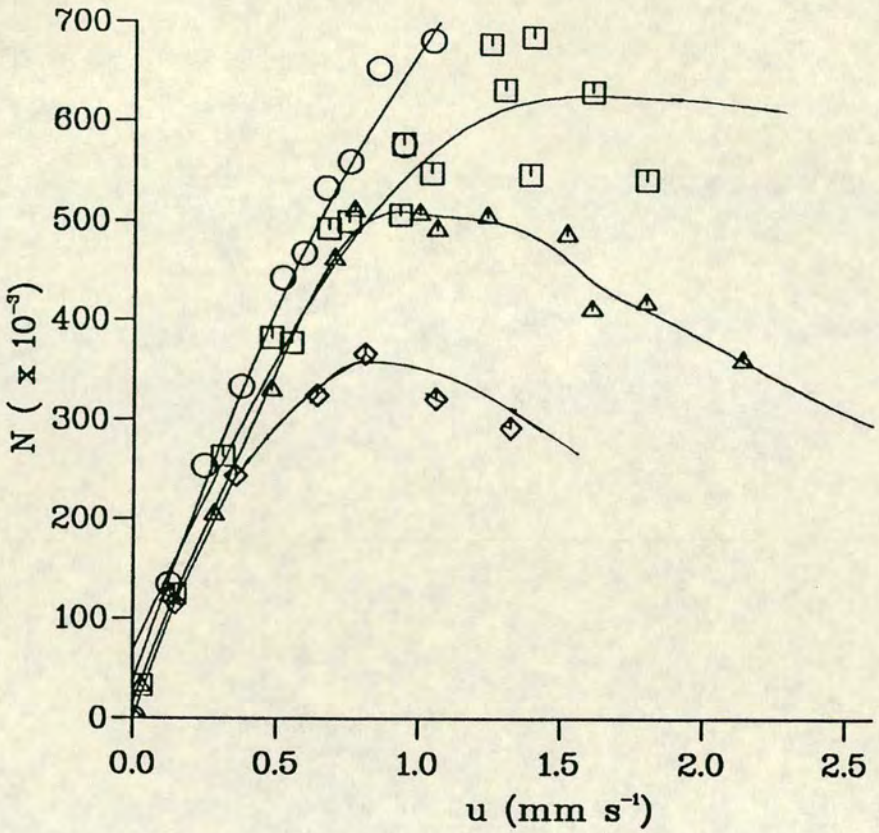

Figure 6.6. Effect of column diameter on N vs u for a charged compound (dns-leucine). Buffer 0.02 M $Na_2B_4O_7$. Column diameter: o 50 μm, □ 75 μm, △ 100 μm, ◇ 150 μm.

seem reasonable to assume that the extra band broadening observed is also an artifact of the increased temperature in the capillary. The actual temperature in the capillary has been briefly mentioned by some investigators [131] but to date no thorough investigation of the actual temperature rise and its effects on the retention times and performance of capillary electrophoresis has been done. The remainder of this thesis is therefore dedicated to means of measuring the capillary temperature, predicting the effect of temperature on the parameters associated with the technique viz. retention times, currents, number of plates achieved, and proposing methods for prevention of excessive temperature rises.

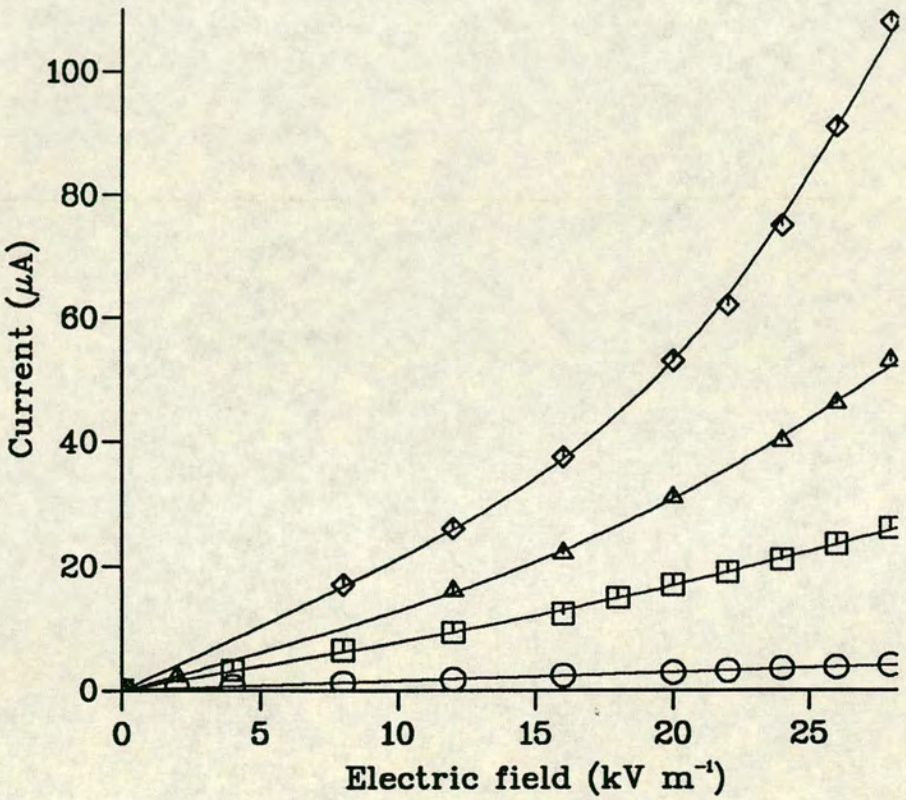

Figure 6.7. Effect of buffer concentration on the linearity of I vs E. Column 50 μm i.d.. Buffer $Na_2B_4O_7$: ○ 0.004 M, □ 0.02 M, △ 0.05 M, ◇ 0.083 M

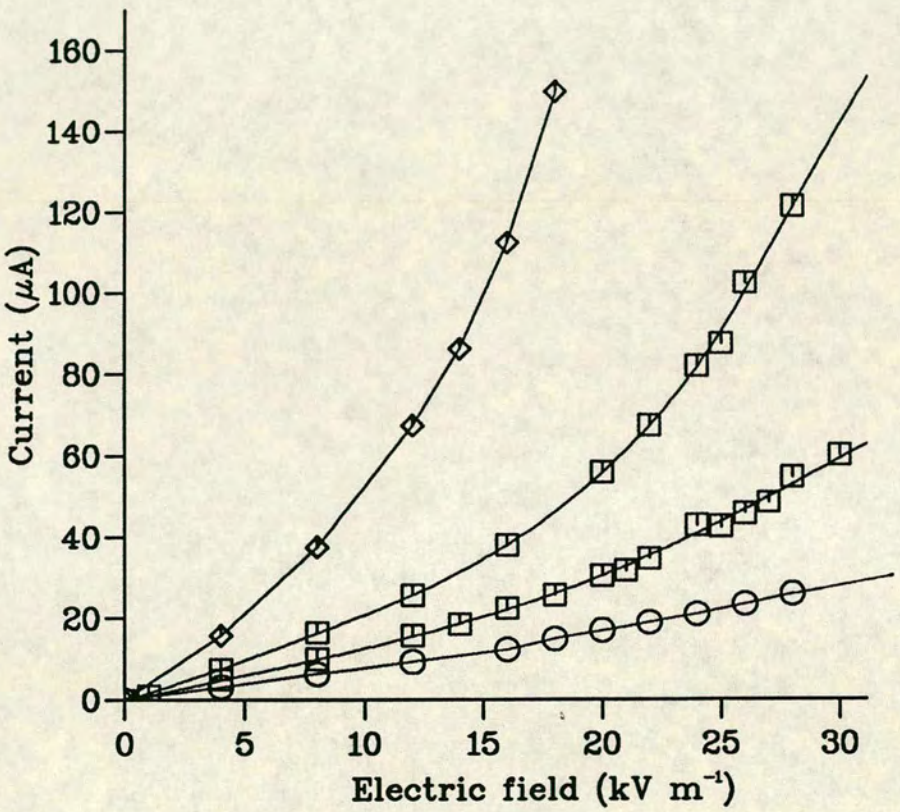

Figure 6.8. Effect of column diameter on the linearity of I vs E. Buffer $Na_2B_4O_7$. Column diameter: o 50 μm, □ 75 μm, △ 100 μm, ◇ 150 μm.

6.2 Temperature dependence of variables in CZE

Assuming that an increase in the temperature of the buffer within the capillary occurs, the temperature dependence of the parameters associated with the basic equations for capillary electrophoresis must be understood. A proper understanding of the temperature dependence of these parameters, namely the viscosity and the dielectric constant of the solutions, and indirectly their effect on the diffusion coefficient and the ζ potential may explain many of the effects observed.

6.2.1 Viscosity

The viscosity of electrolyte solutions in capillary electrophoresis have been assumed to be identical with that of the solvent which is usually water. In fact, the relative viscosity of an electrolyte solution η is given by the Jones-Dole equation [122] as

$$\eta/\eta_o = 1 + A\sqrt{c} + Bc \tag{6.3}$$

where η_o is the viscosity of the solvent at a given temperature and pressure, c is the electrolyte concentration and A and B are constants. The $A\sqrt{c}$ term was first described by Gruneisen and is attributed to long range electrostatic forces between the ions as those in one layer move in shear past those in adjacent layers. The Gruneisen effect occurs in very dilute solutions, up to 0.002 M. Above this concentration a linear variation of viscosity with concentration is noticeable with strong electrolytes, extending to 0.1 M in aqueous solutions. B coefficients can be positive or negative and are generally accepted to be a result of ion-solvent interaction [123, 124]. For some solutions with a predominant negative B term, the viscosity of the solution at moderate concentrations can be less than that

of water e.g. KCl and some of the higher alkali halide salts. B coefficients are temperature dependent, with small or negative B values increasing with temperature, sometimes to positive values, and larger values of B increasing more slowly with temperature. The division of B values into individual ionic contributions has been done [124]. In general, within a group in the periodic table, the smallest ions increase the viscosity the most. The higher the charge on an ion, the greater the B value. Large molecular ions, such as tetra-alkyl ammonium ions, have large B values. A is of the order of 0.01 or less, and B can vary from 0.23 to 0.03 for sodium salts at room temperature. The concentration of buffers used in the experiments never exceeded 0.1 M. Taking a maximum value of A of 0.01 and for B of 0.23, $\eta/\eta_o = 1.026$. It can be assumed that A and B values for the electrolytes used in CZE are lower than than these values, and so the viscosity of the electrolyte solution is less than 2.6% greater than that of the pure solvent. This is a relatively small effect and will be neglected in the following work, in which the viscosity of the buffer solution is taken to be equivalent to that of water.

The viscosity of water is known to decrease with temperature [125]. The dependence of the viscosity on temperature in the temperature range 20–100 °C is given by the following empirical equation.

$$\log_{10} \frac{\eta_T}{\eta_{20}} = \frac{1.3272(20 - T) - 0.001053(T - 20)^2}{T + 105} \tag{6.4}$$

with T in degrees Centigrade.

This is the equation used by Davis [111] in his calculation of thermal effects in CZE. For calculation purposes the simpler Andrade equation can be used

$$\eta_T = A \exp(B/T) \tag{6.5}$$

where A and B are constants.

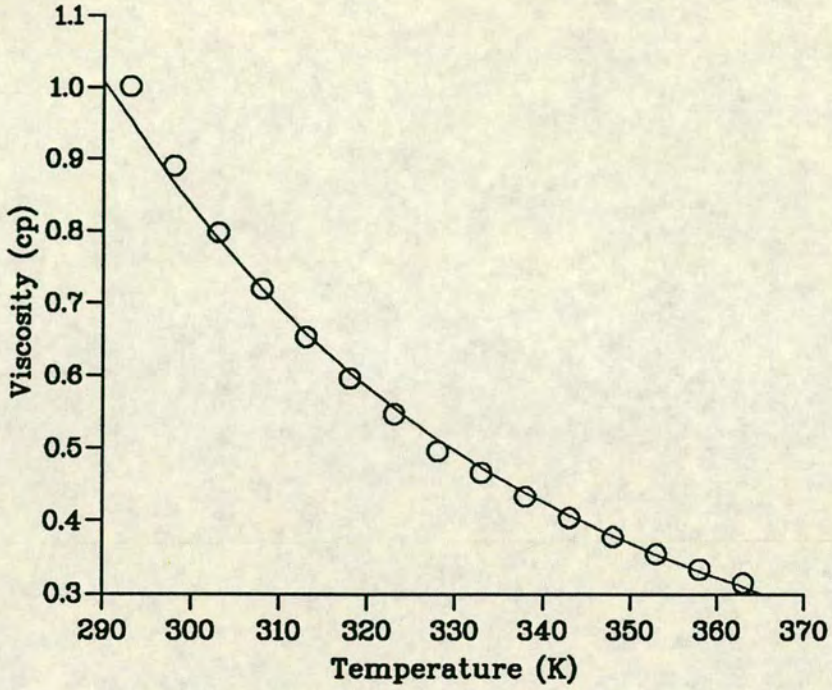

Figure 6.9. Variation of viscosity of water with temperature. o data from reference [125]. Line is a fit of equation 6.6.

The data given for the variation of η with T between 20 °C and 100 °C has been fitted to an Andrade type equation, and found to fit the following

$$\eta_T = 2.761 \times 10^{-6} \exp(1713/T) \tag{6.6}$$

with η_T in kg $m^{-1}s^{-1}$ and T in K.

Figure 6.9 is a plot of viscosity against temperature for a variety of temperatures, and the curve given by equation 6.6. Good agreement is obvious with a maximum error of 2.1% when calculating a viscosity from a temperature above 27 °C.

Alternatively T can be expressed in terms of η to allow calculation of a temperature from a known viscosity, using the following cubic equation

$$T = -251\eta^3 + 624\eta^2 - 570\eta + 215 \tag{6.7}$$

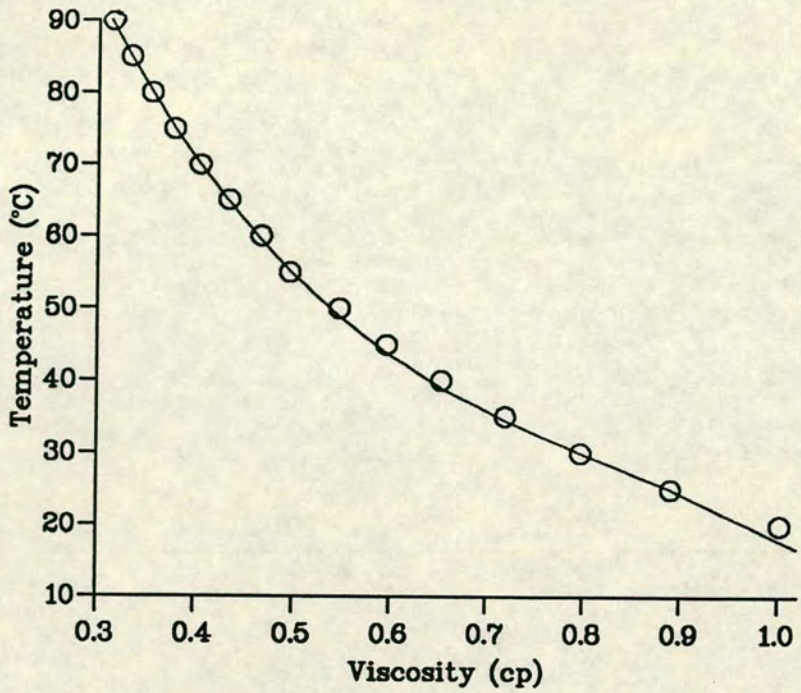

Figure 6.10. Variation of temperature with viscosity of water. o data from reference [125]. Curve is a fit of equation 6.7.

with T in degrees Centigrade and η in cp. Figure 6.10 is a plot of T against η with the curve given by equation 6.7 plotted. Errors in calculated temperature values are less than 1% when T is greater than 23 °C.

6.2.2 Dielectric constant

The dielectric constant or relative permittivity (ϵ_r) of the buffer solution used is taken to be that of the solvent, generally water. The dielectric constant of water is 80.18 at 20 °C and decreases with temperature in an exponential fashion [122].

$$\epsilon_r = 305.7 \exp(-T/219) \tag{6.8}$$

with T in K. Figure 6.11 illustrates the variation of the dielectric constant with temperature with equation 6.8 fitted to the data.

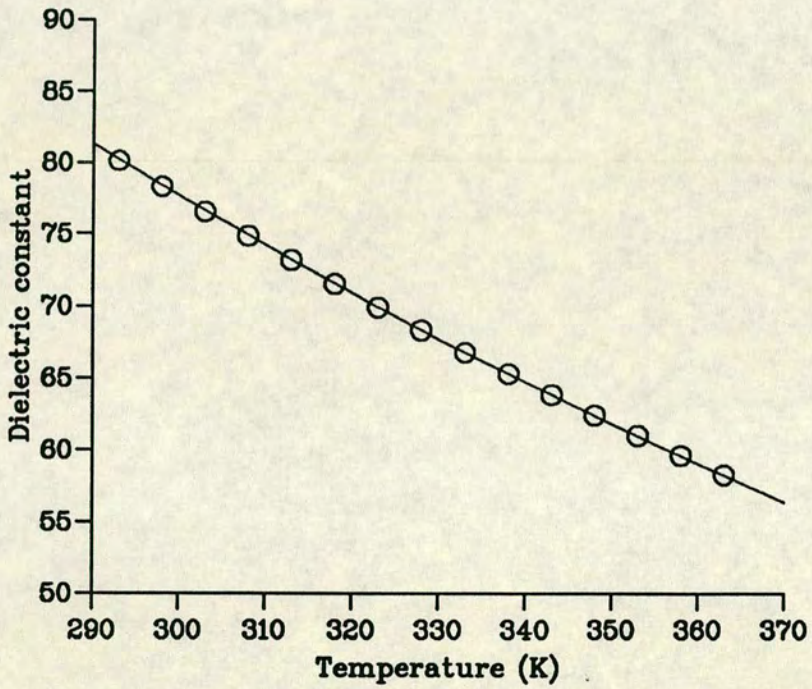

Figure 6.11. Variation of dielectric constant of water with temperature. o data from reference [125]. Curve is a fit of equation 6.8.

6.2.3 Electrical Conductivity

When a potential gradient is applied across a buffer solution a current flows. The magnitude of the current is given by

$$I = k_e A E \tag{6.9}$$

where A is the cross sectional area and k_e is given by equation 6.2.

From the Kohlrausch law of independent migration of ions, the equivalent conductance can be expressed as

$$\lambda = \lambda_+ + \lambda_- \tag{6.10}$$

Combining equations 6.2 and 6.10 and summing for all ions in solution

$$k_e = \sum_j c_j \lambda_j \tag{6.11}$$

Since

$$\mu_j = \lambda_j / F \tag{6.12}$$

where μ_j is the electrophoretic mobility of the ion j in the field, then

$$k_e = F \sum c_j \mu_j \tag{6.13}$$

Considering a cylindrical capillary of radius r, the current flowing in the system becomes

$$I = \pi r^2 E F \sum_j c_j \mid \mu_j \mid \tag{6.14}$$

The ion mobility can be re-written as follows:

$$\mu_j = z_j e / 6\pi a_j \eta \tag{6.15}$$

Substituting into equations 6.13 and 6.14

$$k_e = \frac{F}{\eta} \sum_j c_j \mid \frac{z_j e}{6\pi a_j} \mid \tag{6.16}$$

$$I = \frac{\pi r^2 E F}{\eta} \sum_j c_j \mid \frac{z_j e}{6\pi a_j} \mid \tag{6.17}$$

T °C	$1/\eta$ m s kg^{-1}	k_e / Ω^{-1}m^{-1}						
		Na_2HPO_4 /M				$Na_2B_4O_7$ /M		
		0.02	0.04	0.06	0.08	0.02	0.051	0.08
18.5	961.5	0.320	0.597	0.814	1.049	0.153	0.353	0.557
25.2	1128.1	0.367	0.676	0.949	1.220	0.177	0.415	0.630
30.8	1273.9	0.406	0.751	1.064	1.370	0.190	0.465	0.709
36.5	1431.9	0.456	0.847	1.190	1.544	0.212	0.510	0.796
42.0	1589.6	0.490	0.931	1.310	1.701	0.239	0.556	0.877
47.0	1737.6	0.505	0.998	1.409	1.803	0.246	0.601	0.949
53.0	1921.6	0.586	1.106	1.568	-	0.270	0.655	1.046
59.0	2111.5	0.613	1.184	1.707	-	0.300	0.721	1.142
70.3	2484.2	0.715	1.376	-	-	0.358	0.847	1.337
76.2	2686.4	0.793	1.532	-	-	0.378	0.895	1.472

Table 6.1. Variation of electrical conductivity with temperature.

From equation 6.16, $k_e \propto 1/\eta$ and so $k_e\eta = F\sum_j c_j \mid z_j e/6\pi a_j \mid$ = constant. The electrical (specific) conductance of some of the buffers used in the capillary electrophoresis experiments were measured according to the method in chapter 4 at a variety of temperatures along with the reciprocal of the viscosity. The data is presented in table 6.1. Figure 6.12 illustrates the linearity of k_e against $1/\eta$ for the $Na_2B_4O_7$ buffer solutions used. Substituting equation 6.17 for the current into the equation for the electro-osmotic flow velocity, the following is obtained

$$u_{eo} = \frac{\epsilon_o \epsilon_r \zeta}{\pi r^2 F} \frac{I}{\sum c_j \mid z_j e/6\pi a_j \mid} \tag{6.18}$$

Figures 6.13 and 6.14 are plots of the current against the electro-osmotic velocity for a variety of buffer concentrations and column diameters. The linearity of each is immediately evident. From the above equation in which the only temperature dependent factors expected are ϵ_r and ζ, it is apparent that the product of these factors must be constant at any temperature and, since ϵ_r decreases with temperature, ζ must proportionately increase with temperature.

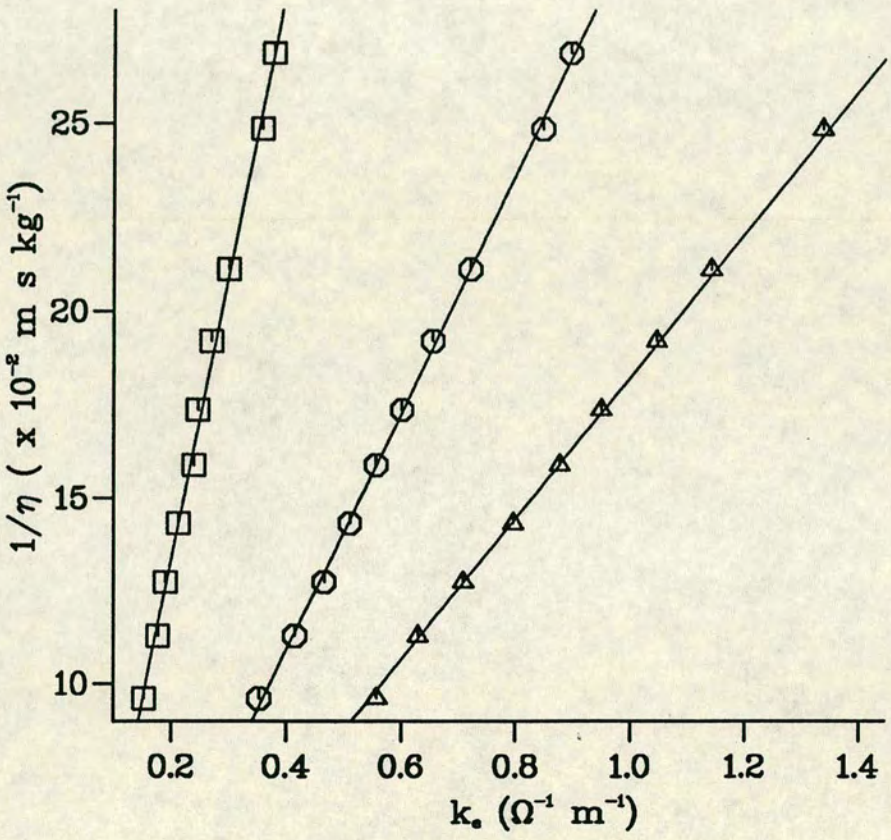

Figure 6.12. Linearity of electrical conductance with reciprocal of viscosity. Buffer $Na_2B_4O_7$: □ 0.02 M, o 0.051 M, △ 0.08 M.

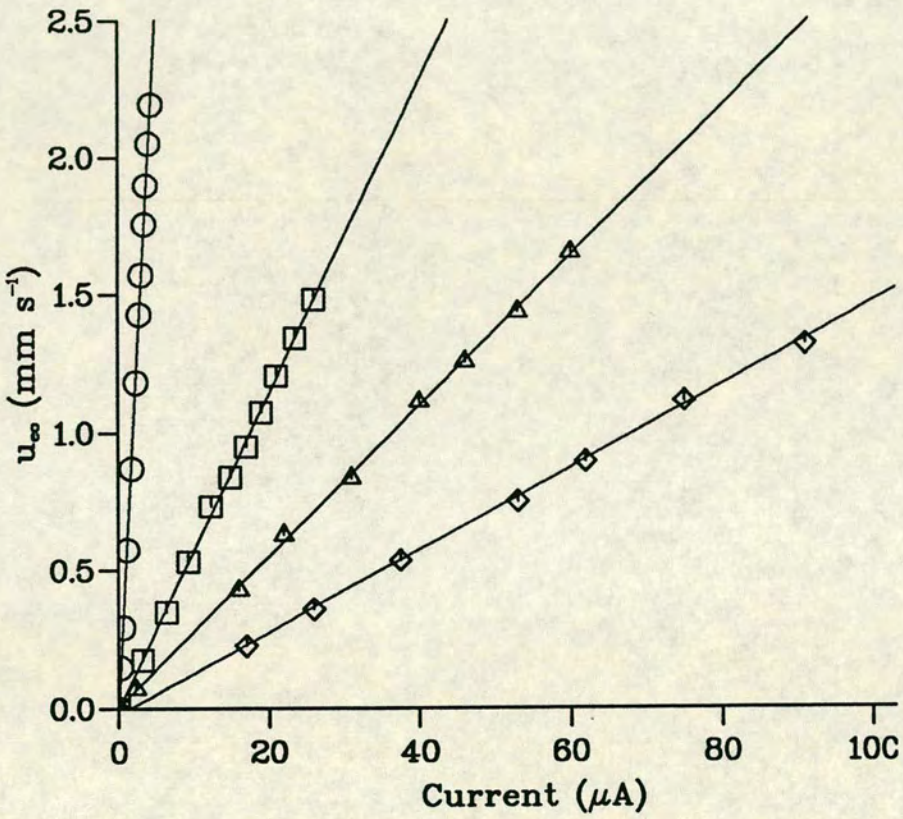

Figure 6.13. Effect of buffer concentration on I vs u_{eo}. Column 50 μm i.d.. Buffer $Na_2B_4O_7$: ○ 0.004 M, □ 0.05 M, △ 0.05 M, ◇ 0.083 M.

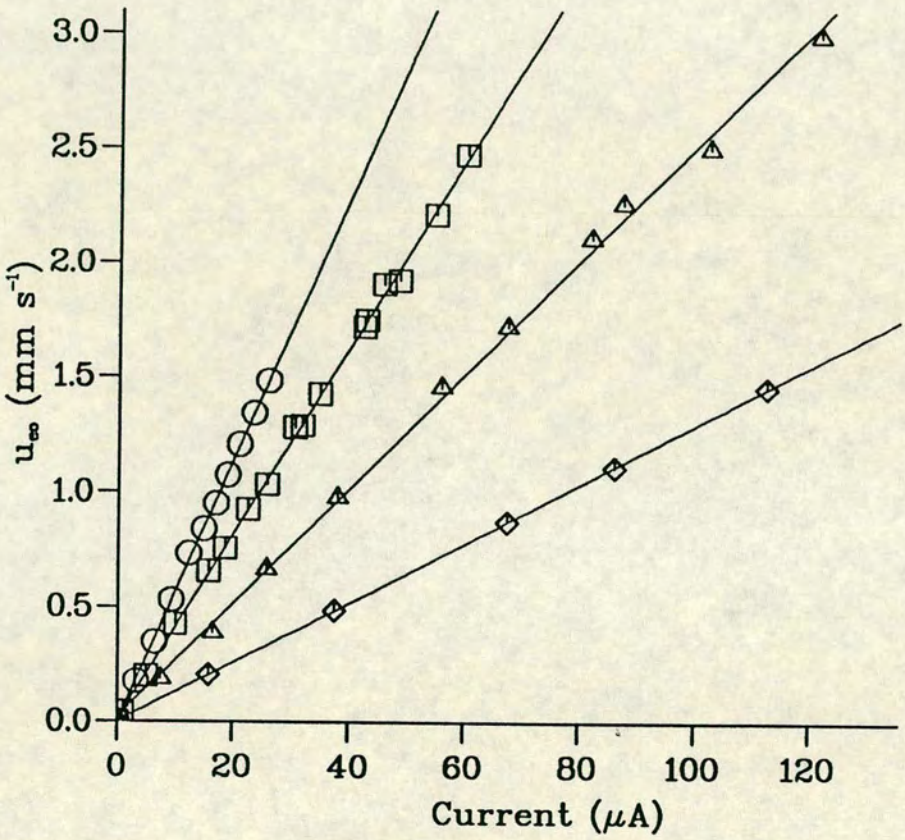

Figure 6.14. Effect of column diameter on I vs u_{eo}. Bufer 0.02 M $Na_2B_4O_7$. Column diameter: o 50 μm, □ 75 μm, △ 100 μm, ◇ 150 μm.

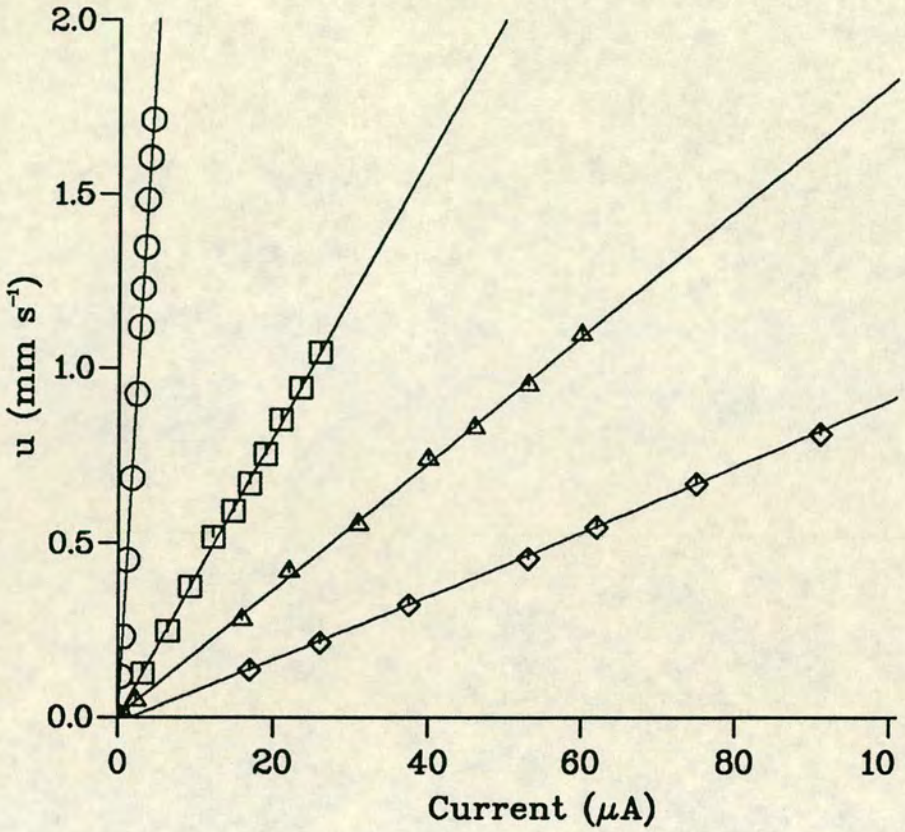

Figure 6.15. Effect of buffer concentration on I vs u for a charged solute (dns-leucine). Column 50 μm i.d.. Buffer $Na_2B_4O_7$: o 0.004 M, □ 0.05 M, △ 0.05 M, ◇ 0.083 M.

In a similar manner, the equations relating the velocity of charged solutes with current becomes

$$u = \frac{\frac{z_s e}{6\pi a_s} + \epsilon_o \epsilon_r \zeta}{\pi r^2 F} \frac{I}{\sum c_j \mid z_j e / 6\pi a_j \mid} \tag{6.19}$$

where s refers to the solute molecule or ion and j refers to the buffer ion and so the velocity of a charged soluted in CZE is linear with the measured current, shown for a charged solute (dns-leucine) in figures 6.15 and 6.16.

The proven linearity of current with velocities, and thus the inverse proportional relationship of retention times with current, suggest that the use of current instead of the applied voltage most commonly used is of greater use in CZE in

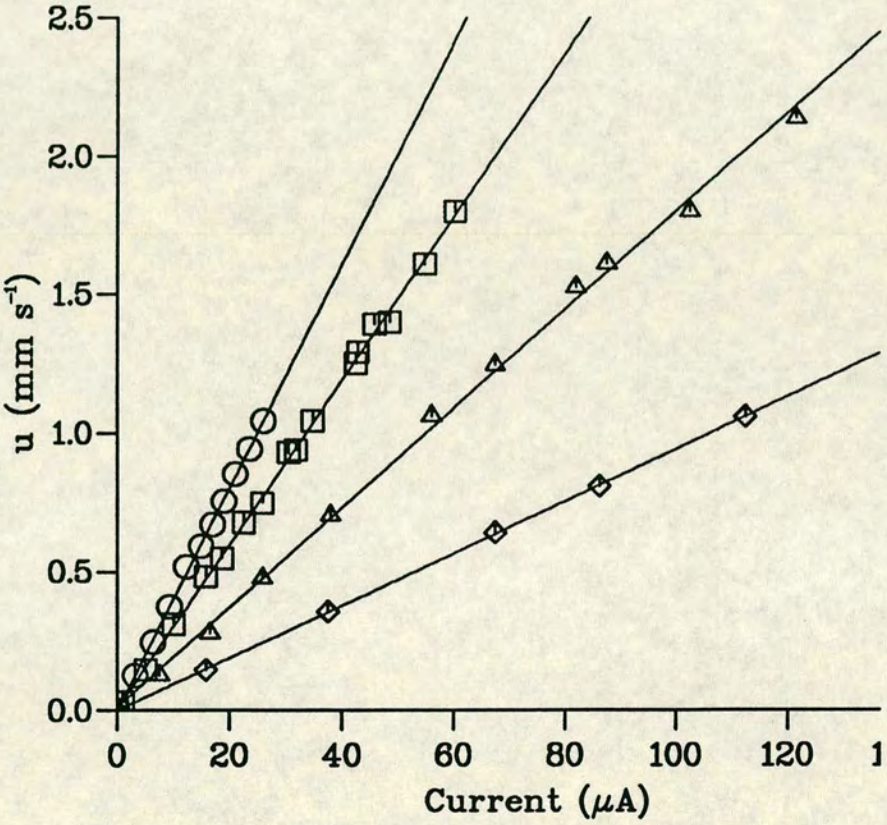

Figure 6.16. Effect of column diameter on I vs u for a charged solute (dns-leucine). Buffer 0.02 M $Na_2B_4O_7$. Column diameter: o 50 μm, □ 75 μm, △ 100 μm, ◇ 150 μ.

the prediction of retention times and velocities of samples from run to run. The conductivity measured in the system from consideration of the applied electric field and the measured current was always greater than the measured values in table 6.1. No satisfactory explanation for this has yet been found.

6.2.4 The zeta potential and surface charge

In chapter 2, equations relating the zeta potential ζ and the charge density at the OHP σ_o were given for a dilute solution as (equation 2.17)

$$\zeta = \sigma_o / \epsilon_o \epsilon_r \kappa$$

By substituting for the reciprocal double layer thickness κ from equation 2.11 and rearranging

$$\epsilon_r \zeta = \frac{\sigma_o}{\epsilon_o} \left(\frac{\epsilon_o \epsilon_r kT}{2e^2 N_A c z^2} \right)^{1/2} \tag{6.20}$$

The left hand side of the equation has already been proved to be constant. The magnitude of $(\epsilon_r T)^{1/2}$ decreases by about 5% as the temperature increases from 20 °C to 90 °C and so the charge density at the OHP must increase slightly with temperature, all other variables being assumed constant.

6.2.5 The Diffusion Coefficient

The diffusion coefficient has been previously mentioned in chapter 3 in which axial or longitudinal diffusion has been one of the principle causes of dispersion in CZE systems and is therefore dependent on the magnitude of the diffusion coefficient.

The diffusion coefficient is the constant D in Fick's first law of diffusion

$$J = -D dc/dx \tag{6.21}$$

which applies in any medium and where J is the molal flux of the species, c the concentration of the diffusing species and x the distance in the direction of diffusion. D is largest for small molecules and decreases with size, being typically of the order of 10^{-9}–10^{-10} m^2s^{-1} for diffusion in liquids. There are many theoretical equations which aim to predict the diffusion coefficient of a solute in a given solvent, taking into account the properties of both solute and solvent. One of the simplest is the Stokes equation

$$D = \frac{kT}{6\pi\eta a_s} \tag{6.22}$$

in which a_s is the radius of the diffusing molecule which is assumed to be spherical.

The Wilke-Chang equation was proposed in 1955 [126] for low solute concentrations in which D was given by

$$D = 7.4 \times 10^8 \left(\frac{(\phi M_2)^{1/2} T}{V_1^{0.6} \eta} \right) \tag{6.23}$$

in which ϕ is an association parameter of the solvent and has a value of 2.6 for water, 1.9 for methanol and ethanol and 1 for benzene and other unassociated solvents. M_2 is the molecular weight of the solvent and V_1 the molal volume of the solute at the normal boiling point. All parameters are in S.I. units.

These two equations are the most common that are used in practice. Many more have however been proposed. The Scheibel equation [127] is

$$D = \frac{KT}{V_1^{1/3} \eta} \tag{6.24}$$

where $K = 8.2 \times 10^{-8}(1 + (3V_2/V_1)^{2/3})$ and $K = 25.2 \times 10^{-8}$ if $V_1 < V_2$ and V_1, V_2 are the molecular volumes of the solute and solvent respectively.

The three preceding equations suggest that D is proportional to T/η. Innes and Albright [128] state in their paper that the above equation is only approximately correct and that the function $D \propto T/\eta$ is too sharp. They recommend

use of the empirical Othmer-Thaker equation [129] which for aqueous solutions reduces to

$$D = \frac{14.0 \times 10^{-5}}{\eta^{1.1} V_1^{0.6}} \tag{6.25}$$

with η in cp. This equation is said to agree with a large amount of data with an average deviation of 5%.

Longsworth [130] investigated the temperature dependence of diffusion between 1°C and 37°C of a variety of samples whose molecular weights ranged from 19 to 68,000. From the experimental diffusion coefficients he calculated the Stokes radius for each molecule from the Stokes equation. The Stokes radius was found to increase with temperature for the smallest molecule (HDO) and decrease with temperature for the largest ones (proteins). For alanine (MW = 89) the Stokes radius was constant with temperature. These results confirmed an earlier observation by Oholm in 1913 that the temperature coefficient of diffusion increased with the size of the diffusing particle. From Longsworth's results, it is apparent that the temperature variation of D for molecules with molecular weights of the same order of magnitude as alanine depends on T/η. The samples used in this study had molecular weights ranging from 90 to 400 and so the temperature dependence is taken to be the same as for the Stoke and Wilke-Chang equations i. e. $D \propto T/\eta$.

The diffusion coefficient of a typical sample used in these studies, 2-naphthalene sulphonic acid (MW = 208.25), was measured by the method described in chapter 4, at temperatures between 20 °C and 60 °C. The values obtained along with the temperature and the viscosity of the solution is presented in table 6.2. Each D value is calculated from the gradient of a plot of σ^2 vs t for 10 or more data points. Combining the Stokes equation 6.22 and equation 6.6 for the viscosity of water with temperature and inserting values for the constants, which

T °C	D $10^{-10}m^2s^{-1}$	η cp
20	8.22	1.002
30	9.43	0.7975
40	10.63	0.6529
45	12.59	0.5960
50	14.47	0.5468
60	16.54	0.4665

Table 6.2. Measured diffusion coefficients of 2-naphthalene sulphonic acid at different temperatures

are all in S.I. units,

$$D = \frac{2.701 \times 10^{-19}}{a_s} T \exp(-1713/T) \tag{6.26}$$

The measured diffusion coefficients are plotted against $T\exp(-1713/T)$ in figure 6.17.

A least squares fit to the data gave a gradient for the line as 7.98×10^{-10} $m^2s^{-1}K^{-1}$, from which an effective radius for 2-naphthalene sulphonic acid can be calculated from equation 6.26 as $a_s = 3.38 \times 10^{-10}$ m.

6.3 Effect of temperature on CZE

The previous sections have illustrated the strong dependence of viscosity on temperature, and as a direct result of this dependence, both the electrical conductivity and the diffusion coefficient exhibit an equally strong dependence on the temperature. If equation 6.6 is substituted into the equation for electro-osmotic flow and equation 6.26 into the plate equation, the following equations are the

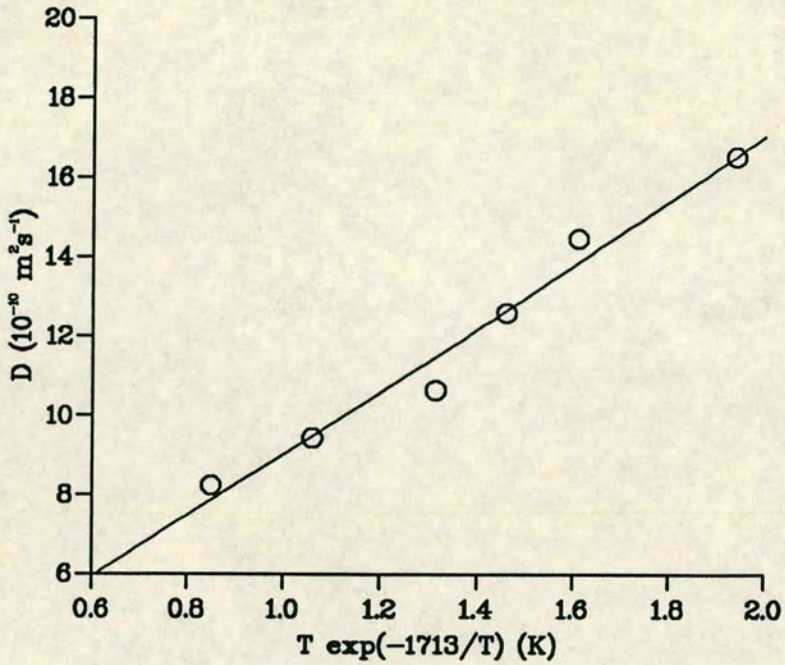

Figure 6.17. Diffusion coefficient of 2-naphthalene sulphonic acid as a function of temperature. o experimental data with least squares best fit line drawn through the data.

result

$$u_{eo} = 3.622 \times 10^5 \epsilon_o \epsilon_r \zeta E \exp(-1713/T) \tag{6.27}$$

$$N = 1.851 \times 10^{18} a_s u L \frac{\exp(1713/T)}{T} \tag{6.28}$$

Equation 6.27 explains the curvature of the plots of electro-osmotic velocity against the electric field. As the temperature increases the exponential term increases and so the velocity is greater than expected.

Ignoring the parabolic velocity gradients which may result from heating the increase in u_{eo} will not necessarily degrade the efficiency of the separation. In fact, increased electro-osmotic flow may be beneficial in certain analyses which may otherwise take a long time.

The temperature dependence of equation 6.28 is more serious. The number of plates that the separation is equivalent to is strongly dependent on the temperature. An increase in temperature of 35 °C from 20 °C to 55 °C at a constant velocity will give less than half the number of plates expected. The conclusion must be that to obtain the maximum or theoretical number of plates in CZE, the temperature rise in the capillary must be prevented or minimised.

6.4 Measurement of the average temperature in capillaries

The strong temperature dependence of viscosity and the effect on the electro-osmotic velocity, current and linear velocity of samples suggests three independent methods for calculating the temperatures in capillaries. As the temperature rise results in increased electro-osmotic velocities, buffer conductivity and electrophoretic mobilities, calculation of the relative increase in any of these parameters above the values at ambient temperatures will allow calculation of the capillary temperature. The three methods are outlined in the following sections. The calculated temperature will be an average of the temperatures at the wall and in the centre of the capillary.

6.4.1 Variation of u_{eo} with E

Rearranging the equation for electro-osmosis

$$\frac{u_{eo}}{E} = \frac{\epsilon_o \epsilon_r \zeta}{\eta} \tag{6.29}$$

Plotting u_{eo}/E against E will give a curve from which the value of $\epsilon_o \epsilon_r \zeta / \eta$ at ambient temperature can be calculated from the intercept. Knowing η and ϵ_r at

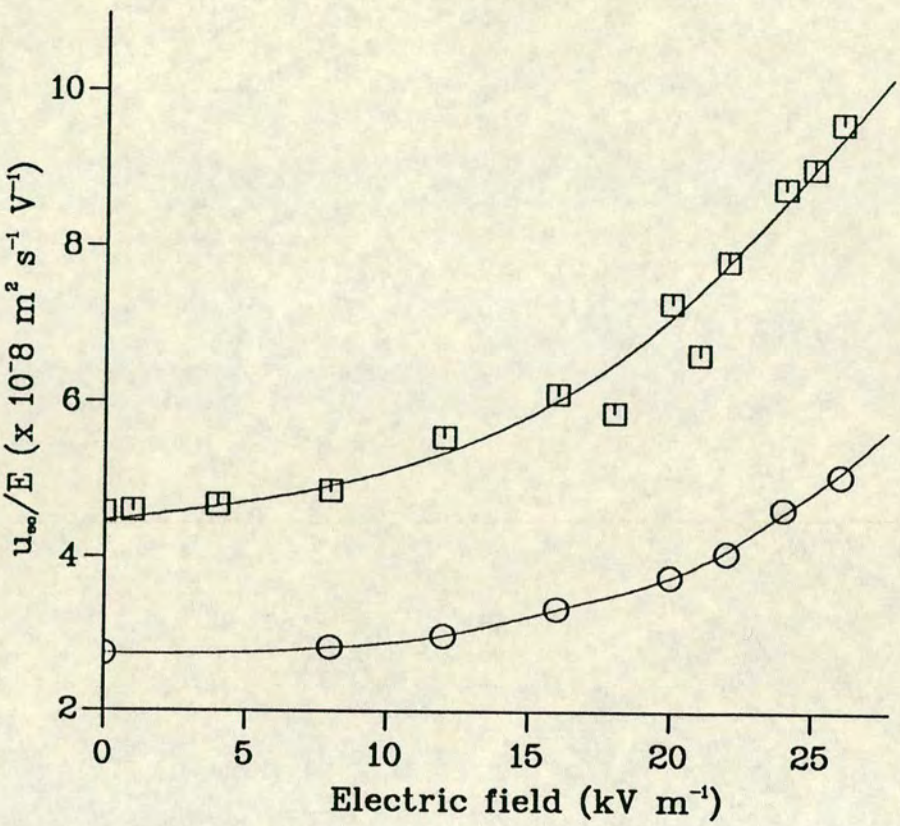

Figure 6.18. u_{eo}/E vs E for the calculation of column temperatures for 0.083 M $Na_2B_4O_7$ in a 50 μm capillary (o) and 0.02 M $Na_2B_4O_7$ in a 100 μm capillary (□).

this temperature allows calculation of ζ. The viscosity at any field strength can then be calculated from

$$\eta = \epsilon_o \epsilon_r \zeta E / u_{eo} \tag{6.30}$$

and the temperature in the capillary calculated from equation 6.7. u_{eo}/E was plotted against E for the seven systems studied. Figure 6.18 illustrates a typical plot for 0.083 M buffer in a 50 μm capillary and for 0.02 M buffer in a 100 μm capillary. Table 6.3 gives the resulting intercepts (as Intercept_1) from which ζ was calculated, along with the calculated values of ζ. Table 6.3 also gives the intercepts from the other two methods to be described. It is immediately

Buffer conc M	Column i.d. μm	Intercept$_1$ 10^{-8} m s^{-1}V^{-1}	ζ mV	Intercept$_2$ 10^{-10} A m V^{-1}	Intercept$_3$ 10^{-7} m^{2}s^{-1}V^{-1}	Intercept$_4$ 10^{-7} m^{2}s^{-1}V^{-1}
0.004	50	7.288	102.9	-	-	-
0.020	50	4.320	61.0	7.8	- 6.20	-12.35
0.050	50	3.540	50.0	11.4	- 5.95	-10.90
0.083	50	2.740	38.7	20.8	- 7.70	-10.90
0.020	75	4.980	70.3	12.2	- 6.00	-13.00
0.020	75	5.220	73.7	-	-	-
0.020	100	4.580	64.6	18.4	- 5.00	-13.00
0.020	150	5.200	73.4	34.6	- 5.00	-13.90

Table 6.3. Intercepts for calculation of capillary temperatures—see text for details.

apparent from the table that ζ decreases with concentration of buffer, expected from double layer theory. Variation of the ζ potential from column to column is also evident.

6.4.2 Variation of k_e with E

The conductance of the buffer solution has been shown to be inversely proportional to the viscosity, so

$$k_e = A/\eta \tag{6.31}$$

where A is a constant. Inserting into equation 6.1 and rearranging

$$\frac{I}{E} = \frac{\pi r^2 A}{\eta} \tag{6.32}$$

As for the first method, plotting I/E against E will give a value for $\pi r^2 A/\eta$ at ambient temperature from the intercept at zero electric field. Knowing η and r at this temperature, A can be calculated. Thus η can be calculated at any value of I and E and from equation 6.7 the temperature found.

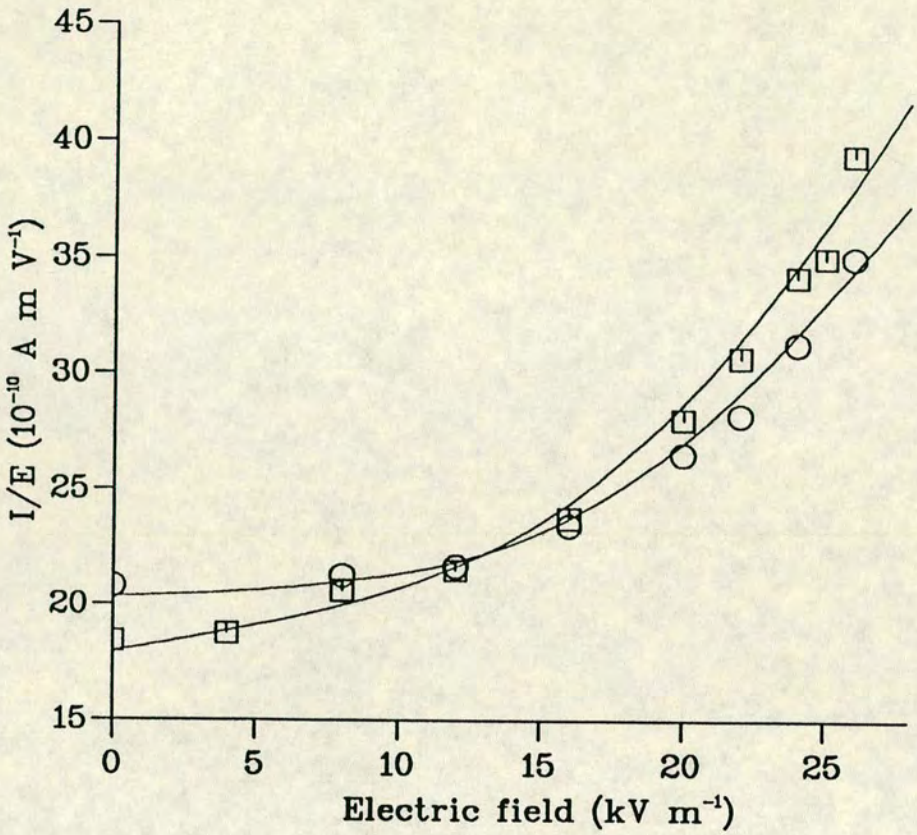

Figure 6.19. I/E vs E for the calculation of column temperatures for a 0.083 M $Na_2B_4O_7$ buffer solution in a 50 μm capillary (o) and 0.02 M $Na_2B_4O_7$ in a 100 μm capillary (□).

Figure 6.19 is a plot of I/E against E with a 0.083 M buffer solution in a 50 μm capillary. The intercepts of the plots for the seven systems studied are shown also in table 6.3 as Intercept_2.

6.4.3 Variation of μ_{ep} with E

For a charged solute, the electrophoretic mobility is inversely proportional to the viscosity. The electrophoretic mobility of a charged solute can be calculated from

experimental data by the following

$$\mu_{ep} = \frac{u - u_{eo}}{E} \tag{6.33}$$

As a result, the following holds

$$\frac{u - u_{eo}}{E} = \frac{A}{\eta} \tag{6.34}$$

where again A is a constant. A plot of $u - u_{eo}/E$ against E will give a value for A/η at ambient temperature from which A can be calculated. Knowing A the viscosity can be calculated at any field strength and the temperature in the capillary estimated as before.

In these studies two negatively charged solutes, 2-naphthol and dns-leucine, were used to estimate the temperature in the capillary. The intercepts of the plots for the seven systems studied are presented in table 6.3 for both samples, as Intercept_3 and Intercept_4 for 2-naphthol and dns-leucine respectively. A representative plot of $u - u_{eo}/E$ for both 2-naphthol and dns-leucine is shown in figure 6.20 for a 50 μm capillary with 0.083 M buffer.

6.4.4 Calculated temperatures

The actual viscosities and temperatures calculated by each method are presented in table 6.4 for 0.083 $Na_2B_4O_7$ buffer in a 50 μm capillary, and in table 6.5 for a 100 μm capillary with the same buffer at a concentration of 0.02 M. The difference between columns is obvious. There is an exceptionally large difference in the values of η_3 and T_3 in table 6.5 compared to the other values. These values were calculated from the electrophoretic mobility of 2-naphthol. The pKa of 2-naphthol is 9.51 and the pH of the buffer solution is 9.2. As the temperature increases the pH also increases and becomes closer in value to the pKa of the sample. As a result the sample would be expected to become more charged or

E kVm^{-1}	EI Wm^{-1}	η_1 cp	η_2 cp	η_3 cp	η_4 cp	T_1 °C	T_2 °C	T_3 °C	T_4 °C
8	0.136	0.9719	0.9808	0.9797	0.9597	21.3	20.9	20.9	21.8
12	0.312	0.9229	0.9618	0.9352	0.9163	23.1	21.7	22.9	23.8
16	0.600	0.8210	0.8891	0.8818	0.8206	28.7	25.1	25.5	28.8
20	1.060	0.7316	0.7865	0.7677	0.7405	33.7	30.6	31.6	33.2
22	1.364	0.6741	0.7396	0.7162	0.6865	37.4	33.2	34.6	36.6
24	1.800	0.5914	0.6669	0.5291	0.5904	44.2	37.9	50.9	44.3
26	2.366	0.5420	0.5955	0.5307	0.5624	49.4	43.8	50.7	46.7
28	3.024	0.4754	0.5404	0.4510	0.4955	58.1	49.6	61.8	54.1

Table 6.4. Calculated viscosities and temperatures for 0.083 M $Na_2B_4O_7$ buffer in a 50 μm capillary.

E kVm^{-1}	EI Wm^{-1}	η_1 cp	η_2 cp	η_3 cp	η_4 cp	T_1 °C	T_2 °C	T_3 °C	T_4 °C
1	-	0.9976	-	1.002	1.002	20.2	-	20.0	20.0
4	0.030	0.9816	0.9833	0.8713	0.8684	20.8	20.8	26.1	26.2
8	0.132	0.9439	0.8941	0.8907	0.9385	21.5	24.8	25.0	22.7
12	0.310	0.8269	0.8575	0.7332	0.8270	24.6	26.8	33.6	28.4
16	0.608	0.7516	0.7763	0.6311	0.7578	32.5	31.1	40.7	32.2
18	-	0.7815	-	0.6937	0.8056	30.8	-	36.1	29.5
20	1.120	0.6303	0.6585	0.4639	0.6595	40.8	38.6	59.8	38.5
21	-	0.6928	-	0.5813	0.7068	36.1	-	45.2	35.2
22	1.485	0.5870	0.6009	0.4144	0.6008	44.7	43.3	68.1	43.4
24	1.968	0.5232	0.5396	0.3536	0.5389	51.6	49.7	80.3	49.8
25	2.188	0.5083	0.5268	0.3450	0.5049	53.5	51.2	82.3	54.0
26	2.665	0.4776	0.4677	0.3139	0.4851	57.8	59.2	76.0	56.7
28	3.402	0.4299	0.4249	0.2719	0.4296	65.3	66.2	101.0	65.4

Table 6.5. Calculation of viscosities and temperatures for 0.02 M $Na_2B_4O_7$ buffer in a 100 μm capillary.

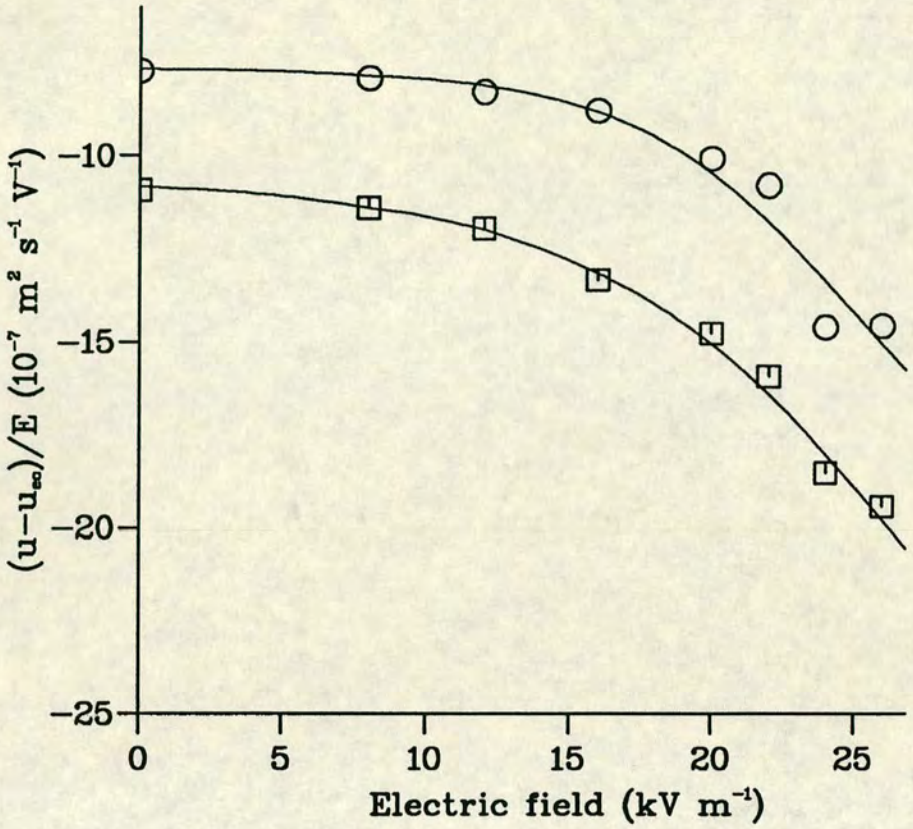

Figure 6.20. $(u-u_{eo})/E$ vs E for the calculation of column temperature. Data shown is for 2-naphthol (o) and dns-leucine (□) in 0.083 M $Na_2B_4O_7$ in a 50 μm capillary.

spend a greater fraction of time as an anion. The electrophoretic mobility would therefore increase at a faster rate than suggested by changes in the viscosity and give a lower value for the calculated viscosity than reality. Care must be taken when using these methods for calculating temperatures that effects such as these do not occur, and use of at least two methods for comparative purposes is recommended. From the figures which were used to calculate the variables at ambient temperature, which were in turn used to calculate the viscosities and thus temperatures, it is apparent that there is a relatively large amount of scatter of deviation from each curve, and so a large error in the intercept. This is as a

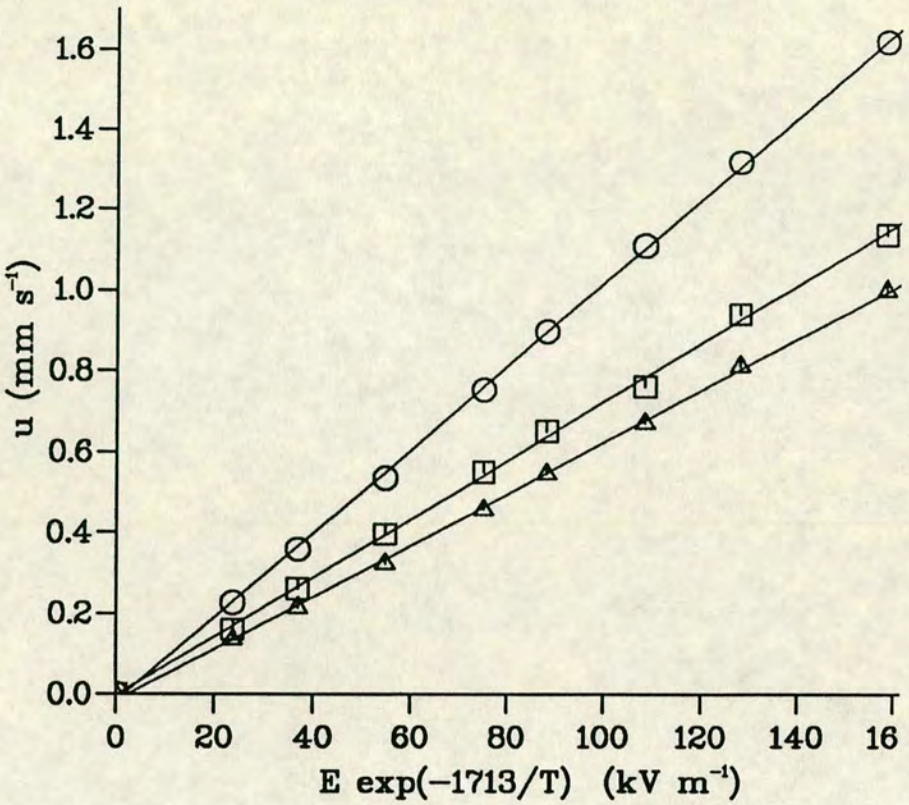

Figure 6.21. u vs $E\exp(-1713/T)$ for 0.083 M $Na_2B_4O_7$ in a 50 μm i.d. capillary. Samples: o cytosine (uncharged), □ 2-naphthol, △ dns-leucine.

result of variations in the ζ potential and current during each set of runs, which in turn affected the measured velocities and currents. In an attempt to cancel the effects of these variations, the average temperature of three calculations (ignoring the value given by 2-naphthol) is used used in further calculations.

Equation 6.27 predicts that u_{eo} is linear with $E\exp(-1713/T)$. The linear velocities of charged solutes would also be expected to be linear with $E\exp(-1713/T)$. Figure 6.21 is a plot of the electro-osmotic velocity and the velocities of two charged compounds against $E\exp(-1713/T)$ in a 0.083 M $Na_2B_4O_7$ buffer in a 50 μm i.d. capillary. The plots are linear as predicted by equation 6.27. The observed linearity of the plots is confirmation that the

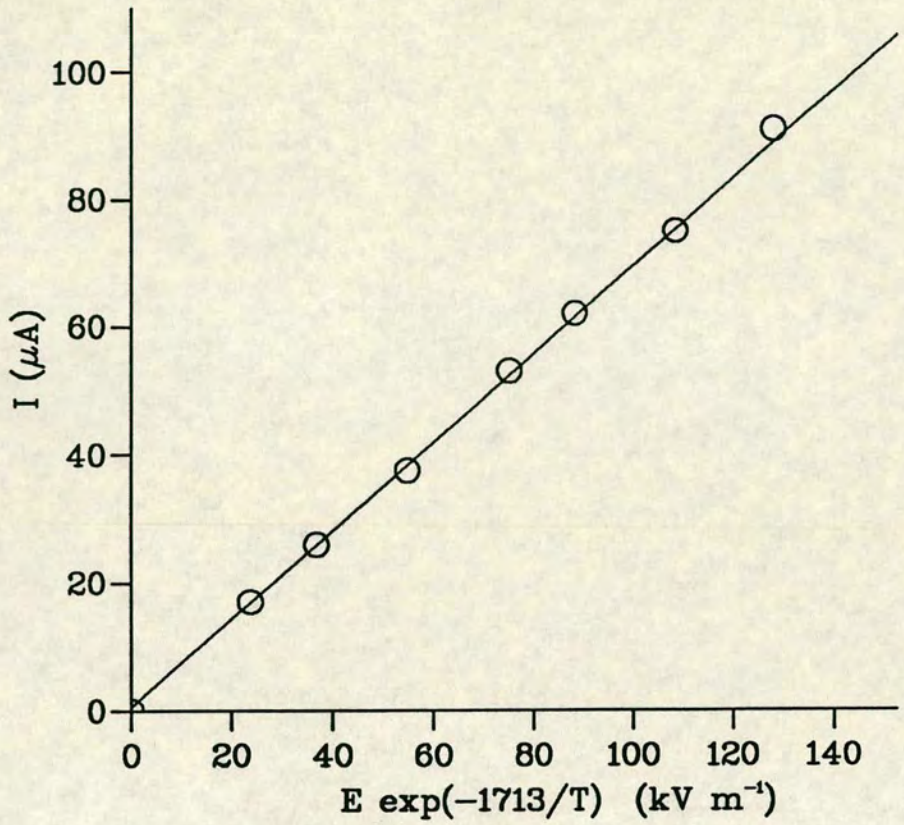

Figure 6.22. I vs $E\exp(-1713/T)$ for 0.083 M $Na_2B_4O_7$ buffer in a 50 μm i.d. capillary.

calculated temperatures are the correct ones. Similarily, it is to be expected that the current against applied electric field plots would be linearised by including the factor $\exp(-1713/T)$. Figure 6.22 is a plot of I vs $E\exp(-1713/T)$ for 0.083 M $Na_2B_4O_7$ buffer in a 50 μm i.d. capillary. Again, the linearity of the plot further confirms the validity of the calculated capillary temperatures.

6.5 Temperature dependence on power

The average temperature calculated for each system was plotted against the power generated (EI) in figure 6.23. The data fall on two curves with the

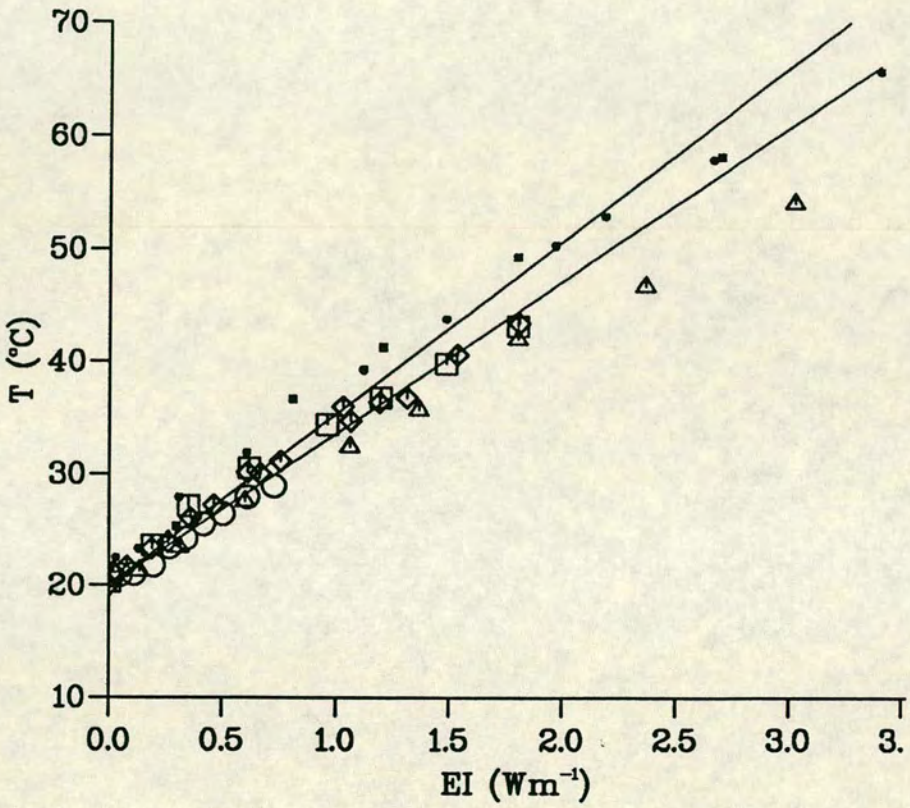

Figure 6.23. Column temperatures vs power generated. Open symbols: 375 μm o.d. capillary. Filled symbols: 250 μm o.d. capillary. Buffer $Na_2B_4O_7$. o 0.02 M 50 μm i.d., □ 0.05 M 50 μm i.d., △ 0.083 M 50 μm i.d., ◇ 0.02 M 75 μm i.d., • 0.02 M 100 μm i.d., ■ 0.02 M 150 μm i.d..

intercept on the Y-axis corresponding to ambient temperature. From the plot it would appear that the temperature rise above ambient, given by θ, is directly proportional to the power generated.

Knox [87] has given a formula for the calculation of θ as a function of the power generated. On rearranging, it becomes

$$\theta = 1.273EI/d_o^{0.3} \tag{6.35}$$

where d_o is the outer diameter of the capillary. In this work, two different column outer diameters were used, one approximately 375 μm o.d. and the other approximately 250 μm o.d.. From equation 6.35 the expected slopes are 13.57 K m W^{-1} and 15.33 K m W^{-1}. The actual slopes are 11.82 K m W^{-1} and 13.08 K m W^{-1} respectively, 15% and 17% lower than those expected.

In fact, the lines in figure 6.23 are not exactly linear. A full discussion of this is presented in chapter 7.

The results in figure 3 of Terabe's paper [131] agree well with these results.

6.6 Effect of temperature on efficiency

It has already been observed that the diffusion coefficient is strongly dependent on temperature and that this is responsible for the extra band broadening and discussed at the beginning of the chapter. To confirm the validity of equation 6.28 the number of plates obtained was plotted against $(u \exp 1713/T)/T$ for the three samples used for all seven systems studied. Figures 6.24, 6.25 and 6.26 illustrate the results. Except for the data for 100 μm i.d. capillary (• in figure 6.24), the data now all fall more or less on a common curve with a greater degree of linearity than before (figures 6.3, 6.4, 6.5 and 6.6). There is no obvious explanation for the exceptionally poor performance of the cytosine sample in the 100 μm capillary. However there is still curvature at the higher

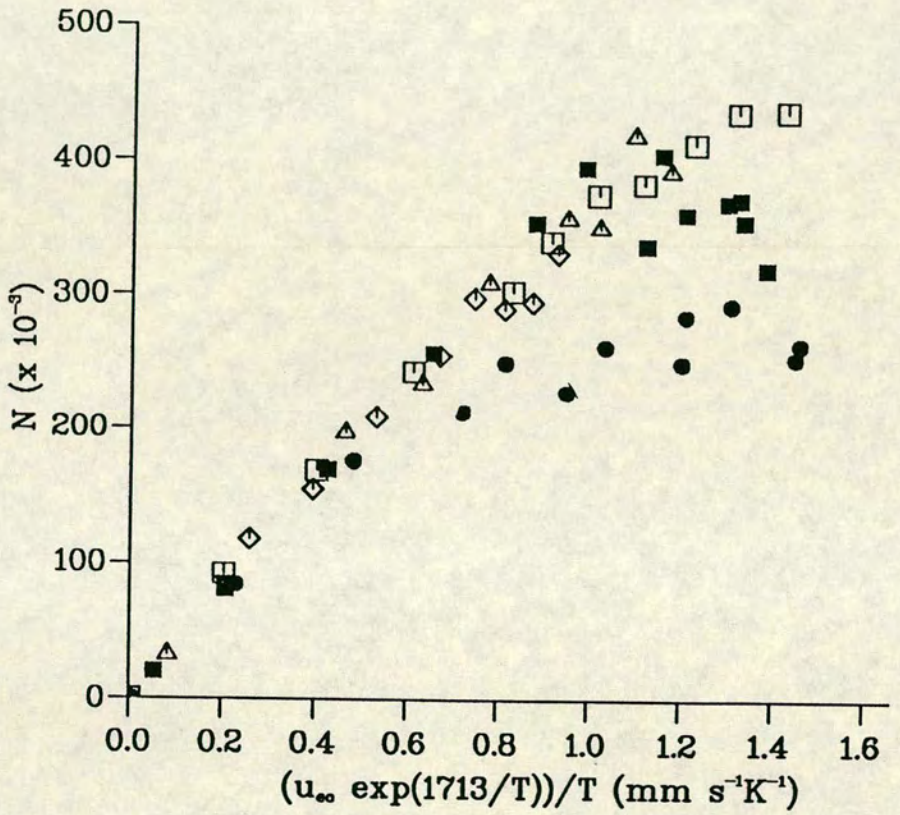

Figure 6.24. N vs $(u_{eo} \exp 1713/T)T$ with cytosine as sample. Open symbols: 375 μm o.d.. Filled symbols: 250 μm o.d.. Buffer $Na_2B_4O_7$. ○ 0.02 M 50 μm i.d., □ 0.05 M 50 μm i.d., △ 0.083 M 50 μm i.d., ◇ 0.02 M 75 μm i.d., ● 0.02 M 100 μm i.d., ■ 0.02 M 150 μm i.d..

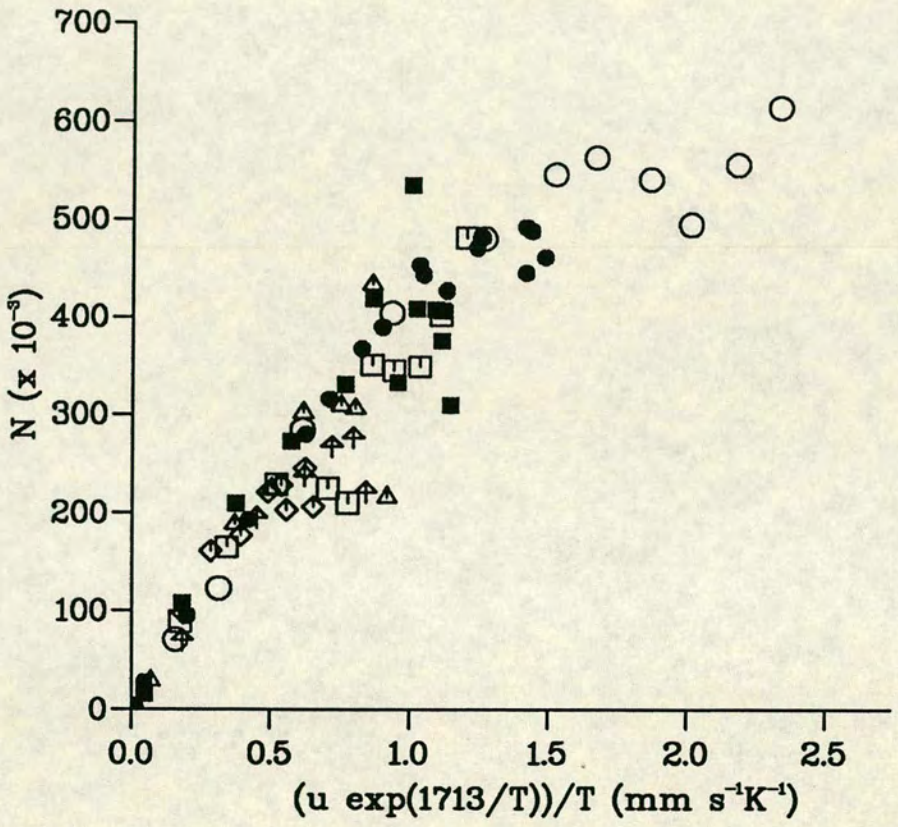

Figure 6.25. N vs $(u \exp 1713/T)/T$ with 2-naphthol as sample. Open symbols: 375 μm o.d.. Filled symbols: 250 μm o.d.. Buffer $Na_2B_4O_7$. ○ 0.02 M 50 μm i.d., □ 0.05 M 50 μm i.d., △ 0.083 M 50 μm i.d., ◇ 0.02 M 75 μm i.d., ● 0.02 M 100 μm i.d., ■ 0.02 M 150 μm i.d..

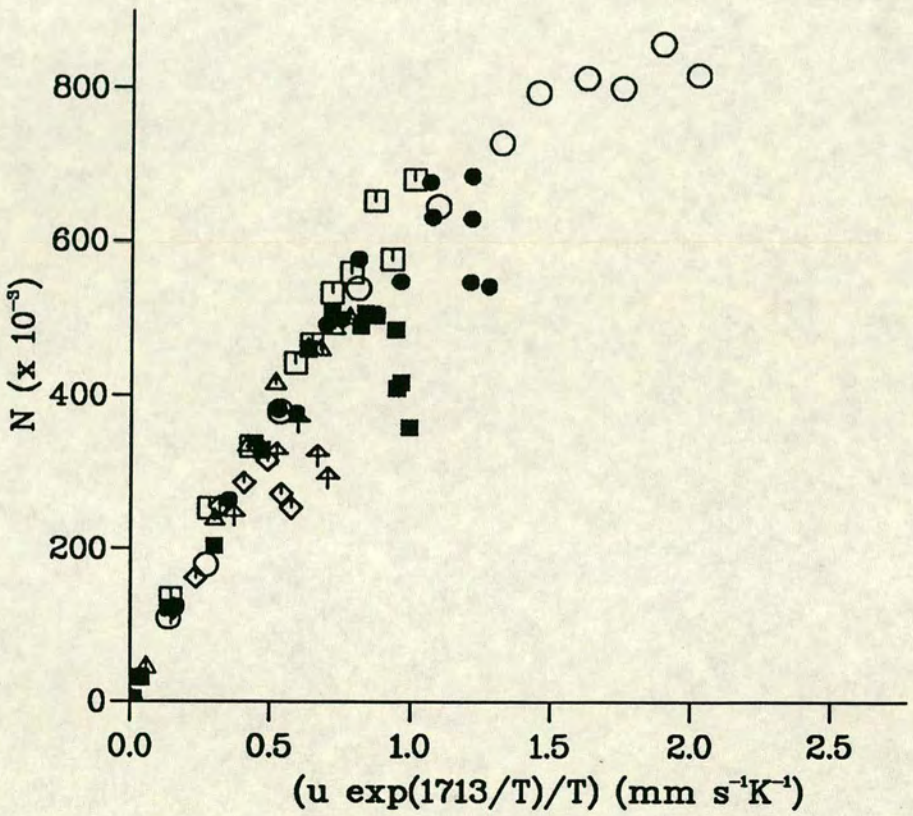

Figure 6.26. N vs $u \exp 1713/T)/T$ with dns-leucine as sample. Open symbols: 375 μm o.d.. Filled symbols: 250 μm o.d.. Buffer $Na_2B_4O_7$. ○ 0.02 M 50 μm i.d., □ 0.05 M 50 μm i.d., △ 0.083 M 50 μm i.d., ◇ 0.02 M 75 μm i.d., ● 0.02 M 100 μm i.d., ■ 0.02 M 150 μm i.d..

u mms^{-1}	N_{diff} $\times 10^{-3}$	$N_{inj+det+diff}$ $\times 10^{-3}$	$N_{inj+det+diff}/N_{diff} \times 100$
0.1	79	78	98.7
0.5	395	371	93.8
1.0	790	698	88.4
1.5	1185	989	83.5
2.0	1580	1250	79.1
2.5	1975	1485	75.2
3.0	2370	1698	71.7

Table 6.6. Effect of length of injection and detection zones on N achieved as u varies. $D = 5 \times 10^{-10}$ m^{2}s^{-1}, $l_{inj} = 1$ mm, $l_{det} = 0.5$ mm, $l_{eff} = 0.79$m

values of $(u \exp 1713/T)/T$, in particular for the lowest concentration of buffer for which heating in the capillary is negligible. At these high values of N, effects of injection and detection become important as discussed in chapter 3. Table 6.6 shows the increasing importance of injection and detection length as a function of u for a constant diffusion coefficient of 5×10^{-10} m^{2}s^{-1} using values for injection and detection as used in these studies. At a typical velocity of 2 mm s^{-1} only 79 % of the expected effeciency would be obtained. This partially accounts for the remaining curvature of the plots in the three figures, but there is still some unexplained curvature.

6.7 Effect of temperature on resolution

The resolution has been given as

$$R_s = 0.177(\mu_1 - \mu_2)\left[\frac{V}{D(\bar{\mu} + \mu_{eo})}\right]^{1/2}$$

Since $\mu \propto 1/\eta$ and $D \propto T/\eta$ the viscosity dependence cancels from the above equation and $R_s \propto 1/\sqrt{T}$. For a temperature rise of 40 °C from 20 °C a reduction

of the resolution by a factor of 1.066 would be expected. This may be significant in borderline separations but is not a major effect.

6.8 Expansion of buffer in the capillary

As the temperature is increased, the density of water increases (above 4 °C), or equivalently the specific volume (ml/g) increases. The specific volume (V_a) of the liquid in the capillary at ambient temperature is given by

$$V_a = \pi r^2 l / m_a \tag{6.36}$$

where r and l are the radius and length of the capillary respectively, and m_a is the mass of the liquid contained in the capillary. As the temperature is increased, the volume needed to contain the mass m_a increases. Since r is constant (assuming negligible expansion of the silica capillary), the change in volume must occur through an increase in the length occcupied by the mass of liquid. Since the capillary is constant in length, the net result is an expulsion of liquid from both ends of the capillary.

If V_T is the specific volume of the liquid at temperature T then

$$V_T = \frac{\pi r^2 l_T}{m_T} = \frac{\pi r^2 l_a}{m_a} \tag{6.37}$$

$$l_T = \frac{V_T}{V_a} l_a \tag{6.38}$$

Therefore the increase in length of capillary necessary to contain the liquid at a given temperature T above that of ambient is given by the ratio of the specific volumes at the two temperatures.

If the entire length of the capillary is thermostatted at the same temperature, then it can be assumed that equal volumes are expelled from both ends and the

θ °C	l_{exp} $T_a = 20°C$ mm	l_{exp} $T_a = 30°C$ mm
0	0.00	0.00
5	0.58	0.81
10	1.28	1.73
15	2.10	2.74
20	3.02	3.85
25	4.03	5.05
30	5.15	6.33
35	6.35	7.70
40	7.63	9.15
45	9.00	10.7
50	10.4	12.3
55	12.0	14.0
60	13.6	15.7

Table 6.7. Amount expelled from capillary due to volume expansion as temperature in capillary rises.

amount of liquid expelled from any end l_{exp} is given by

$$l_{exp} = \frac{1}{2}\left(\frac{V_T l_a}{V_a} - l_a\right) = \left(\frac{V_T/V_a - 1}{2}\right) l_a \tag{6.39}$$

The amount expelled is given in mm when l_a is in mm and will depend on the ambient temperature. The magnitude of l_{exp} is given in table 6.7 for temperature rises within the capillary above ambient (θ) for ambient temperatures of 20 °C and 30 °C, values typically used in CZE analyses. With $\theta = 50$ and ambient temperature of 20 °C, expulsion of 10.45 mm of liquid from each end of the capillary is predicted. As injection lengths are of the order of 1 mm, these values predict that all the sample would be ejected from the capillary.

However whether the injected sample is expelled or not depends on the distance moved by the sample in the time taken for the temperature to reach its maximum value. It can be assumed that the relative increase in length of the

capillary necessary to contain the sample with temperature, $\Delta l/\Delta T$, and the increase in temperature with applied voltage, $\Delta T/\Delta E$, are practically instantaneous. In the time t that it takes the voltage to reach the set level, the buffer solution will expand and attempt to leave the capillary. Opposing this is the linear velocity of the sample. Simplistically, if the velocity of sample u varies linearly from 0 to the the steady state value in time t, then the average length travelled in this time is $0.55u$ or $0.55l_{eff}t/t_r$ where l_{eff} is the effective length of the capillary or the distance to the detection zone and t_r is the retention time of the sample. If none of the injected sample is to be expelled from the capillary then the following must hold

$$\frac{0.55l_{eff}t}{t_r} > l_{exp} \tag{6.40}$$

Substituting from equation 6.39 for l_{exp}

$$\frac{0.55l_{eff}t}{l_a t_r} > \frac{V_T}{V_a} - 1 \tag{6.41}$$

Using the condition expressed by equation 6.40 in the form $t_r < 0.55l_{eff}t/l_{exp}$ then a maximum retention time can be calculated for a variety of temperatures below which no sample should be lost from the capillary due to heating and expansion of the buffer. For an ambient temperature of 20 °C with a capillary 1000 mm long and 800 mm to the detector, in which $t = 2$ s, then the conditions under which no sample is lost are as follows

$\theta = 10\ ^\circ$ then $t_r < 687.5$ s

$\theta = 20\ ^\circ$ then $t_r < 291.3$ s

$\theta = 30\ ^\circ$ then $t_r < 170.9$ s

$\theta = 40\ ^\circ$ then $t_r < 115.3$ s

These conditions are in fact quite stiff, and from the temperature excesses achieved fairly routinely in previous sections in this chapter, it is apparent that sample can be easily lost from the capillary at the beginning of a run due to

volume expansion of the buffer. It is also apparent that within a sample mixture, the proportion of injected sample lost by this mechanism will vary from component to component, depending on their relative retention times. This fact will make the use of internal standards more difficult in CZE.

The conditions under which no sample will remain on the capillary depends on the length of the injection zone l_{inj}. If all the sample is to be lost, the condition is

$$\frac{0.55 l_{eff} t}{t_r} + l_{inj} < l_{exp} \tag{6.42}$$

In other words, if the sum of the distance the sample moves in time t and the injection zone length are less than the amount that would be expected to be expelled at the final buffer temperature, then no sample will remain on the capillary. This condition can be expressed in terms of retention times as follows, with $l_{inj} = 1$ mm

if $\theta = 10$ °C then $t_r > 3142.9$ s

if $\theta = 20$ °C then $t_r > 435.6$ s

if $\theta = 30$ °C then $t_r > 212.0$ s

if $\theta = 40$ °C then $t_r > 132.7$ s

The conditions at which all the sample is lost from the capillary are not that extreme and are likely to occur in practice. The solution to this problem is to apply a low voltage to the capillary for a few seconds to move all the sample sufficiently into the capillary so that on application of the running voltage, none of the sample is lost. This will of course affect the measured retention times, and make calculation of exact mobilities difficult or inaccurate. The existence of this phenomena is further evidence that the temperature rise within capillaries must be eliminated or minimised.

Chapter 7

Temperature in CZE (2)

7.1 Introduction

The previous chapter has illustrated the detrimental effect of the temperature rise within the capillary on the separation efficiency, the resolution and sample injection. In addition, large temperature rises within the capillary are to be avoided when dealing with thermally labile samples. For unthermostatted capillaries operated at ambient temperature, the temperature rise θ has been given as a linear function of the power per unit length. If $\theta \leq 4$ K then

$$\frac{u_{T+\theta}}{u_T} = \frac{\eta_T}{\eta_{T+\theta}} \tag{7.1}$$

If $T = 293$ K and $\theta = 4$ K then $u_{T+\theta}/u_T = 1.10$ by substituting in values for the viscosity, and so the velocity of the sample increases by less than 10%. To prevent excessive band broadening and deviation from linearity of the curves, a maximum value for θ of 4 K is allowed. Combining with Knox's value for θ

$$1.273EI/d_o^{0.3} \leq 4 \tag{7.2}$$

Replacing $I = \pi r^2 \lambda c E$ and rearranging

$$E^2 r^2 \lambda c/d_o^{0.3} \leq 1.000 \tag{7.3}$$

If the system is operated under these conditions, then the resulting electropherogram will obey the classical CZE equations as originally proposed by Jorgenson and Lukacs, with velocity and currents linear with the potential gradient, and the number of theoretical plates also linear with potential gradient or velocity, subject to injection and detection restraints as discussed. Under typical conditions, if $d_c = 50$ μm, $c = 0.01$ M, $\lambda = 0.015$ $m^2\Omega^{-1}mol^{-1}$ and $d_o = 375$ μm, then $E_{max} = 15.8$ kV m^{-1}. If it is desired to double the voltage in order to halve the analysis time or improve the separation efficiency then either d_c must be halved or c or λ reduced by a factor of four.

The above conditions for operating CZE ststems are more restrictive than those given by Knox and Grant [4]. This is because they considered only the effects of a parabolic temperature gradient across the capillary on the separation efficiency, and did not consider the effect of the actual temperature rise above ambient.

There are many reasons why the analyst would find the conditions imposed by equation 7.3 too restrictive. If working with molecules with small diffusion coefficients which are well resolved , then whether the separation effeciency is 400,000 or 800,000 plates may be irrelevant. However for molecules with larger diffusion coefficients ($\sim 10^{-9}$ m^2s^{-1}) and/or a low resolution separation, the efficiency becomes critical and so the temperature needs to be controlled. For sensitivity purposes, particularily with uv detection, the path length should be as large as possible. Typically capillaries of 50–75 μm i.d. are used, but it would be of advantage to be able to use capillaries of 100–200 μm i.d.. The potential gradient should be maximised to increase the speed of the analysis, particularily important in industrial settings. Commercial instruments in general have an upper limit of 30 kV for the applied voltage which, depending on the length of the capillary, can allow potential gradients of up to 60 kV m^{-1} to be

applied. The ability to apply high potential gradients becomes more important with low pH buffer solutions where the ζ potential on the wall is much reduced compared to the value at pH 9. It would also be advantageous to be able to use a high concentration of buffer to prevent migrational dispersion and, with protein samples, to prevent adsorption to the walls of the capillary. Most researchers use buffer concentrations of the order of 0.01–0.05 M. Where micellar solutions are used, the concentration of the micelle forming component must be above the critical micelle concentration, which also contributes to the net current and power generated. SDS concentrations as high as 0.05 M are often used in MECC.

It has been observed by Issaq *et al* [132] that correct choice of buffer will reduce the current at a given voltage and thus reduce the power generated. As discussed in the previous chapter, the current at a given voltage is dependent on the mobility of the ions in solution, and for electro-osmotic flow towards the cathode (common in CZE) the mobility of the cation has the most effect on the current produced. As a result, using a sodium salt buffer instead of a potassium one will result in a lower current and a higher electro-osmotic velocity. Issaq gives examples in which a 0.1 M sodium acetate buffer gives a current of 147 μA with 20 kV applied, while a potassium acetate buffer at the same concentration and voltage produced a current of 195 μA. Clearly, correct choice of buffer will have a major impact on the power generated and, as a result, on the temperature excess.

One means of improving the efficiency obtained for a separation is to reduce the ambient temperature. For a 0.05 M $Na_2B_4O_7$ buffer for which $\lambda = 7.28 \times 10^{-3}$ $m^2\Omega^{-1}mol^{-1}$, $k_e = 0.364$ $\Omega^{-1}m^{-1}$ and $\eta = 1.002 \times 10^{-3}$ kg $m^{-1}s^{-1}$ at 20 ^{0}C. With an applied potential of 30 kV m^{-1} across a 100 μm i.d. capillary with an outer diameter of 375 μm, the expected temperature rise is 34.9 °C and the temperature in the capillary is 54.9 °C. If the ambient temperature were reduced

to 4 °C, then $\eta = 1.567 \times 10^{-3}$ kg m^{-1}s^{-1} and $k_e = 0.233\ \Omega^{-1}$m^{-1}. To maintain the same analysis time, the applied voltage must be multiplied by the viscosity factor and increases to 46.9 kV m^{-1}. The temperature rise expected is then 55.1 °C with a temperature in the capillary of 59.1 °C. The temperature in the capillary is thus higher than at 20 °C and a net reduction in the efficiency would be observed due to the increased diffusion coefficient. An improvement in the separation efficiency will only be observed if the temperature excess at the higher temperature is less than the difference between the two ambient temperatures. By keeping the same conditions in the example above but halving the column diameter the temperature in the capillary operated at 20 °C is reduced to 28.7 °C while the temperature in the capillary operated at the lower ambient temperature is reduced to 17.7 °C. Since

$$\begin{aligned} \frac{D_{T_1}\eta_{T_1}}{T_1} &= \frac{D_{T_2}\eta_{T_2}}{T_2} \\ D_{17.7} &= 0.745 D_{28.7} \end{aligned}$$

As a result an improvement in the number of theoretical plates generated by a factor of $1/0.745 = 1.343$ can be expected.

The maximum improvement is to be expected when $\theta \sim 0$. For temperatures of 4 °C and 20 °C as above, $D_4 = 0.605 D_{20}$ and so $N_{4°C} = 1.645 N_{20°C}$ where $N_{4°C}$ and $N_{20°C}$ are the number of plates obtained at 4 °C and 20 °C respectively.

From the above then, reducing the ambient temperature will result in an improvement in the efficiency at low power levels where the temperature excess is not a problem. At higher power levels, while maintaining the same analysis time, reduction of ambient temperature may in fact result in a worsening of the situation.

7.2 Heating equations

In 1988, Knox [105] proposed that the temperature rise within capillaries could be reduced if the heat generated within the capillary was more effectively dissipated by forced convection or air flow over the surface. His calculations show that with a flow of 1 m s^{-1} of air over the surface of a 100 μm capillary at 300 W cm^{-3}, $\theta = 17$ K, compared to $\theta = 44$ K for natural convection.

In order to consider the effects of cooling of the capillary it is necessary to use the heat conduction and convection equations of heat transfer.

The law of heat conduction is named after the French mathematical physicist, Joseph Fourier, who used it in his analytic theory of heat. The law states that the rate of heat flow by conduction is proportional to the cross sectional area perpendicular to the direction of flow of the heat and to the temperature gradient in that direction. For heat flow in the x direction

$$Q_x = -k_{th} A dT/dx \tag{7.4}$$

$$q_x = -k_{th} dT/dx \tag{7.5}$$

where Q_x is the rate of heat flow through area A in W and q_x is the heat flux in W m^{-2}. The proportionality constant k_{th} is the thermal conductivity of the material in W $m^{-1}K^{-1}$.

For cylinders, the one dimensional time dependent heat conduction equation for the system is given in radial co-ordinates as

$$\frac{1}{r}\frac{\partial}{\partial r}\left(r k_{th}\frac{\partial T}{\partial r}\right) + g = \rho c_p \left(\frac{\partial T(r,t)}{\partial t}\right) \tag{7.6}$$

where g is the heat generation rate in W m^{-3} and ρ and c_p are the density and heat capacity of the material.

For steady state heat conduction equation 7.6 reduces to

$$\frac{1}{r}\frac{d}{dr}\left(rk_{th}\frac{dT}{dr}\right)+g=0 \tag{7.7}$$

and if k_{th} is independent of temperature then

$$\frac{1}{r}\frac{d}{dr}\left(r\frac{dT}{dr}\right)+\frac{g}{k_{th}}=0 \tag{7.8}$$

In considering the total temperature drop from the centre of the capillary to the air/fluid temperature outside i.e. the ambient temperature, heat transfer by convection becomes relevant. The results of the previous chapter have shown that the temperature within the capillary can be as high as 45 °C. When fluid flows over a heated surface, the motion of the fluid relative to the surface results in heat transfer between the fluid and the surface. In free convection, the fluid motion is a result of density differences within the fluid caused by temperature differences. Newton's law of cooling gives the heat transfer as

$$q=h(T_w-T_f) \tag{7.9}$$

where h is the heat transfer coefficient. T_w and T_f are the temperatures at the wall and in the bulk fluid. h varies with the type of flow, geometry of the body, flow passage area and physical properties of the fluid.

The fused silica capillaries used in CZE can be considered as composite cylinders i.e. cylinders composed of layers of differing materials, for the purposes of calculating heat transfer and temperature distribution. r_1 is the inner radius of the cylinder or capillary or the radius of the buffer solution with thermal conductivity k_w (taken to be the same as for water), r_2 is the radius from the centre to the outer surface of the silica, with thermal conductivity k_s and r_3 is the total radius to the outer surface, with the thermal conductivity of the polymer coating given as k_p. The temperature at the centre of the capillary is T_c, with T_1, T_2 and T_3 the temperatures at each of the interfaces respectively.

Solving equation 7.8 for the inner buffer containing portion with the boundary conditions $dT/dr = 0$ and $T = T_c$ at $r = 0$, and $T = T_1$ at $r = r_1$

$$T_c - T_1 = \frac{r_1^2 g}{4k_w} \tag{7.10}$$

Solving for the silica layer with the boundary conditions that at $r = r_1$, $T = T_1$ and at $r = r_2$, $T = T_2$, and since Q must be constant at any point i.e. $g_1 r_1^2 = g_2 r_2^2 = g_3 r_3^2$

$$T_1 - T_2 = \frac{r_1^2 g}{2k_s} \ln \frac{r_2}{r_1} \tag{7.11}$$

Similarily for the polyimide layer

$$T_3 - T_2 = \frac{r_1^2 g}{2k_p} \ln \frac{r_3}{r_2} \tag{7.12}$$

Using Newton's law of cooling to solve for the temperature difference between the capillary outer surface and the surrounding fluid

$$T_3 - T_f = \frac{q}{h} = \frac{r_1^2 g}{2r_3 h} \tag{7.13}$$

Combining equations 7.10, 7.11, 7.12 and 7.13, the temperature between the centre of the capillary and the surrounding fluid is given by

$$T_c - T_f = \frac{r_1^2 g}{2} \left(\frac{1}{2k_w} + \frac{1}{k_s} \ln \frac{r_2}{r_1} + \frac{1}{k_p} \ln \frac{r_3}{r_2} + \frac{1}{r_3 h} \right) \tag{7.14}$$

Substituting $g = EI/\pi r_1^2$ into the above

$$T_c - T_a = \frac{EI}{2\pi} \left(\frac{1}{2k_w} + \frac{1}{k_s} \ln \frac{r_2}{r_1} + \frac{1}{k_p} \ln \frac{r_3}{r_2} + \frac{1}{r_3 h} \right) \tag{7.15}$$

Substituting the same expression for g into equation 7.10 gives an expression for the temperature excess within the capillary as

$$T_c - T_1 = \frac{EI}{4\pi k_w} \tag{7.16}$$

Equations 7.10 to 7.15 have been derived under the assumption that the thermal conductivity is independent of temperature. In fact, it is known that k_{th} is

temperature dependent. For water, k_w varies from 0.574 W $m^{-1}K^{-1}$ at 280 K to 0.680 W $m^{-1}K^{-1}$ at 370 K [125], an increase of 18%. As the temperature gradient is inversely proportional to k_w use of the value at ambient temperature will lead to a higher value of $T_c - T_1$ by 18%. In the case of water with a power generation of 10 W m^{-1} (about the about the limit of what can be used in practice) use of k_w at 280 K gives $T_c - T_1 = 1.39$ K and using k_w at 370 K gives $T_c - T_1 = 1.17$ K. Clearly the difference is negligible compared to the errors encountered in calculations of the temperatures in capillaries and so use of k_w at ambient temperature is justified. If a more accurate temperature distribution is required an initial calculation using k_w at T_f may be done to obtain an estimated value for T_c. The value may be used to determine the best value of k_w to use and enable recalculation of T_c for a more accurate temperature profile.

The addition of the first three terms of equation 7.15 gives the temperature difference between the capillary centre and the wall. Inserting typical values of $k_w = 0.594$ W $m^{-1}K^{-1}$, $k_s = 1.5$ W $m^{-1}K^{-1}$, $k_p = 0.155$ W $m^{-1}K^{-1}$, $r_3 = 187.5$ μm, $r_2 = 172.5$ μm, $r_1 = 25$ μm and $EI = 3$ W m^{-1} gives $T_c - T_3 = 1.05$ K. Experimentally $T_c - T_a = 34.1$ K at this power level so it is obvious that the greatest temperature drop occurs between the wall and the surroundings. If $\theta = T_3 - T_f$, substituting into equation 7.13 with $g = EI/\pi r_1^2$

$$\theta = \frac{EI}{2\pi} \frac{1}{r_3 h} \tag{7.17}$$

In order to calculate θ and compare it with experimental data it is necessary to evaluate h, the heat transfer coefficient. Basic engineering textbooks [114, 133, 138] express h in the form of the dimensionless Nusselt number Nu

$$Nu = \frac{h d_o}{k_f} = \frac{2 h r_3}{k_f} \tag{7.18}$$

where k_f is the thermal conductivity of the surrounding fluid and d_o is the characteristic dimension of the system, in this case, the capillary outer diameter. The

Nusselt number can be interpreted as the ratio of heat transfer by convection to conduction across the fluid layer of thickness d. Combining equations 7.17 and 7.18

$$Nu = \frac{EI}{\pi\theta k_f} \tag{7.19}$$

in which both sides of the equation are dimensionless.

Calculation of Nu is dependent on the type of convection present in the system i.e. free or forced convection. For free convection,

$$Nu = f(GrPr) \tag{7.20}$$

that is, the Nusselt number is a function of the dimensionless Grashof (Gr) and Prandtl (Pr) numbers.

The Grashof number is defined as

$$Gr = \frac{g\beta d_o^3(T_3 - T_f)}{\nu^2} \tag{7.21}$$

and represents the ratio of buoyancy force to the viscous force acting on the fluid where ν is the kinematic viscosity $= \eta/\rho$, g is the acceleration due to gravity and β is the reciprocal of the film temperature T_{film} which is defined as the average temperature of the wall and fluid, and is the temperature at which ν and k_f and any other temperature dependent variables are to be calculated.

The Prandtl number is defined as

$$Pr = \frac{c_p\eta}{k_f} = \frac{\nu}{\alpha} \tag{7.22}$$

where α is the molecular diffusivity of heat. The Prandtl number is about 0.7 for linear diatomic gases and decreases slightly with temperature.

Combining equations 7.19, 7.20 and 7.21

$$f\left(\frac{g\beta d_o^3\theta}{\nu^2}Pr\right) = \frac{EI}{\pi\theta k_f} \tag{7.23}$$

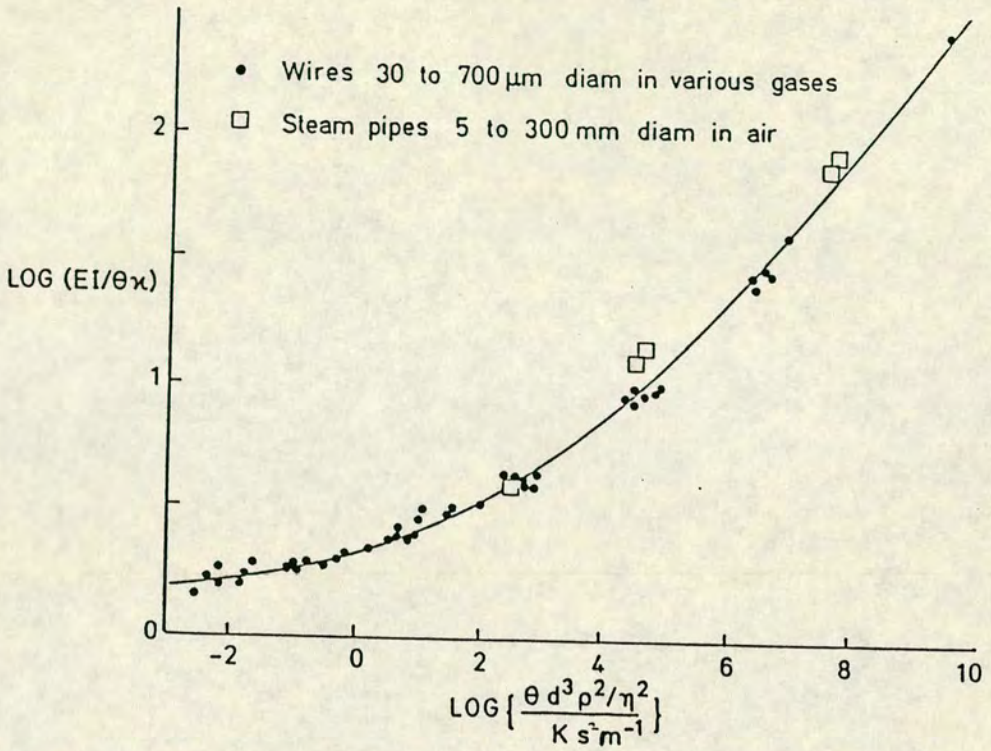

Figure 7.1. Universal plot for natural convection after Knox and Roberts.

As g, Pr and π are constants, plotting $d_o^3\theta\beta/\nu^2$ against $EI/\theta k_f$ gives a universal plot or curve for any cylinder undergoing natural convection. Figure 7.1 shows one such curve, adapted from Roberts [134] by Knox, where the log values have been plotted, for wires and steam pipes up to 700 mm in various gases.

The functional dependence of Nu on Gr and Pr cannot be derived theoretically. A number of empirical solutions based on experimental results have been derived by various investigators.

Churchill and Chu [135] proposed the following for free convection on an isothermal horizontal cylinder

$$Nu^{1/2} = 0.60 + \frac{0.387Ra^{1/6}}{(1 + (0.559/Pr)^{9/16})^{8/27}} \tag{7.24}$$

for $10^{-4} < Ra < 10^{12}$ and where $Ra = GrPr$ and is the dimensionless Rayleigh number.

Ra	b	n
10^{-12}–10^{-2}	0.675	0.058
10^{-2}–10^{2}	1.02	0.148
10^{2}–10^{4}	0.85	0.188
10^{4}–10^{7}	0.48	0.250
10^{7}–10^{12}	0.125	0.333

Table 7.1. b and n used in the calculation of Ra.

Morgan [136] gave the following simpler correlation:

$$Nu = bRa^{n} \tag{7.25}$$

where b and n used depend on the magnitude of Ra and are given in table 7.1 Equation 7.25 is reported to correlate well with experimental data [133], and since it is simpler in form than equation 7.24 will be used in calculations. With the dimensions and θ values usual in CZE experiments, Ra values are generally in the range 10^{-2}–10^{2} and therefore

$$Nu = 1.02Ra^{0.148} \tag{7.26}$$

Combining equations 7.23 and 7.26

$$1.02\left(\frac{gd_o^3\beta\theta Pr}{\nu^2}\right)^{0.148} = \frac{EI}{\pi\theta k_f} \tag{7.27}$$

Equation 7.27 indicates that the linear dependence assumed of θ on EI is not in fact correct and explains the curvature of θ against EI observed in figure 6.23. If all other terms in equation 7.27 were constant, it would be expected that $\theta^{1.148} \propto EI$. However Pr, ν and k_f are all temperature dependent and so obviously is β where

$$\beta = \frac{2}{T_3 + T_f} = \frac{1}{T_f + \theta/2} \tag{7.28}$$

T	ρ	c_p	η	k_f	Pr	ν
		10^{-4}	10^{-5}	10^{-2}		10^{-5}
K	kg m^{-3}	J kg^{-1}K^{-1}	kg s^{-1}m^{-1}	W m^{-1}K^{-1}		m^{2}s^{-1}
275	1.285	5.741	1.719	2.428	0.715	1.338
280	1.261	5.741	1.743	2.468	0.713	1.382
285	1.240	5.741	1.767	2.506	0.711	1.425
290	1.217	5.743	1.790	2.548	0.710	1.471
295	1.197	5.743	1.814	2.586	0.709	1.515
300	1.177	5.746	1.839	2.624	0.708	1.562
305	1.158	5.746	1.863	2.664	0.707	1.609
310	1.139	5.748	1.885	2.702	0.705	1.655
315	1.121	5.748	1.907	2.740	0.704	1.701
320	1.104	5.750	1.931	2.780	0.703	1.749
325	1.086	5.753	1.955	2.816	0.702	1.800
330	1.070	5.753	1.977	2.854	0.701	1.847
335	1.054	5.755	1.999	2.890	0.700	1.897
340	1.038	5.758	2.021	2.928	0.699	1.947
345	1.024	5.760	2.044	2.965	0.698	1.996
350	1.009	5.762	2.066	3.003	0.697	2.048
355	0.995	5.762	2.088	3.043	0.696	2.098
360	0.980	5.765	2.109	3.079	0.695	2.152
365	0.967	5.767	2.130	3.115	0.694	2.203
370	0.953	5.772	2.152	3.150	0.693	2.258

Table 7.2. Thermodynamic properties of air (taken from reference [137]).

Substituting equation 7.28 into equation 7.27 and rearranging so that all temperature dependent factors are on one side of the equation

$$\theta k_f \left(\frac{\theta Pr}{(T_a + \theta/2)\nu^2} \right)^{0.148} = \frac{EI}{1.02\pi(2gd_o^3)^{0.148}} \tag{7.29}$$

The values of k_f, Pr, ν, η and ρ for air at various temperatures are given in table 7.2 taken from reference [137]. Taking T_f as 295 K and evaluating Pr, ν and k_f at the film temperature, the log values of $k_f\theta(\beta\theta Pr/\nu^2)^{0.148}$ were plotted against $\log\theta$ for various θ values in figure 7.2. The plot was linear with a gradient of

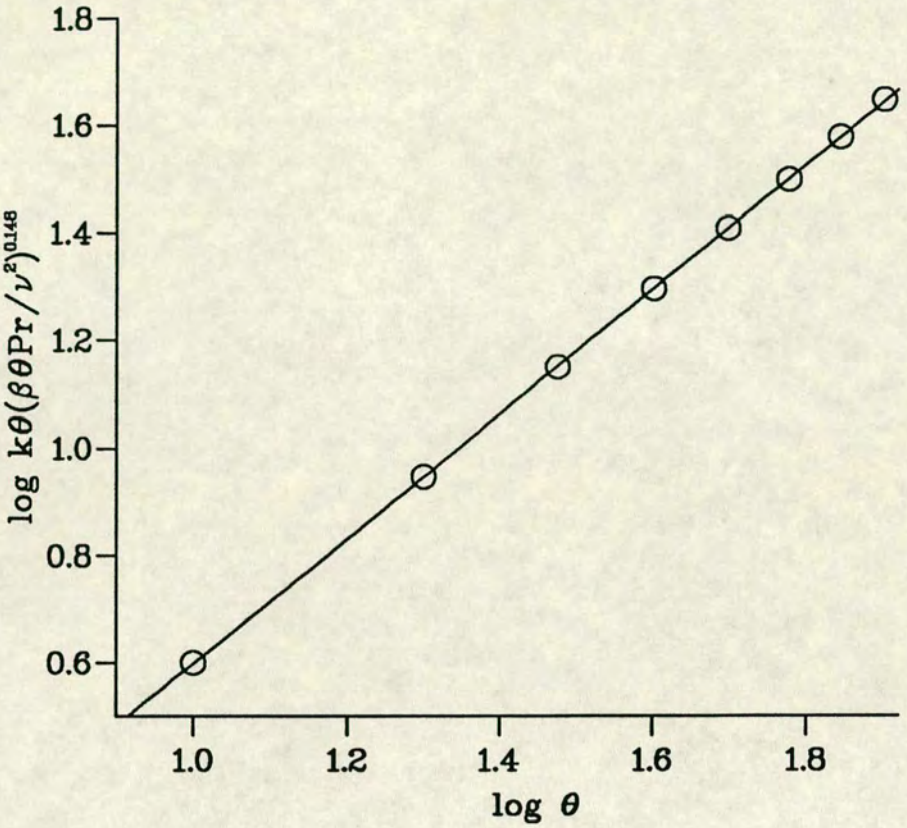

Figure 7.2. Log θ vs $k_f\theta(\beta\theta Pr/\nu^2)^{0.148}$.$T_f$ = 295 K.

1.160 and an intercept of −0.5606. Therefore

$$k_f\theta\left(\frac{\beta\theta Pr}{\nu^2}\right)^{0.148} = 0.275\theta^{1.160} \tag{7.30}$$

Substituting into 7.29, giving values to the constants and rearranging

$$\theta = 0.8333\frac{(EI)^{0.8621}}{d_o^{0.3828}} \tag{7.31}$$

Plots of θ against $(EI)^{0.8621}$ are shown in figure 7.3 for the data from chapter 6 with 375 μm and 250 μm diameter capillaries with natural convection. The best fit slopes of 13.70 and 15.70 are approximately 80% of those expected from equation 7.31 and are more linear than the plots of θ against EI of figure 6.23.

Equation 7.31 has shown the dependence of θ on the outer capillary diameter.

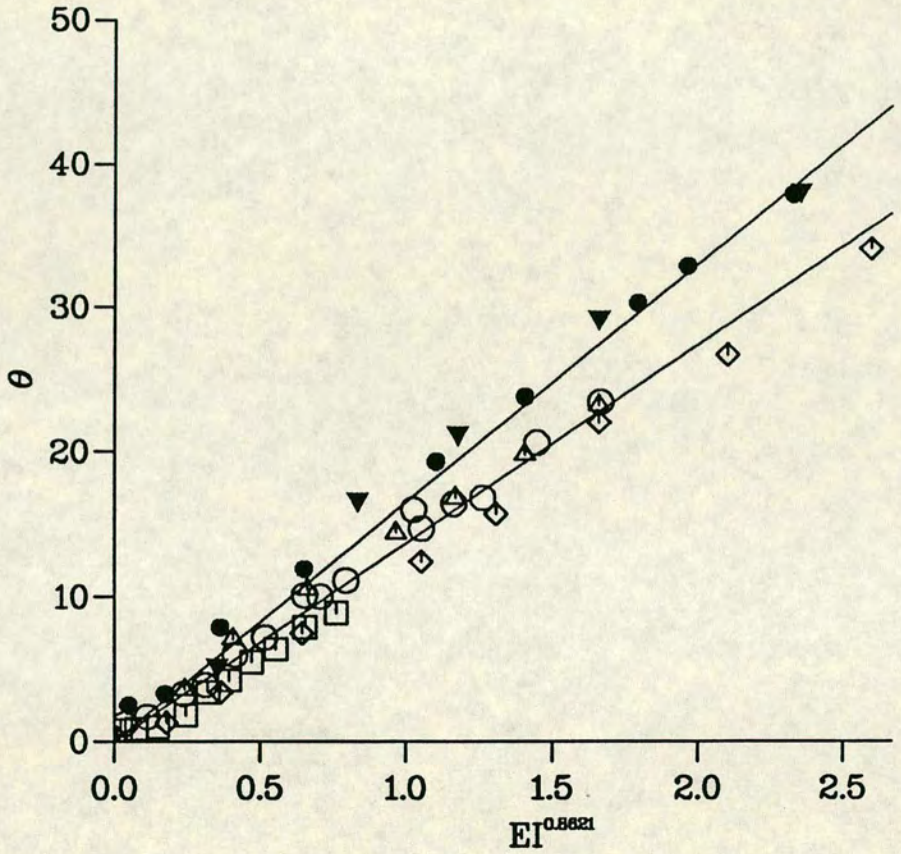

Figure 7.3. Temperature excess as a function of the power generated. Open symbols: 375 μm o.d.. Filled symbols: 250 μm o.d.. Buffer $Na_2B_4O_7$. ○ 0.02 M 50 μm i.d., □ 0.05 M 50 μm i.d., △ 0.083 M 50 μm i.d., ◇ 0.02 M 75 μm i.d., ● 0.02 M 100 μm i.d., ▼ 0.02 M 150 μm i.d..

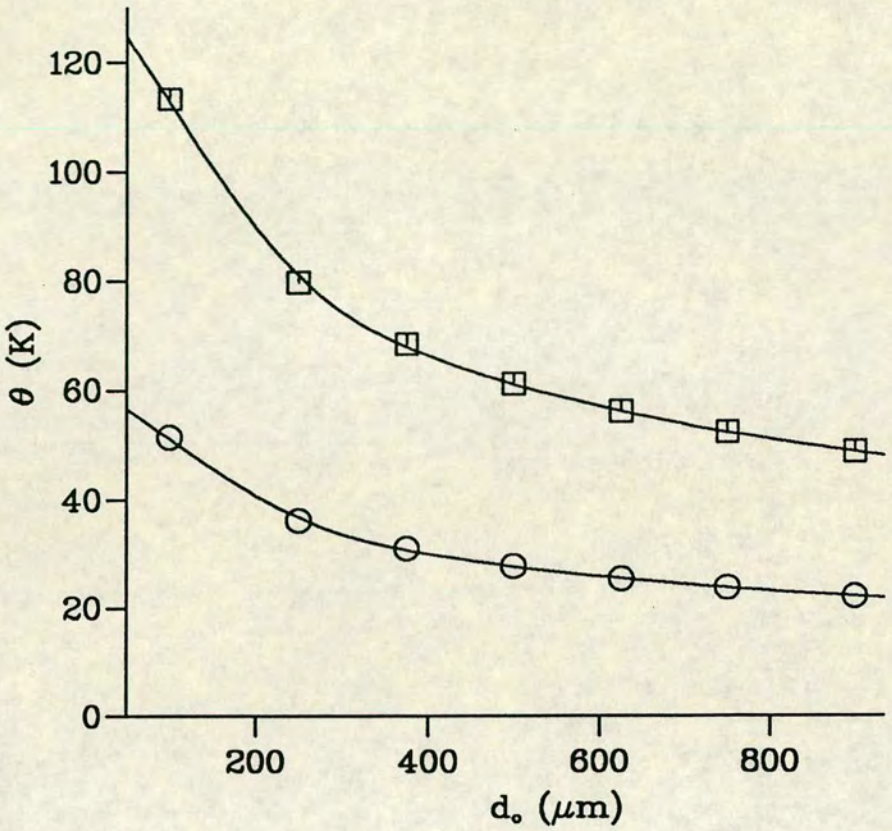

Figure 7.4. The temperature excess as a function of column outer diameter for natural convective cooling. o $EI = 2$ W m^{-1}, □ $EI = 5$ W m^{-1}.

Intuitively, a dependence on d_o is to be expected as a larger surface area would be expected to be more effective at allowing heat dissipation. The temperature dependence of θ as a function of the outer diameter is illustrated in figure 7.4 for fixed power levels of 2 and 5 W m^{-1} with data generated from equation 7.31. It is clear from the figure that even with an outer diameter of 900 μm, an unacceptably high value of θ is obtained at 5 W m^{-1}. With 2 W m^{-1} applied, more reasonable values are achieved but with the ultimate penalty of long run times as the applied potential is correspondingly reduced.

If the diffusion coefficient is limited to a rise of 25% then $T_2\eta_1/T_1\eta_2 < 1.25$. If $T_1 = 20$ °C then $\theta_{max} = 9$ °C. A value of EI_{max} to be used can be calculated

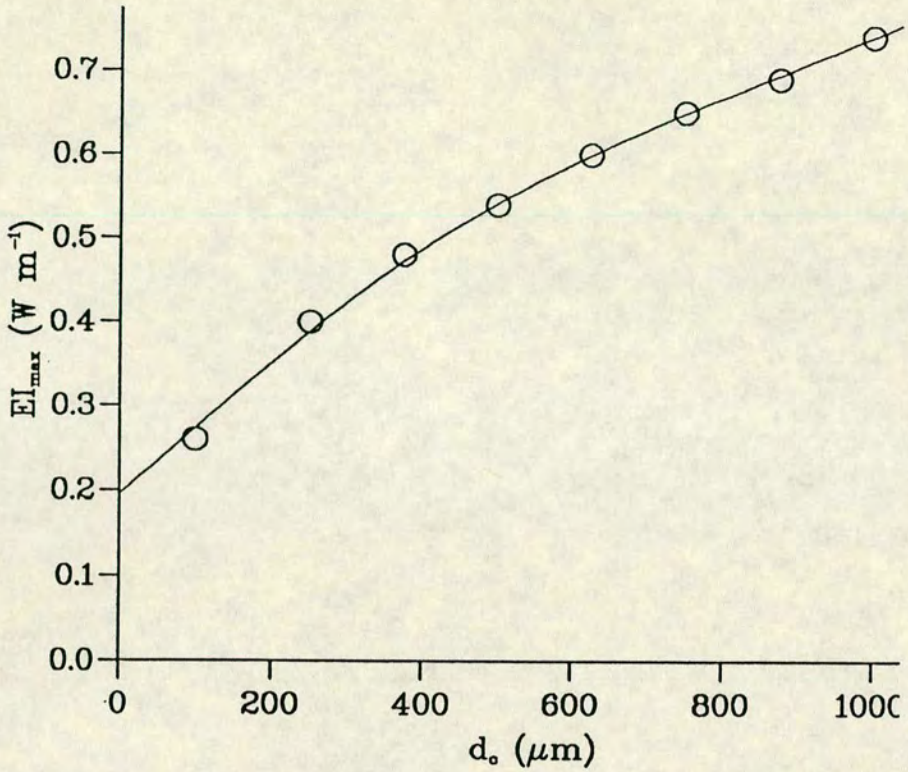

Figure 7.5. EI_{max} for a maximum temperature excess of 9 °C as a function of column outer diameter.

for d_o and is illustrated in figure 7.5 for a temperature excess limited to 9 °C. Obviously an increase in d_o will allow an increase in the maximum power that can be used, and since EI is dependent on E^2, c and r^2, thus an increase in one or other of these parameters is possible. Even so, the maximum power allowable with the above restraint is too low to be practically useful in most situations.

7.3 Forced convection

A solution to preventing excessive temperature rises, as pointed out by Knox is to actively cool the outside of the capillary using a flow of air. Using forced convection, the dimensionless Nusselt number now becomes a function of the

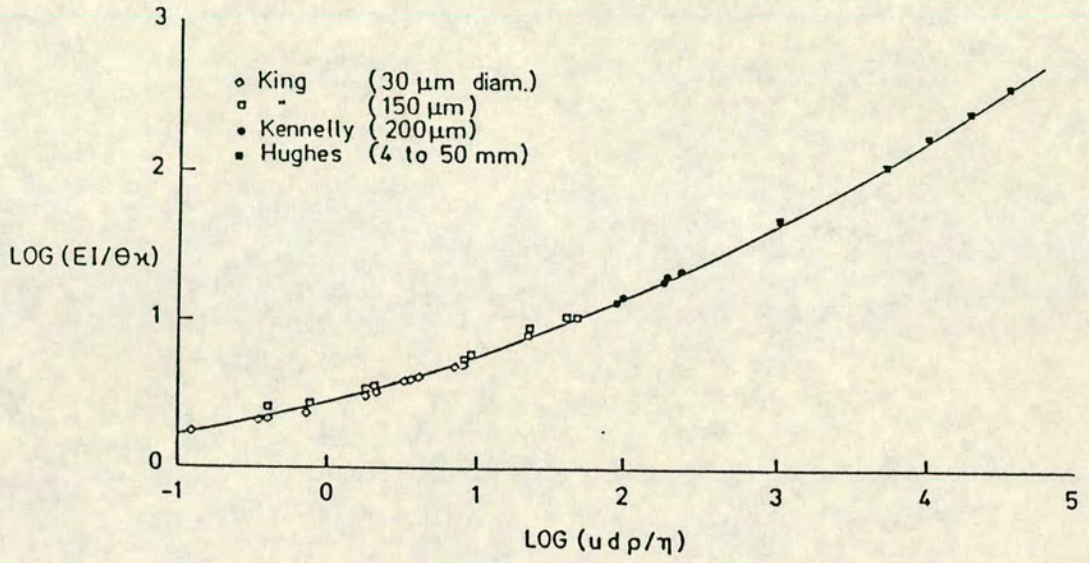

Figure 7.6. Universal plot for forced convective cooling over cylinders after Knox and Roberts.

Reynold's number, well known in fluid dynamics where

$$Re = u_f d_o / \nu \tag{7.32}$$

where u_f is the fluid velocity past the object in question, in this case the capillary. The Nusselt number is a function of the Reynolds number for forced convection. Similar to natural convection, there is a dimensionless plot of $\log Nu$ against $\log Re$ (figure 7.6) adapted by Knox from Roberts. Knox has fitted a curve of the form

$$\log \frac{EI}{k_f \theta} = 0.46 + 0.28 \log \frac{u_f d_o}{\nu} + 0.04 \left(\log \frac{u_f d_o}{\nu} \right)^2 \tag{7.33}$$

through the data. As before, k_f and ν are to be evaluated at the film temperature. Knowing u_f, d_o and EI, equation 7.33 can be used to calculate θ. An iterative process must be used due to the requirement that variables are evaluated at the

Re	n	b
1–4	0.33	0.891
4–40	0.385	0.821
40–4000	0.466	0.615
4000–4 $\times 10^4$	0.618	0.174
4 $\times 10^4$ – 2.5 $\times 10^5$	0.805	0.0239

Table 7.3. b and n for calculating Nu numbers from Re for forced convection.

film temperature, which is unknown. θ can be estimated by first calculating k_f and ν at ambient temperature, calculating a rough value for θ and then modifying the values of k_f and ν used to obtain a more accurate value for θ. Two or three cycles are generally sufficient.

The curve may also be expressed over various ranges by the following

$$Nu = b(Re)^n \tag{7.34}$$

McAdams [138] has given values for b and n depending on Re and these values are given in table 7.3. As d_o in these systems is small (< 0.001 m), Re will always be less than 4000, which limits calculations to the first three sets of values.

Combining equations 7.19 and 7.34 and substituting for Re

$$b\left(\frac{u_f d_o}{\nu}\right)^n = \frac{EI}{\pi\theta k_f} \tag{7.35}$$

Rearranging with the temperature dependent terms on one side

$$\frac{k_f\theta}{\nu^n} = \frac{EI}{\pi b(u_f d_o)^n} \tag{7.36}$$

The values of b and n to be used will depend on which range of Reynold's numbers the calculated value falls into. θ is seen to be proportional to the reciprocal of the product of the fluid velocity and capillary outer diameter. As Nu and k_f are temperature dependent, equation 7.36 does not indicate whether θ is linear

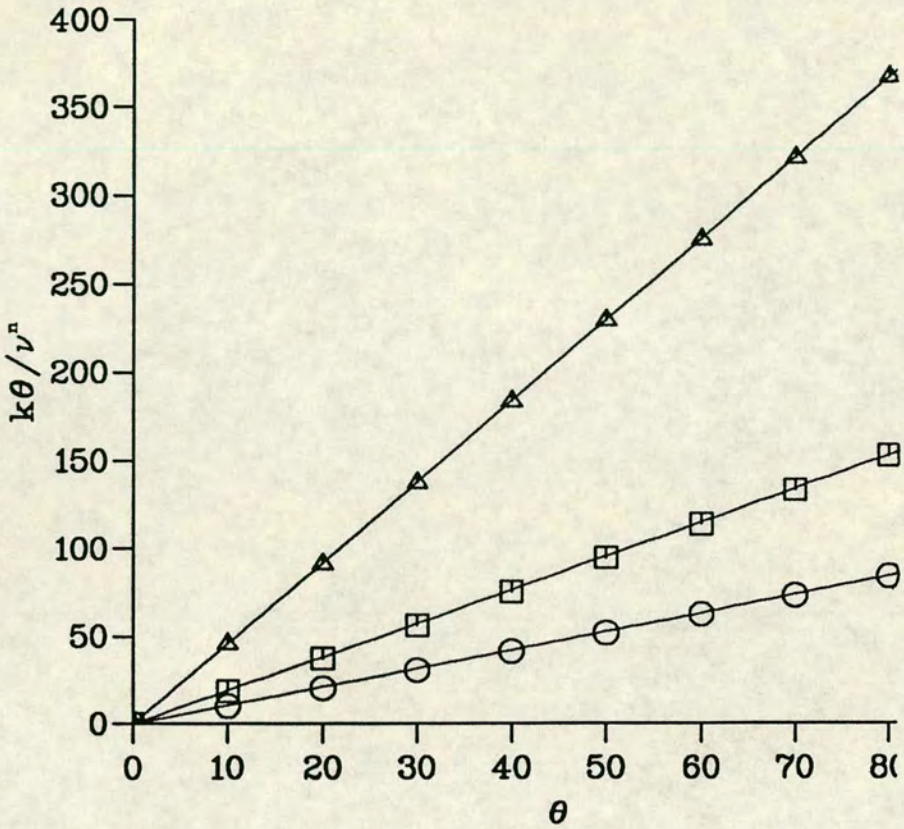

Figure 7.7. $k_f\theta/\nu^n$ vs θ for forced convection. $T_f = 300$ K. $\circ$ $n = 0.33$, $\square$ $n = 0.385$, $\triangle$ $n = 0.466$.

with EI. $k_f\theta/\nu^n$ has been plotted against θ for the three values of n expected to be applicible $(0.33, 0.385, 0.466)$. The data is shown in figure 7.7 where room or ambient temperature has been taken to be 300 K. The data is obviously linear with θ with the slope m increasing as n increases. Replacing $k_f\theta/\nu^n$ in equation 7.36 with $m\theta$ and rearranging

$$\theta = \frac{EI}{\pi m b (u_f d_o)^n} \tag{7.37}$$

For fixed u_f and d_o, θ is thus seen to be linear with EI. The data in table 7.3 can be recalculated to give a range of values of $u_f d_o$ and the corresponding values of m, b and n to be used (table 7.4). The values for $u_f d_o$ have been calculated

Re	$u_f d_o$	b	n	m	Slope
1–4	1.56×10^{-5}–6.25×10^{-5}	0.891	0.33	1.053	$0.3393/(u_f d_o)^{0.33}$
4–40	6.25×10^{-5}–6.25×10^{-4}	0.821	0.385	1.912	$0.2028/(u_f d_o)^{0.385}$
40–4000	6.25×10^{-4}–6.25×10^{-2}	0.615	0.466	4.593	$0.1127/(u_f d_o)^{0.466}$

Table 7.4. Constants for the calculation of θ from EI for forced convective cooling according to equation 7.37.

using ν at 300 K and 'slope' is the value by which EI must be multiplied to give θ i.e. $1/\pi m b(u_f d_o)^n$. m varies slightly with ambient temperature.

The effect of u_f and d_o is illustrated in figure 7.8. The θ values were calculated according to equation 7.37 from table 7.4 at a constant power level of 5 W m^{-1} and some values are given in table 7.5 with values for natural convection calculated according to equation 7.31. The effect of $u_f d_o$ on the temperature rise is quite dramatic, application of $u_f = 0.5$ m s^{-1} more than halving the temperature rise compared to natural convective cooling with the same applied power. While u_f and d_o are seen to have the same effect on θ, in practice it is easier to change u_f. To halve the temperature rise an increase of d_o by a factor of 6 is necessary, from say 250 μm to 1500 μm, while it is easier to increase u_f by the same amount, from say 0.2 to 1.2 m s^{-1}.

Using Knox's equation 7.33, taking logs and letting $g(Re)$ represent the log function $0.46 + 0.28\log(u_f d_o/\nu) + 0.04(\log(u_f d_o/\nu))^2$

$$k_f 10^{g(Re)}\theta = EI \tag{7.38}$$

Again k_f and $g(Re)$ are temperature dependent. $k_f\theta 10^{g(Re)}$ has been evaluated for a range of u_f values with $d_o = 375\mu$m, ambient temperature of 300 K and a variety of θ values. The plots in figure 7.9 are all linear, indicating, as already proven, that θ is linear with EI. However due to the complicated nature of the

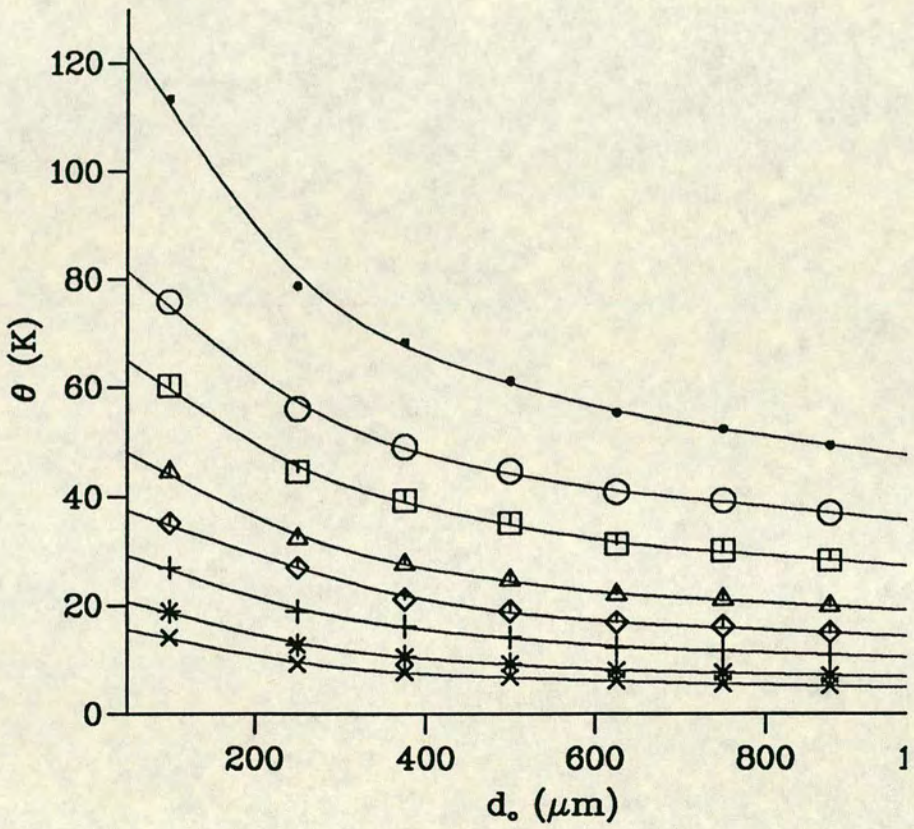

Figure 7.8. Effect of column outer diameter d_o and fluid velocity u_f on the temperature excess within the capillary for a fixed power level of 5 W m^{-1}. Natural convection •, u_f (m s^{-1}): ○ 0.1, □ 0.2, △ 0.5, ◇ 1.0, + 2.0, * 5.0, × 10.0.

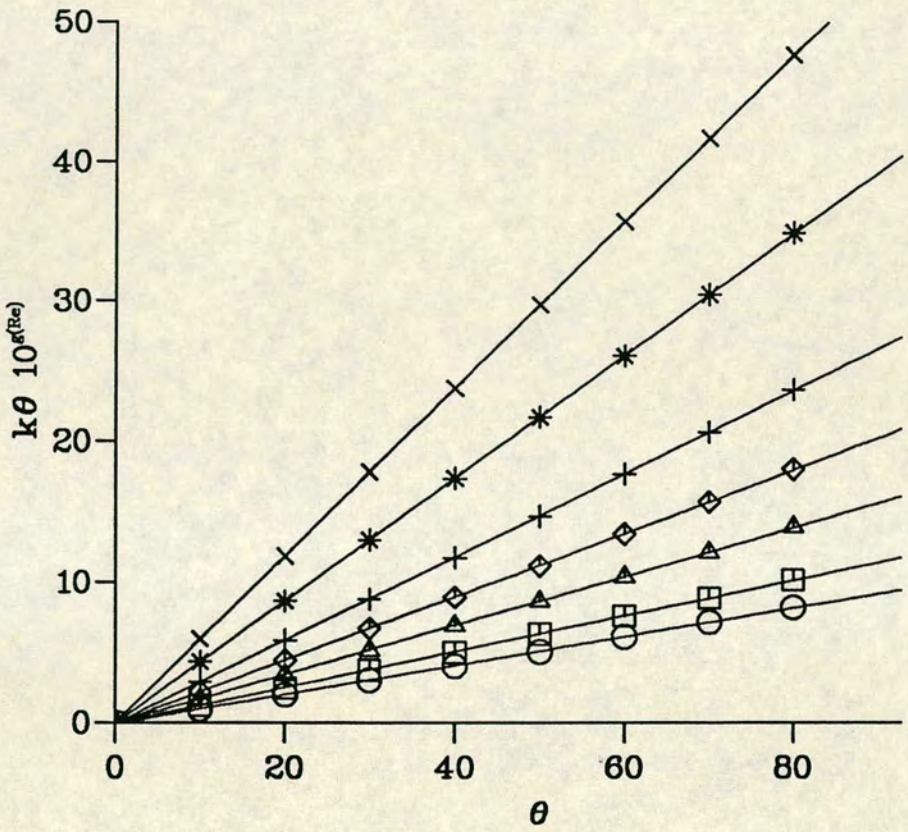

Figure 7.9. $k_f\theta 10^{g(Re)}$ vs θ for the Knox equation where $g(Re) = 0.46 + 0.28\log(u_f d_o/\nu) + 0.04(\log(u_f d_o/\nu))^2$. $T_f = 300$ K. u_f (m s^{-1}): ○ 0.1, □ 0.2, △ 0.5, ◇ 1.0, + 2.0, * 5.0, × 10.0.

u_f m s^{-1} → d_o μm ↓	0.1	0.2	0.5	1.0	2.0	5.0	10	Natural convection
100	75.8	60.3	44.6	35.2	26.9	18.9	14.1	113.4
250	56.0	44.6	32.3	26.9	18.9	12.7	9.2	78.8
375	49.0	39.3	27.6	21.1	16.1	10.5	7.6	68.4
500	44.6	35.2	24.7	18.9	14.1	9.2	6.7	61.2
625	40.9	31.3	22.0	16.9	12.3	8.0	6.0	55.4
750	39.3	30.1	21.1	16.1	11.7	7.6	5.5	52.4
875	37.0	28.3	19.9	15.0	10.9	7.1	5.1	49.4
1000	35.2	26.9	18.9	14.1	10.2	6.7	4.8	47.0

Table 7.5. Temperature rise in capillaries with forced and natural convection as a function of column outer diameter and fluid velocity for a fixed power of 5 W m^{-1}.

u_f m s^{-1} →	0.1	0.2	0.5	1.0	2.0	5.0	10.0
$1/k_f 10^{g(Re)}$	9.78	7.87	5.74	4.44	3.38	2.29	1.68
$1/\pi mb(Re)^n$	9.80	7.86	5.52	4.23	3.22	2.10	1.52

Table 7.6. Comparison of equations 7.37 and 7.38 for the calculation of temperature excesses within the capillary. T_f = 300 K. d_o = 375 μm.

function $g(Re)$, the slopes vary according as $u_f d_o$ is changed and does not present as simple a method of calculating θ as equation 7.37. Equations 7.37 and 7.38 have been compared in table 7.6 for a variety of u_f values with d_o = 375 μm. The values are seen to compare well and thus justify use of the simpler equation 7.37.

θ values for a range of concentrations of $Na_2B_4O_7$ buffer have been obtained in a forced convection system (ABI 270A) operated at 303 K. The values were calculated according to the methods presented in chapter 6 and each value is the average of three separate calculations as before. The plot of θ against EI

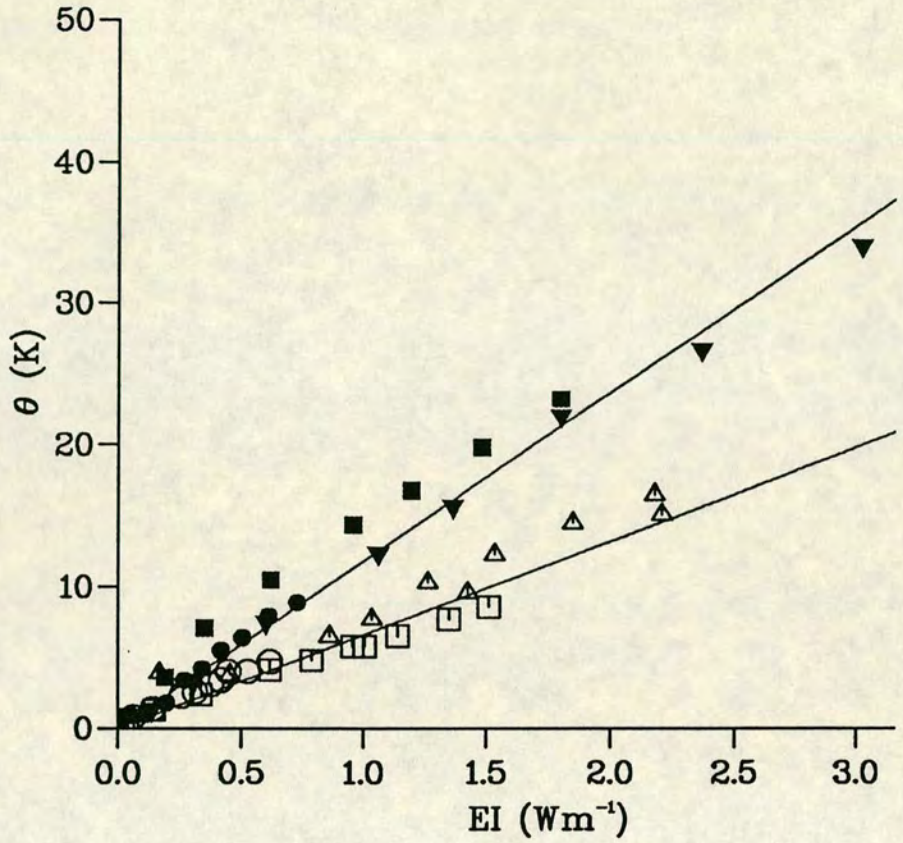

Figure 7.10. Temperature excess vs power generated for systems undergoing natural (filled symbols) and forced (open symbols) convective cooling. Column 50 μm i.d., 375 μm o.d.. Buffer $Na_2B_4O_7$: ○ ● 0.02 M, □ ■ 0.05 M, ▼ 0.0767 M, △ 0.083 M.

is shown in figure 7.10. The best fit least squares gradient is 6.6 K m W^{-1} and is obviously much lower than the data on an equivalent diameter column with natural convection also shown. The dependence of θ on EI is not strictly linear as previously discussed, but is plotted for comparative purposes.

The manufacturers could not supply a value of u_f for the system used. Using equation 7.37, with $d_o = 375$ μm, $m = 1.912$, $b = 0.821$ and $n = 0.385$, $u_f = 0.314$ m s^{-1}. However, the use of a grid is known to increase the turbulence of the fluid and increase the heat dissipating effect of the system. In the ABI system,

u_f m s^{-1} → d_o μm ↓	0.1	0.2	0.5	1.0	2.0	5.0	10.0	Natural convection
100	0.59	0.75	1.01	1.28	1.67	2.38	3.19	0.26
250	0.80	1.01	1.39	1.82	2.38	3.54	4.90	0.40
375	0.92	1.04	1.63	2.13	2.79	4.28	5.91	0.48
500	1.01	1.28	1.82	2.38	3.19	4.90	6.76	0.54
625	1.07	1.39	1.98	2.57	3.54	5.43	7.50	0.60
750	1.15	1.50	2.13	2.79	3.86	5.91	8.17	0.65
875	1.22	1.59	2.26	3.00	4.15	6.35	8.78	0.69
1000	1.28	1.67	2.38	3.19	4.41	6.76	9.34	0.74

Table 7.7. EI_{max} (W m^{-1}) if θ_{max} = 9 K as a function of capillary outer diameter and fluid velocity for natural and forced convective cooling.

there is a grid between the capillary and the fan so the actual air velocity may be less than that calculated.

If as before, D is constrained to increase by less than 25%, so limiting θ to 9 K, it is possible to calculate the maximum power allowed under these conditions. The values of EI_{max} are given in table 7.7 for natural and forced convection using equation 7.37 to calculate EI_{max} for forced convection and equation 7.31 for natural convection. The effect of velocity is very noticeable—a wind/air velocity of 0.2 m s^{-1} doubles the maximum power that can be used compared to natural convection, while an increase of u_f to 1 m s^{-1} more than quadruples the power allowed. Table 7.7 shows most clearly the advantage of using forced convection and larger outer diameters in CZE. As $EI = \pi r^2 \lambda c E^2$ a quadrupling of the power allowed will allow a quadrupling of either c or λ with all other conditions remaining constant or an increase in r or E by a factor of 2, thus allowing greater sensitivity or faster analysis times, or a combination of both.

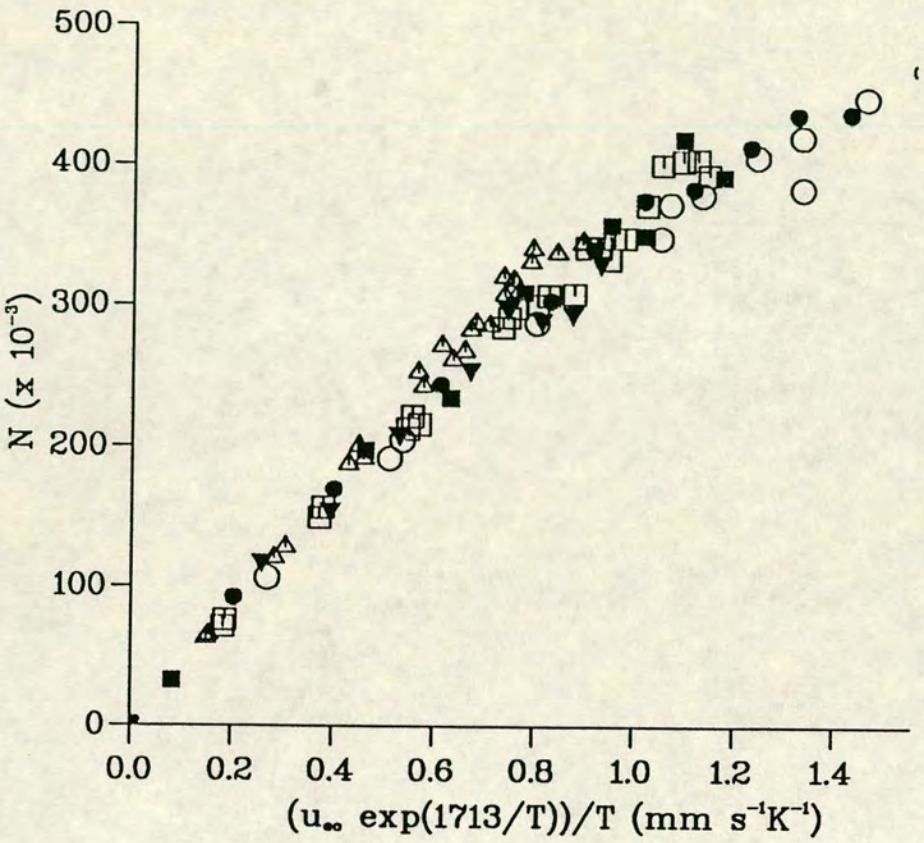

Figure 7.11. Comparison of natural and forced convectively cooled systems. Data for cytosine (uncharged). Open symbols: Forced convection. Closed symbols: Natural convection. Buffer $Na_2B_4O_7$. o • 0.02 M, □ ■ 0.05 M, ▼ 0.077 M, △ 0.083 M.

7.3.1 Comparison of natural and forced convection

The previous chapter has illustrated the fact that curvature of plots of the number of theoretical plates generated against the linear velocity can be 'linearised' by taking into account the temperature of the buffer. This chapter has concentrated on the beneficial aspects of forced convective cooling in prevention of excessive temperature increases. In figures 7.11, 7.12 and 7.13 the number of theoretical plates obtained has been plotted against the linear velocity corrected for temperature for all three samples. Each plot has the results for both nat-

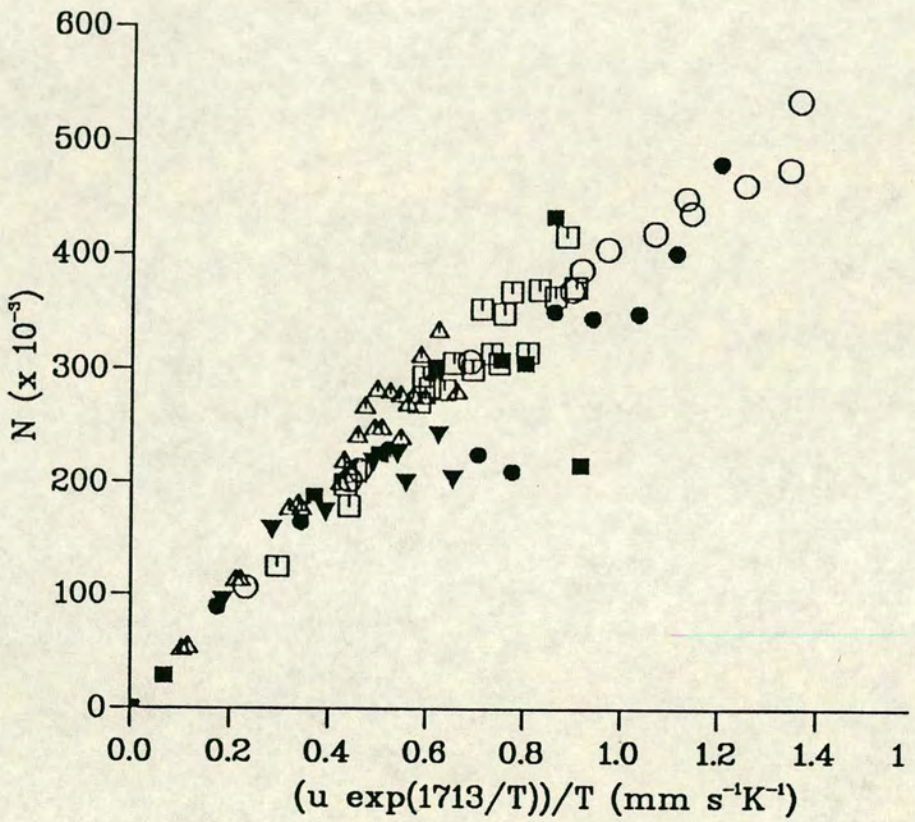

Figure 7.12. Comparison of natural and forced convectively cooled systems. Data for 2-naphthol. Open symbols: Forced convection. Filled symbols: Natural convection. Buffer $Na_2B_4O_7$. ○ ● 0.02 M, □ ■ 0.05 M, ▼ 0.077 M, △ 0.083 M.

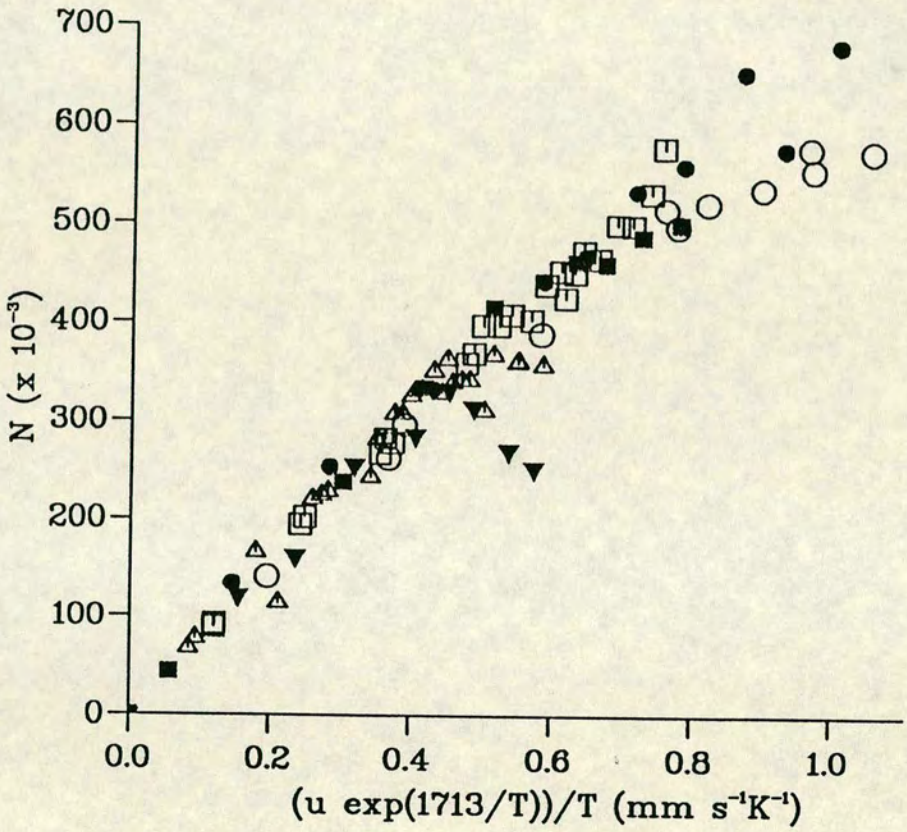

Figure 7.13. Comparison of natural and forced convectively cooled systems. Data for dns-leucine. Open symbols: Forced convection. Filled symbols: Natural convection. Buffer $Na_2B_4O_7$. ○ ● 0.02 M, □ ■ 0.05 M, ▼ 0.077 M, △ 0.083 M.

ural and forced convective cooling for three different concentrations of $Na_2B_4O_7$ buffer. In each case, the data all fall on a common curve. For each plot the data were obtained in different systems, with different capillaries, different buffer concentrations and different ambient temperatures. The fact that all the data falls on a common curve is further proof of the fact that curvature of N vs u plots is due to temperature rises within the capillary and shows that different systems can be compared by the simple means of correcting for the temperature increase.

7.3.2 Use of cooling fluids other than air

Equation 7.37 indicates that the temperature rise also depends on the properties of the fluid. Choosing a fluid with a value of ν^n/k_f smaller than that for air will result in more effective heat dissipation. As liquids in general have higher thermal conductivities and lower kinematic viscosities than gases, using liquids to cool the capillaries would be expected to be more effective than gaseous cooling. The kinematic viscosities, thermal conductivities and Prandtl numbers for a variety of liquids at 298 K are given in table 7.8 from reference [137], along with the values of $1/Nu\pi k_f b$. As this term is the value by which EI must be multiplied to give the temperature excess, the lower this value the better the heat dissipating capacity of the system. Calculation of the Nusselt number with liquids as the coolant is different to that used for gases. The following equation has been taken from McAdams and is due to Ulsamer

$$Nu = b_1(Re)^n(Pr)^m \tag{7.39}$$

where the values of the constants depend on the Reynolds as follows: Re : 0.1–50, $b_1 = 0.91$, $n = 0.385$, $m = 0.31$ and Re : 50–10,000, $b_1 = 0.60$, $n = 0.5$, $m = 0.31$. The table shows that using water as a coolant will give a 180 fold improvement over air as coolant at the same velocity. Due to the high electric

Fluid	ν m^2s^{-1}	k_f $W\ m^{-1}K^{-1}$	Pr	Re	$1/Nu\pi k_f$ $m\ K\ W^{-1}$
Air	1.562×10^{-5}	0.0264	0.7	24.0	4.350
CCl_2F_2	1.960×10^{-5}	0.0720	5.1	19.1	1.730
CCl_4	5.740×10^{-7}	0.1036	8.2	653.3	0.104
Toluene	6.381×10^{-7}	0.1332	7.5	587.7	0.094
$CHCl_3$	3.618×10^{-7}	0.1176	4.5	1036.5	0.088
Hexane	4.534×10^{-7}	0.1246	5.4	827.1	0.088
H_2O	8.540×10^{-7}	0.6090	6.3	439.1	0.023

Table 7.8. Thermodynamic constants of some fluids (taken from reference [137]) and calculated values of $1/Nu\pi k_f$ with $u_f = 1\ m\ s^{-1}$, $d_o = 375\ \mu m$ and $T_f = 298$ K.

fields used in CZE, water is not a practical coolant. However toluene or hexane show an improvement over air of over forty fold. Use of liquid cooling presents great advantages as regards prevention of temperature rises, but will necessitate the development of more sophisticated systems to allow pumping of the fluid along with easy exchange of capillaries and suitable detection. The problems are not insurmountable and the advantages in terms of power levels allowed are substantial. If again a maximum temperature increase of 9 K is allowed, then by using an organic liquid such as hexane as a coolant, the maximum power allowed increases to over 100 $W\ m^{-1}$, compared to 2.13 $W\ m^{-1}$ for air.

7.4 Temperature gradients within the capillary

It has become clear that excessive band broadening due to increased diffusion coefficients of sample molecules as a result of increasing temperatures can be

prevented by using thick walled capillaries with flow of a coolant over the capillary. Prevention of this 'extra' band broadening, or accurate prediction of it, allows other band broadening mechanisms to become important, most noticeably 'thermal' band broadening as described by Knox and Grant [4] and previously discussed in chapter 3. The general consensus appears to be that at power levels currently used, this effect is negligible. The previous discussion has concentrated on the temperature drop between the wall of the capillary and the surrounding fluid, assuming that the temperature gradient across the capillary bore is negligible, which is justified at high θ values. However $T_c - T_1$ or ΔT is linearly related to EI as proved in an earlier section with $\Delta T = EI/4\pi k_w$. As the maximum power allowed increases as a result of cooling or large d_o, the effect of a temperature gradient across the capillary becomes important. According to the section on liquid cooling, it should be possible to use powers of up to 100 W m^{-1} before extra diffusional band broadening becomes excessive. These sort of power levels are unlikely to be ever needed in CZE. With a capillary of 200 μm i.d., $c = 0.05$ M, $\lambda = 0.015$ $m^2\Omega^{-1}mol^{-1}$ and $E = 50$ kV m^{-1} then $EI = 58.9$ W m^{-1}. With adequate cooling, this power level would not be expected to cause an excessive temperature rise. However, $(d_c/\mu m)^3(E\ /kV\ m^{-1})^3(c\ /mol\ l^{-1}) = 8.17 \times 10^{10}$ which exceeds the value of 3.3×10^9 given as an upper limit by Knox if thermal gradients are not to significantly contribute to band broadening. Thus while cooling of the capillary will prevent excessive diffusional band broadening, the ultimate performance of the system is limited by the parabolic temperature gradient developed across the capillary at high power levels.

If the plate height is considered to be a result of diffusional band broadening and the thermal gradient alone, then the total plate height can be expressed as

$$H = \frac{2D\eta}{\epsilon_o\epsilon_r\zeta E} + \frac{7 \times 10^{-9}\epsilon_o\epsilon_r\zeta\lambda^2 d_c^6 c^2 E^5}{D\eta k_{th}^2} \tag{7.40}$$

	$D = 10^{-9}$ m^2 s^{-1}		$D = 5 \times 10^{-10}$ m^2 s^{-1}		$D = 10^{-10}$ m^2 s^{-1}	
d_c μm	E_{max} kV m^{-1}	N_{max} $\times 10^{-3}$ m^{-1}	E_{max} kV m^{-1}	N_{max} $\times 10^{-3}$ m^{-1}	E_{max} kV m^{-1}	N_{max} $\times 10^{-3}$ m^{-1}
50	110.7	1629	87.8	2586	51.4	7552
75	73.8	1086	58.6	1724	34.2	5035
100	55.3	815	43.9	1293	25.7	3776
125	44.3	652	35.1	1034	20.5	3021
150	36.9	543	29.3	862	17.1	2517
175	31.6	465	25.1	739	14.7	2158
200	27.7	407	22.0	647	12.8	1888

Table 7.9. E_{max} and N_{max} as a function of diffusion coefficient of sample and inner diameter of capillary when diffusional and thermal band broadening are present. The power levels in order of decreasing diffusion coefficient are 18.1, 11.4, 3.86 W m^{-1} respectively under these conditions.

As the first term decreases with E and the second term increases with E there will be a value of E for which H is a minimum, or N a maximum. Differentiating equation 7.40, equating with zero, taking square roots and rearranging

$$E_{max}^3 = \frac{7559 D \eta k_{th}}{\epsilon_o \epsilon_r \zeta \lambda d_c^3 c} \tag{7.41}$$

The value of E_{max} for which the minimum plate height is achieved is dependent on a number of factors. Perhaps the most surprising is the fact that E_{max} is weakly dependent on the magnitude of the diffusion coefficient, which will vary from sample to sample. Inserting the values for ϵ_o, η, k_{th} and ϵ_r at 20 °C, fixing $\zeta = 50$ mV and $\lambda = 0.015$ m$^2\Omega^{-1}$mol^{-1}, $c = 0.05$ M then

$$E_{max} = 5533.8 D^{1/3}/d_c \tag{7.42}$$

The values of E_{max} expected under these conditions has been calculated and presented in table 7.9 for a variety of column diameters and diffusion coeffecients. The power level has also been calculated. It is apparent that while the magnitude

of the diffusion coefficient has an effect on the applied voltage at which the maximum number of plates is obtained, the maximum number of plates obtained at this voltage increases as the diffusion coefficient decreases. It is also obvious that while relatively high plate numbers can be obtained from columns with large inner diameters, the maximum plate numbers achieved will never equal those from columns with smaller diameters.

7.5 Conclusions

The main conclusions which can be drawn from the work on capillary zone electrophoresis are as follows:

1. Even under moderate conditions the temperature rise within the capillary is considerable.

2. The temperature rise is detrimental to the performance of the technique through its effect on the diffusion coefficient of the sample, which increases with temperature and thus limits the number of plates which can be obtained from a given separation.

3. The temperature must therefore be eliminated or minimised. Use of thick walled capillaries or forced convective air cooling of the capillary is effective at reducing the temperature excess. Cooling with organic fluids would be even more effective.

4. Even with effective heat dissipation, the ultimate performance of capillary zone electrophoresis is limited by the temperature gradients which exist across the capillary bore at high power levels.

Appendix A

Exact Solution to the P-B Equation

Given from the Poisson-Boltzmann equation that

$$\frac{d^2\psi}{dx^2} = +\frac{2zen_o}{\epsilon_o\epsilon_r}\sinh\left(\frac{ze\psi}{kT}\right) \tag{A.1}$$

Let $A = 2zen_o/\epsilon_o\epsilon_r$ and $B = ze/kT$

$$\frac{d^2\psi}{dx^2} = A\sinh(B\psi) \tag{A.2}$$

Using

$$\frac{d^2\psi}{dx^2} = \frac{1}{2}\frac{d}{d\psi}\left(\frac{d\psi}{dx}\right)^2$$

Then

$$\frac{d}{d\psi}\left(\frac{d\psi}{dx}\right)^2 = 2A\sinh(B\psi) \tag{A.3}$$

Integrating

$$\left(\frac{d\psi}{dx}\right)^2 = \frac{2A}{B}\cosh(B\psi) + C$$

With the boundary conditions that at $x = \infty$, $\psi = 0$ and $d\psi/dx = 0$, $C = -2A/B$ and

$$\left(\frac{d\psi}{dx}\right)^2 = \frac{2A}{B}(\cosh(B\psi) - 1) \tag{A.4}$$

Since $\cosh(2x - 1) = 2\sinh^2 x$

$$\left(\frac{d\psi}{dx}\right)^2 = \frac{4A}{B}\sinh^2\left(\frac{B\psi}{2}\right) \tag{A.5}$$

Taking square roots

$$\frac{d\psi}{dx} = -\sqrt{\frac{4A}{B}}\sinh\left(\frac{B\psi}{2}\right) \tag{A.6}$$

Rearranging

$$\csc\left(\frac{B\psi}{2}\right)d\psi = -\sqrt{\frac{4A}{B}}dx \tag{A.7}$$

Integrating

$$\frac{2}{B}\ln\mid\tanh B\psi/4\mid = -\sqrt{4A/B}x + C \tag{A.8}$$

With the boundary conditions that at $x = 0$, $\psi = \psi_o$, $C = (2/B)\ln\mid\tanh B\psi_o/4\mid$

$$\ln\mid\frac{\tanh B\psi/4}{\tanh B\psi_o/4}\mid = -\sqrt{AB}x$$

and substituting back in for A and B

$$\tanh\mid\frac{ze\psi}{kT}\mid = \tanh\left(\frac{ze\psi_o}{4kT}\right)\exp\left(-\sqrt{\frac{2z^2e^2n_o}{\epsilon_o\epsilon r kT}}x\right) \tag{A.9}$$

Replacing $\sqrt{2z^2e^2n_o/\epsilon_o\epsilon_r kT}$ by κ then

$$\tanh\mid\frac{ze\psi}{kT}\mid = \tanh\left(\frac{ze\psi_o}{4kT}\right)(\exp -\kappa x) \tag{A.10}$$

When $x \leq 0.5 \Rightarrow \tanh x \sim x$ and the equation reduces to the Debye-Huckel approximation $\psi = \psi_o \exp -\kappa x$. When $x \geq 2.7 \Rightarrow \tanh x \rightarrow 1$ and the dependence of ψ on x becomes

$$\psi = \frac{4kT}{ze}\tanh^{-1}(\exp(-\kappa x))$$

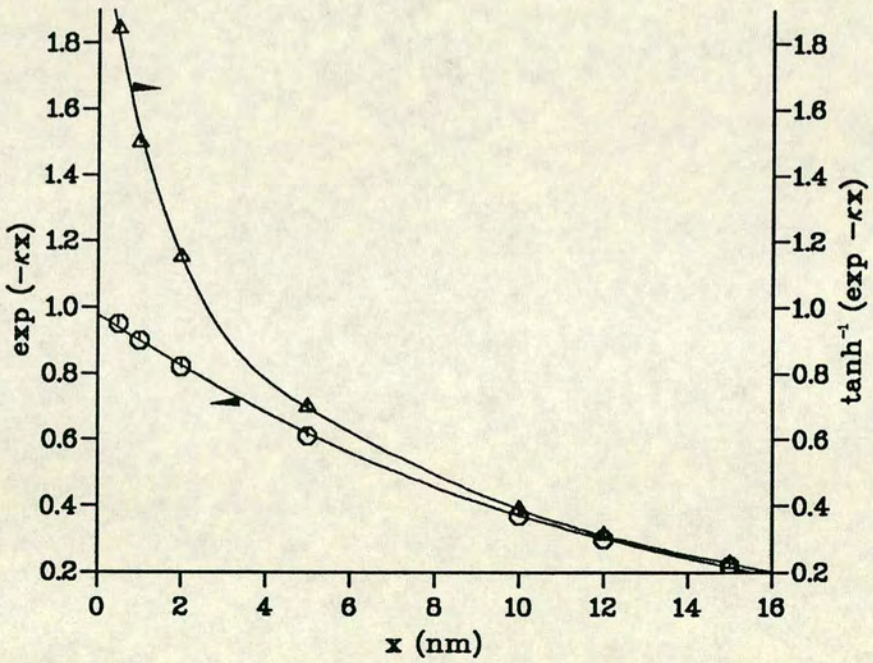

Figure A.1. $\exp(-\kappa x)$ and $\tanh^{-1}(\exp(-\kappa x))$ vs x. $\kappa = 10^8$ m^{-1}

Figure A.1 shows $\exp(-\kappa x)$ and $\tanh^{-1}(\exp(-\kappa x))$ against x where $\kappa = 10^8$ m^{-1} and x varies from 0 to 15 nm. The function $\tanh^{-1}(\exp(-\kappa x))$ falls off much more rapidly than $\exp(-\kappa x)$. Thus at high surface potentials (high surface charge) the diffuse layer does not extend quite so far into the bulk solution. The high surface potentials necessary to satisfy the condition that $\tanh x \rightarrow 1$ are greater than 280 mV, not encountered in practice in CZE where $\psi_o < 200$ mV generally. Using the approximation that $\tanh x \sim x$, even for surface potentials as high as 100 mV leads to a 30 % error, which is acceptable.

Philip and Wooding [139] have made the following approximation

$$\sinh x = x \quad 0 \leq x < 1 \tag{A.11}$$

$$\sinh x = (1/2)\exp x \quad x > 1 \tag{A.12}$$

Equation A.10 is the previously defined Debye-Huckel approximation where at room temperature, ψ must be less than 25 mV to fulfil the condition. For CE experiments in which ζ or ψ are normally greater than 25 mV, equation A.12 should be applicable.

Appendix B

Surface Charge and Potential

The relationship between σ_o and ψ_o, where σ_0 is the charge at the Outer Helmholtz Plane and ψ_o is the potential at that point, is obtained by intergrating the ρ, the charge excess, over the solution

$$\sigma_o = \int_0^\infty -\rho dx \tag{B.1}$$

Substituting in equations 2.5 and A.6

$$\sigma_o = -\sqrt{\frac{\epsilon_o \epsilon_r z^2 e^2 n_o}{2kT}} \int_{\psi_o}^0 \frac{\sinh ze\psi/kT}{\sinh ze\psi/2kT} d\psi \tag{B.2}$$

Since $\sinh 2x / \sinh x = -2\cosh x$

$$\sigma_o = +\sqrt{\frac{2\epsilon_o \epsilon_r z^2 e^2 n_o}{kT}} \int_{\psi_o}^0 \cosh\left(\frac{ze\psi}{2kT}\right) d\psi \tag{B.3}$$

Integrating

$$\sigma_o = \sqrt{8\epsilon_o \epsilon_r n_o kT} \sinh \frac{ze\psi_o}{kT} \tag{B.4}$$

Using the Debye-Huckel approximation that $\sinh x = x$ for small x and rearranging

$$\sigma_o = \epsilon_o \epsilon_r \kappa \psi_o \tag{B.5}$$

where κ has been previously defined.

Appendix C

Natural Convection Data

The data in the following tables in this appendix have been obtained on the home-made system 2 described in chapter 4, and have been used in the figures of chapter 6.

E kV m^{-1}	I μA	u^*_{eo}	u^*_n	u^*_l	N_c $\times10^{-3}$	N_n $\times10^{-3}$	N_l $\times10^{-3}$
2	0.30	0.149	0.135	0.117	66	71	109
4	0.60	0.294	0.267	0.231	110	123	179
8	1.13	0.575	0.521	0.451	213	284	379
12	1.73	0.872	0.791	0.685	270	404	539
16	2.35	1.183	1.073	0.925	270	480	646
20	2.80	1.428	1.290	1.116	251	546	729
22	3.07	1.571	1.416	1.227	243	563	795
24	3.45	1.754	1.580	1.347	-	541	814
26	3.65	1.896	1.704	1.484	-	495	801
28	4.00	2.051	1.848	1.605	-	556	859
30	4.33	2.194	1.977	1.713	264	614	818

Table C.1. Data for 0.004 M $Na_2B_4O_7$. Capillary 50 μm i.d., 375 μ o.d., 1000 mm long, 790 mm to detector. Concentration of samples: cytosine 3.1 $\times10^{-4}$ M, 2-naphthol 1 $\times10^{-4}$ M, dns-leucine 8.8 $\times10^{-5}$ M. Injection 2 kV for 7 s. Ambient temperature 20 °C. c, n, and l represent the samples cytosine (neutral), 2-naphthol and dns-leucine respectively and N is the number of theoretical plates generated. * in mm s^{-1}.
η_{ave} and T_{ave} are the calculated average viscosities and capillary temperatures respectively.

E kV m^{-1}	I μA	u^*_{eo}	u^*_n	u^*_l	N_c $\times10^{-3}$	N_n $\times10^{-3}$	N_l $\times10^{-3}$	η_{ave} cp	T_{ave} °C
4	3.2	0.176	0.151	0.126	92	89	134	0.984	20.8
8	6.4	0.348	0.297	0.246	169	165	253	0.981	20.9
12	9.3	0.531	0.452	0.374	243	229	333	0.977	21.0
16	12.3	0.734	0.623	0.518	303	225	442	0.959	21.8
18	14.9	0.839	0.712	0.592	340	210	467	0.925	23.4
20	17.0	0.950	0.805	0.670	375	351	533	0.905	24.2
22	19.0	1.073	0.904	0.754	383	345	559	0.882	25.5
24	21.0	1.205	1.015	0.852	413	349	653	0.866	26.4
26	23.5	1.341	1.128	0.942	436	402	576	0.838	27.9
28	26.0	1.481	1.247	1.044	437	481	681	0.818	28.9

Table C.2. Data for 0.02 M $Na_2B_4O_7$. Injection 2 kV for 10 s. All other conditions as table C.1. * in mm s^{-1}.

E kV m^{-1}	I μA	u^*_{eo}	u^*_n	u^*_l	N_c $\times 10^{-3}$	N_n $\times 10^{-3}$	N_l $\times 10^{-3}$	η_{ave} cp	T_{ave} ^{o}C
2	2.3	0.071	0.059	0.049	32	29	44	0.995	20.3
12	16	0.427	0.341	0.280	197	188	238	0.915	23.6
16	22	0.630	0.502	0.418	234	225	334	0.852	27.1
20	31	0.836	0.664	0.555	309	302	415	0.787	30.5
24	40	1.111	0.880	0.740	357	309	461	0.719	34.4
26	46	1.256	0.989	0.831	350	306	459	0.683	36.8
28	53	1.436	1.130	0.952	419	433	487	0.644	39.8
30	60	1.650	1.289	1.096	392	216	500	0.602	43.2

Table C.3. Data for 0.05 M $Na_2B_4O_7$. * in mm s^{-1}. Injection 2 kV for 12 s. All other conditions as for table C.1.

E kV m^{-1}	I μA	u^*_{eo}	u^*_n	u^*_l	N_c $\times 10^{-3}$	N_n $\times 10^{-3}$	N_l $\times 10^{-3}$	η_{ave} cp	T_{ave} ^{o}C
8	17	0.226	0.163	0.135	118	97	121	0.971	21.3
12	26	0.357	0.258	0.214	155	161	162	0.934	23.4
16	37.5	0.535	0.395	0.322	209	177	255	0.844	27.5
20	53	0.751	0.550	0.456	255	221	286	0.753	32.4
22	62	0.896	0.649	0.546	298	228	333	0.700	35.7
24	75	1.114	0.764	0.670	290	203	315	0.616	42.0
26	91	1.317	0.939	0.812	295	245	271	0.567	46.7
28	108	1.617	1.138	1.000	331	206	253	0.504	54.1

Table C.4. Data for 0.083 M $Na_2B_4O_7$. * in mm s^{-1}. Injection 2 kV for 12 s. All other conditions as for table C.1.

E kV m^{-1}	I μA	u^*_{eo}	u^*_n	u^*_l	N_c $\times 10^{-3}$	N_n $\times 10^{-3}$	N_l $\times 10^{-3}$	η_{ave} cp	T_{ave} °C
1	1	0.045	0.039	0.032	20	28	33	1.129	-
4	5	0.200	0.175	0.145	84	95	124	0.974	21.2
8	10	0.425	0.370	0.312	176	193	263	0.962	21.7
12	15.8	0.658	0.574	0.483	213	280	382	0.925	23.3
14	18.6	0.755	0.659	0.549	250	316	377	0.910	23.9
16	22.5	0.924	0.803	0.677	228	368	492	0.873	26.0
18	25.8	1.033	0.898	0.749	262	390	499	0.849	27.2
20	30.5	1.279	1.100	09.38	250	453	577	0.794	30.1
21	31.8	1.286	1.113	0.930	285	443	506	0.797	30.0
22	34.8	1.425	1.232	1.043	293	427	548	0.777	31.1
24	42.9	1.752	1.500	1.295	254	471	632	0.695	36.0
25	42.5	1.716	1.483	1.250	264	481	678	0.715	34.7
26	45.8	1.906	1.634	1.391	262	445	547	0.688	36.4
27	48.5	1.924	1.658	1.398	271	488	686	0.683	36.8
28	54.8	2.209	1.886	1.610	230	492	630	0.632	40.6
30	60.2	2.470	2.098	1.798	220	461	542	0.599	43.5

Table C.5. Data for 75 μ i.d. capillary. * in mm s^{-1}. All other conditions as for table C.1.

E kV m^{-1}	I μA	u^*_{eo}	u^*_n	u^*_l	N_c $\times 10^{-3}$	N_n $\times 10^{-3}$	N_l $\times 10^{-3}$	η_{ave} cp	T_{ave} °C
1	-	0.046	0.041	0.033	20	16	32	1.000	20.1
4	7.5	0.187	0.164	0.127	81	108	122	0.944	22.5
8	16.5	0.389	0.344	0.278	170	210	204	0.926	23.3
12	25.8	0.666	0.584	0.477	257	273	329	0.837	27.9
16	38.0	0.977	0.850	0.702	354	331	461	0.762	31.9
18	-	1.057	0.927	0.766	395	419	510	0.794	30.2
20	56.0	1.456	1.240	1.061	337	333	491	0.649	39.3
21	-	1.391	1.210	1.004	405	535	507	0.700	35.7
22	67.5	1.720	1.454	1.243	361	409	504	0.596	43.8
24	82.0	2.105	1.765	1.525	369	408	486	0.534	50.3
25	87.5	2.257	1.894	1.612	372	376	410	0.513	52.9
26	102.5	2.498	2.083	1.800	355	407	417	0.477	57.9
28	121.5	2.989	2.473	2.140	320	310	359	0.428	65.7

Table C.6. Data for 100 μm i.d., 250 μm o.d. capillary. * in mm s^{-1}. All other conditions as table C.1.

E kV m^{-1}	I μA	u^*_{eo}	u^*_n	u^*_l	N_c $\times 10^{-3}$	N_n $\times 10^{-3}$	N_l $\times 10^{-3}$	η_{ave} cp	T_{ave} °C
4	15.8	0.205	0.183	0.146	86	70	115	0.8511	-
8	37.5	0.486	0.430	0.356	185	195	243	0.885	25.3
12	67.5	0.873	0.764	0.641	214	237	324	0.684	36.7
14	86.2	1.108	0.972	0.809	230	267	366	0.624	41.3
16	112.5	1.454	1.264	1.059	242	276	321	0.544	49.3
18	150.0	1.830	1.582	1.324	234	221	292	0.475	58.2

Table C.7. Data for 150 μm i.d., 250 μm o.d. capillary. * in mm s^{-1}. All other conditions as for table C.1.

Appendix D

Forced Convection Data

The data presented in the following tables in this appendix have been obtained with the ABI Instrument, Model 270A and have been used in the figures of chapter 7.

E kV m^{-1}	I μA	u^*_{eo}	u^*_n	u^*_l	N_c $\times 10^{-3}$	N_n $\times 10^{-3}$	N_l $\times 10^{-3}$	η_{ave} cp	T_{ave} °C
5	3.0	0.288	0.247	0.209	106	106	141	0.793	30.2
10	6.2	0.581	0.499	0.422	204	211	296	0.783	30.8
10	6.2	0.553	0.476	0.398	191	202	262	0.783	30.7
15	9.5	0.879	0.753	0.640	287	307	389	0.772	31.4
15	9.5	0.840	0.721	0.606	271	281	382	0.769	31.5
20	12.9	1.195	1.025	0.868	372	387	497	0.756	32.3
20	12.9	1.146	0.983	0.825	352	372	489	0.757	32.2
20	13.0	1.179	1.007	0.853	348	369	515	0.753	32.5
22	14.2	1.275	1.092	0.921	379	405	521	0.750	32.6
22	14.4	1.299	1.110	0.941	405	411	522	0.729	33.8
24	15.7	1.412	1.212	1.019	406	419	536	0.742	33.1
24	15.8	1.438	1.227	1.040	416	409	570	0.744	32.9
25	16.7	1.523	1.303	1.110	420	450	555	0.737	33.4
25	16.3	1.459	1.250	1.055	404	438	553	0.739	33.3
26	17.2	1.545	1.323	1.119	383	437	577	0.727	34.0
26	17.4	1.570	1.339	1.138	422	426	590	0.733	33.6
28	18.7	1.693	1.452	1.224	448	462	574	0.727	34.0
28	18.7	1.719	1.465	1.244	404	454	630	0.722	34.2
30	20.5	1.880	1.608	1.365	460	536	641	0.714	34.7
30	20.3	1.827	1.564	1.319	449	525	598	0.708	35.1
30	20.3	1.862	1.585	1.347	469	476	658	0.712	34.9

Table D.1. Data for 0.02 M $Na_2B_4O_7$. * in mm s^{-1}. Column 50 μm i.d., 375 μm o.d., 1000 mm long, 780 mm to detection zone. Ambient temperature 30 °C. Detection 200 nm UV. Concentration of samples: Cytosine (uncharged) 3×10^{-4} M, 2-naphthol 1.8×10^{-4} M, dns-leucine 1.98×10^{-4} M. Injection 5 kV 4.0 s. c, n, and l represent the samples cytosine, 2-naphthol and dns-leucine and N is the number of theoretical plates generated. η_{ave} and T_{ave} are the calculated average viscosities and capillary temperatures respectively.

E kV m^{-1}	I μA	u^*_{eo}	u^*_n	u^*_l	N_c $\times 10^{-3}$	N_n $\times 10^{-3}$	N_l $\times 10^{-3}$	η_{ave} cp	T_{ave} °C
5	7.1	0.196	0.155	0.128	71	-	89	0.792	30.3
5	7.2	0.202	0.160	0.131	76	-	92	0.784	30.7
10	14.6	0.415	0.296	0.272	156	158	202	0.773	31.3
10	15.2	0.410	0.325	0.267	149	125	194	0.767	31.6
15	22.4	0.639	0.508	0.420	215	209	277	0.754	32.4
15	23.3	0.630	0.499	0.412	221	179	282	0.746	32.9
15	23.3	0.613	0.484	0.399	212	198	267	0.755	32.3
20	30.8	0.866	0.703	0.583	298	284	397	0.726	34.1
20	32.2	0.872	0.690	0.570	291	294	369	0.722	34.3
20	31.3	0.840	0.665	0.547	284	271	359	0.734	33.3
22	35.8	0.975	0.772	0.639	307	306	408	0.713	34.8
22	34.9	0.931	0.736	0.607	300	282	397	0.727	34.0
24	39.8	1.085	0.858	0.711	341	353	438	0.698	35.8
24	38.9	1.034	0.818	0.672	308	300	403	0.713	34.8
25	40.2	1.152	0.914	0.760	348	349	450	0.698	35.8
25	40.9	1.123	0.886	0.738	341	314	452	0.695	36.0
26	43.8	1.196	0.946	0.786	348	368	472	0.687	36.5
26	43.1	1.136	0.897	0.741	333	306	425	0.701	35.6
28	48.1	1.319	1.041	0.866	400	370	499	0.670	37.7
28	47.1	1.255	0.991	0.817	371	315	464	0.685	36.7
30	50.3	1.465	1.157	0.967	393	372	577	0.658	38.6
30	52.9	1.445	1.139	0.949	404	416	513	0.654	38.9
30	51.8	1.378	1.087	0.897	403	364	498	0.667	37.9

Table D.2. Data for 0.0507 M $Na_2B_4O_7$. * in mm s^{-1}. Injection 5 kV 4.8 s. All other conditions as for table D.1.

E kV m^{-1}	I μA	u^*_{eo}	u^*_n	u^*_l	N_c $\times 10^{-3}$	N_n $\times 10^{-3}$	N_l $\times 10^{-3}$	η_{ave} cp	T_{ave} °C
5	9.1	0.167	0.125	0.102	65	53	77	0.782	30.8
5	8.4	0.161	0.112	0.091	63	51	67	0.790	30.4
10	16.8	0.352	0.256	0.208	128	112	166	0.729	33.9
10	18.5	0.314	0.233	0.189	-	-	-	0.770	31.5
10	19.0	0.312	0.233	0.185	120	112	114	0.769	31.6
15	30.2	0.532	0.398	0.326	191	176	228	0.730	33.8
15	29.1	0.494	0.368	0.326	187	176	220	0.733	33.6
15	33.3	0.541	0.405	0.328	200	180	224	0.701	35.6
20	43.0	0.750	0.560	0.460	271	240	308	0.688	36.5
20	41.4	0.677	0.504	0.409	242	218	281	0.691	36.3
20	41.4	0.704	0.524	0.428	252	198	243	0.705	35.3
22	47.0	0.798	0.593	0.486	261	266	308	0.670	37.7
22	51.2	0.827	0.616	0.502	267	247	326	0.670	37.7
24	52.6	0.902	0.671	0.549	287	247	332	0.636	40.3
24	51.9	0.864	0.641	0.523	282	281	331	0.652	39.0
25	57.0	1.000	0.745	0.615	310	275	342	0.645	39.6
25	55.9	0.956	0.709	0.585	285	279	351	0.624	41.3
25	63.2	1.004	0.743	0.604	307	276	329	0.619	41.7
26	59.0	1.015	0.753	0.622	320	238	363	0.613	42.3
26	63.0	1.018	0.755	0.618	318	268	339	0.626	41.2
28	66.0	1.139	0.845	0.698	331	311	357	0.589	44.5
28	68.9	1.125	0.835	0.638	340	274	342	0.598	43.6
30	73.6	1.303	0.965	0.804	345	279	361	0.582	45.1
30	74.4	1.305	0.968	0.805	344	278	360	0.581	45.2
30	72.6	1.265	0.936	0.776	337	333	368	0.568	46.5
30	72.3	1.204	0.890	0.732	344	295	311	0.584	44.9

Table D.3. Data for 0.0767 M $Na_2B_4O_7$. * in mm s^{-1}. Injection 5 kV 5.0 s. All other conditions as for table D.1.

Appendix E

Glossary of symbols

A, B, b, C	constants
a	capillary or ion radius
c	buffer concentration
D	diffusion coeffecient (m^2s^{-1})
d_c	capillary inner diameter
d_o	capillary outer diameter
d_p	particle diameter
E	electric field gradient
e	electronic charge (1.602×10^{-19}C)
F	Faraday constant (96487 C mol^{-1})
f	volume flow rate
G	acceptable increase in H relative to the theoretical minimum
g	heat generation rate (W m^{-3})
g	acceleration due to gravity (9.81 m^2s^{-1})
$g(Re)$	log function of Reynolds number
Gr	Grashof number
H	absolute value of plate height

h	reduced plate height ($h = H/d_p$)
H	difference in levels of buffer reservoirs
I	current
I_o	zero order modified Bessel function of the first kind
k	Boltzmann constant (1.3806×10^{-23} J K^{-1})
k_e	specific or electrical conductivity (Ω^{-1} m^{-1})
k_{th}	thermal conductivity (W $m^{-1}K^{-1}$)
k_f	thermal conductivity of fluid surrounding capillary
k_w	thermal conductivity of water
k_s	thermal conductivity of silica
k_p	thermal conductivity of polyimide coating
k'	phase capacity ratio
L	length of capillary or column
l_{eff}	effective length of capillary to detection zone
l_{inj}	length of injection zone
l_{det}	length of detection zone
l_{exp}	length of sample expelled from capillary due to volume expansion
m	mass of buffer in capillary
m	constant
N	number of theoretical plates
N_A	Avogadro's number (6.023×10^{23} mol^{-1})
Nu	Nusselt number
Pr	Prandtl number
ΔP	Pressure gradient
Q	rate of heat flow (W)
q	effective charge on ion

q	heat flux (W m^{-2})
R	universal gas constant (8.314 J $K^{-1}mol^{-1}$)
Ra	Rayleigh number
Re	Reynolds number
Rs	resolution
r	capillary radius
T	temperature
T_{film}	film temperature or average temperature of capillary wall and surrounding fluid
ΔT	temperature across capillary bore
t	time
t_r	retention time
u	linear velocity
u_f	velocity of fluid flow (for forced convection)
u_{eo}	electro-osmotic velocity
V	applied voltage
β	reciprocal of film temperature
δ	double layer thickness
ϵ	porosity of packed bed
ϵ_o	permittivity of free space (8.85×10^{-12} $C^2N^{-1}m^{-2}$)
ϵ_r	dielectric constant
η	coefficient of viscosity (kg $m^{-1}s^{-1}$)
κ	reciprocal of double layer thickness
λ	molar conductivity ($m^2\Omega^{-1}mol^{-1}$)
μ_{eo}	electro-osmotic mobility
μ_{ep}	electrophoretic mobility
ν	reduced velocity ($\nu = ud_p/D$)

ν	kinematic viscosity (η/ρ) (m^2s^{-1})
ρ	density
σ^2	peak variance
σ_o	charge on Outer Helmholtz Plane
τ	time constant
ψ_o	potential at Outer Helmholtz Plane
ψ_s	potential at surface
θ	temperature excess
ζ	zeta potential at plane of shear of liquid and surface

Appendix F

Courses and conferences attended

In accordance with the University of Edinburgh regulations the following lecture courses and conferences were attended throughout the period of study.

1. FORTRAN Programming
2. EMAS Scribe Course
3. Surface Chemistry
4. Theoretical Chemistry
5. Membrane Science
6. Chromatography
7. Recent Advances in Physical Chemistry
8. Surfaces and Interfaces
9. Meetings of the East of Scotland HPLC Users Group
10. 13th Symposium on Column Liquid Chromatography, 1989
11. 14th Symposium on Column Liquid Chromatography, 1990
12. International Symposium on Capillary Electrophoresis, 1990
13. 18th International Symposium on Chromatography, 1990

Bibliography

[1] Michaelis L., Biochem. Zeit. **1909** *16* 81

[3] Lodge O., British Association Reports **1886**

[2] Picton, Linder, J. Chem. Soc. **1892** *61* 148

[4] Knox J.H., Grant I.H., Chromatographia **1987** *24* 135

[5] Tsuda T., Anal. Chem. **1987** *59* 521

[6] Tiselius A., Trans. Faraday Soc. **1937** *33* 524

[7] Hjerten S., Chromatogr. Rev. **1967** *2* 122

[8] Brakke M.K., Arch. Biochem. Biophys. **1955** *55* 175

[9] Smith I., Chromatographic and Electrophoretic Techniques, 2nd Edition **1968** *II* 217

[10] Ornstein L., Ann. N.Y. Acad. Sci. **1964** *121* 321

[11] Davis B.T., Ann. N.Y. Acad. Sci. **1964** *121* 404

[12] Catsimpoolas N., Separ. Sci. **1973** *8* 71

[13] Laurell C.B., Anal. Biochem. **1965** *10* 358

[14] Laurell C.B., Anal. Biochem. **1966** *15* 45

[15] Jorgenson J.W., Lukacs K.D., Anal. Chem. **1981** *53* 1298

[16] Mikkers F.E.P., Everaerts F.M., Verheggen Th.P.E.M., J. Chromatogr. **1979** *169* 11

[17] Jorgenson J.W., Lukacs K.D., Clin. Chem. **1981** *27* 1551

[18] Jorgenson J.W., Lukacs K.D., J. Chromatogr **1981** *218* 209

[19] Olefirowicz T.M., Ewing A.G., Anal. Chem. **1990** *62* 1872

[20] Hjerten S., J. Chromatogr. **1985** *347* 191

[21] Altria K.D., Simpson C.F., Anal. Proc. **1986** *23* 453

[22] Wallingford R.A., Ewing A.G., Anal. Chem. **1987** *59* 1762

[23] Huang X., Luckey J.A., Gordon M.J., Zare R.N., Anal. Chem. **1989** *61* 766

[24] Yu M., Dovichi N.J., Mikrochim. Acta (Wien) **1988** *III* 27

[25] Liu J., Shirota O., Novotny M., Anal. Chem. **1991** *63* 413

[26] Nickerson B., Jorgenson J.W., J. H.R.C. & C.C. **1988** *11* 878

[27] Christenson P.L., Yeung E.S., Anal. Chem. **1989** *61* 1344

[28] Sweedler J.V., Shear J.B., Fishman H.A., Zare R.N., Sheller R.H., Anal . Chem. **1991** *63* 496

[29] Chen C.Y., Demana T., Huang S.D., Morris M.D., Anal. Chem. **1989** *61* 1590

[30] Pentoney S.L., Zare R.N., Quint J.F., Anal. Chem. **1989** *61* 1642

[31] Lee E.D., Muck W., Henion J.D., Covey T.R., J. Chromatogr. **1988** *458* 313

[32] Smith R.D., Olivares J.A., Nguyen N.T., Udseth H.R., Anal. Chem. **1988** *60* 436

[33] Kuhr W.G., Yeung E.S., Anal. Chem. **1988** *60* 2642

[34] Lauer H.H., McManigill D., Tr.A.C. **1986** *5* 11

[35] Grossman P.D., Colburn J.C., Lauer H.H., Nielsen R.G., Riggin R.M., Sittampalam G.S., Rickard E.C., Anal. Chem. **1989** *61* 1186

[36] Gross L., Yeung E.S., J. Chromatogr. **1989** *480* 169

[37] Tsuda T., Nomura K., Nakagawa G., J. Chromatogr. **1983** *264* 385

[38] Fujiwara S., Honda S., Anal. Chem. **1986** *58* 1811

[39] Wainwright A., J. Microcol. Sep. **1990** *2* 166

[40] Altria K.D., Simpson C.F., J. Pharm. Biomed. Anal. **1988** *6* 801

[41] Van Orman B.B., McIntire G.L., J. Microcol. Sep. **1989** *1* 289

[42] Lauer H.H., McManigill D., Anal. Chem. **1986** *58* 166

[43] Grossman P.D., Soane D.S., Anal. Chem. **1990** *62* 1592

[44] Zhu A., Chen Y., J. Chromatogr. **1989** *470* 251

[45] Terabe S., Otsuka K., Ichikawa K., Tsuchiya A., Ando T., Anal. Chem. **1984** *56* 111

[46] Wallingford R.A., Curry P.D., Ewing A.G., J. Microcol. Sep. **1989** *1* 23

[47] Rasmussen H.T., Goebel L.K., McNair H.M., J. Chromatogr. **1990** *517* 549

[48] Nishi H., Tsumagari N., Terabe S., Anal. Chem. **1989** *61* 2434

[49] Cohen A.S., Terabe S., Smith J.A., Karger B.L., Anal. Chem. **1987** *59* 1021

[50] Nishi H., Fukuyama T., Matsuo M., Terabe S., J. Microcol. Sep. **1989** *1* 234

[51] Dobashi A., Ono T., Hara S., Yamaguchi J., Anal. Chem. **1989** *61* 1984

[52] Otsuka K., Terabe S., Ando T., J. Chromatogr. **1985** *348* 39

[53] Nishi H., Tsumagari N., Kakimoto T., Terabe S., J. Chromatogr. **1989** *465* 331

[54] Saitoh T., Hoshino H., Yotsuyanagi T., J. Chromatogr. **1989** *465* 175

[55] Swaile D.F., Burton D.E., Balchunas A.T., Sepaniak M.J., J. Chromatogr. Sci. **1988** *26* 406

[56] Liu J., Banks F., Novotny M., J. Microcol. Sep. **1989** *1* 137

[57] Northrop D.M., Martire D.E., MacCrehan W.A., Anal. Chem. **1991** *63* 1038

[58] Weinberger R., Lurie I.S., Anal. Chem. **1991** *63* 823

[59] Walbroehl Y., Jorgenson J.W., Anal. Chem. **1986** *58* 479

[60] Gozel P., Gassmann E., Michelsen H., Zare R.N., Anal. Chem. **1987** *59* 44

[61] Swaile D.F., Sepaniak M.J., Anal. Chem. **1991** *63* 179

[62] Clark B.J., Van der Greef J., Large T., Poster presented at 18th I.S.C., Amsterdam **1990**

[63] Cohen A.S., Karger B.L., J. Chromatogr. **1987** *397* 409

[64] Drossman H., Luckey J.A., Kostichka A.J., D'Cunha J., Smith L.M.,Anal. Chem. **1990** *62* 900

[65] Cohen A.S., Najarian D., Smith J.A., Karger B.L., J. Chromatogr. **1988** *458* 323

[66] Guttman A., Cohen A.S., Henger D.N., Karger B.L., Anal. Chem. **1990** *62* 137

[67] Guttman A., Paulus A., Cohen A.S., Grinberg N., Karger B.L., J. Chromatogr. **1988** *448* 41

[68] Yin H-F., Lux J.A., Schomburg G., Poster presented at 18th I.S.C., Amsterdam **1990**

[69] Lux J.A., Yin H-F., Schomburg G., J. H.R.C. **1990** *13* 437

[70] Zhu M., Hansen D.L., Burd S., Gannon F., J. Chromatogr. **1989** *480* 311

[71] Olechno J.D., Tso J.M.Y., Thayer J., Wainwright A., International Lab **1991** *May* 42

[72] Lecoq H., bulletin de la societé Royale des Sciences de Liège **1944** *13* 20

[73] Grant I.H., PhD Thesis, University of Edinburgh **1990**

[74] Pretorius V., Hopkins B.J., Schieke J.D., J. Chromatogr. **1974** *99* 23

[75] Strain H.H., J. Am. Chem. Soc. **1939** *61* 1292

[76] Tsuda T., Nomura K., Nakagawa G., J. Chromatogr. **1982** *248* 241

[77] Tock P.P.H., PhD Thesis, University of Amsterdam **1990**

[78] Pfeffer W.D., Yeung E.S., Anal. Chem. **1990** *62* 2178

[79] Rice C.L., Whitehead R., J. Phys. Chem. **1965** *69* 4017

[80] Grieser F., Lamb R.N., Wiese R.N., Yates D.E., Cooper R., Healy T.W., Radiat. Phys. Chem. **1984** *23* 172

[81] Snyder L.R., Sep. Sci. **1966** *1* 191

[82] Lambert W.J., Middleton D.L., Anal. Chem. **1990** *60* 1585

[83] Wood L.A., J. Am. Chem. Soc. **1946** *68* 437

[84] Towns J.K., Regnier F.E., J. Chromatogr. **1990** *516* 69

[85] Healy T.W., White L.R., Adv. Colloid Interface Sci. 1978 9 303

[86] Laskowski J. , Kitchener J.A., J. Colloid Interface Sci. 1969 29 670

[87] Knox J.H., High Performance Liquid Chromatography, Edinburgh University Press, **1978**

[88] Martin A.J.P., Synge R.L.M., Biochem J. **1941** *35* 1358

[89] Giddings J.C., J. Chromatogr. **1987** *395* 19

[90] Taylor G.I., Proc. Roy. Soc. (London) **1953** *A219* 186

[91] Golay M.J.E. in Gas Chromatography, ed. Desty D.H., Butterworths, London, **1959** 36

[92] Aris R., Proc. Roy. Soc. (London) **1953** *A235* 67

[93] Sternberg J.C., Advances in Chromatography **1966** *2* 205

[94] Huang X., Coleman W.F., Zare R.N., J. Chromatogr. **1989** *480* 95

[95] Burton D.E., Sepaniak M.J., Maskarinec M.P., Chromatographia **1986** *21* 583

[96] Wallingford R.A., Ewing A.G., Anal. Chem. **1988** *60* 1972

[97] Grushka E., McCormick R.M., J. Chromatogr. **1989** *471* 421

[98] Otsuka K., Terabe S., J. Chromatogr. **1989** *480* 91

[99] Huang X., Pang T-K. J., Gordon M.J., Zare R.N., Anal. Chem. **1987** *59* 2747

[100] Green J.S., Jorgenson J.W., J. Chromatogr. **1989** *478* 63

[101] Jorgenson J.W., Lukacs K.D., Science **1983**

[102] Reijenga J.C., Aben, Verheggen, Everaerts, J. Chromatogr. **1983** *260* 241

[103] Mikkers F.E.P., Everaerts F.M., Verheggen Th.P.E.M., J. Chromatogr. **1979** *169* 1

[104] Thormann W., Michaud J-P, Mosher R.A., Electrophoresis **1986** 267

[105] Knox J.H., Chromatographia **1988** *26* 329

[106] Coxon M., Binder M.J., J. Chromatogr. **1974** *101* 1

[107] Brown J.F., Hinckley J.O.N., J. Chromatogr. **1975** *109* 218

[108] Jones A.E., Grushka E., J. Chromatogr. **1989** *466* 219

[109] Virtanen R., Acta Polytech. Scand. **1974** *123*

[110] Grushka E., McCormick R.M., Kirkland J.J., Anal. Chem. **1989** *61* 241

[111] Davis J.M., J. Chromatography **1990** *517* 521

[112] Jones H.K., Nguyen N.T., Smith R.D., J. Chromatogr. **1990** *504* 1

[113] Davis J., Anal. Chem. **1989** *61* 2455

[114] Holman J.P., Heat Transfer, International Edition **1985**, McGraw-Hill Book Co..

[115] Terabe S., Otsuka K., Ando T., Anal. Chem. **1989** *61* 251

[116] Huang X., Gordon M.J., Zare R.N., Anal. Chem. **1988** *60* 375

[117] Walbroehl Y., Jorgenson J.W., J. Microcol. Sep. **1989** *1* 41

[118] Tsuda T., Novotny M., Anal. Chem. **1978** *50* 271

[119] Tsuda T., Tanaka I., Nakagawa G., Anal. Chem. **1984** *56* 1249

[120] Kennedy R.T., Jorgenson J.W., Anal. Chem. **1989** *61* 1128

[121] Ghaemi Y., Wall R.A., J. Chromatogr. **1980** *198* 397

[122] Jones G., Dole M., J. Am. Chem. Soc. **1929** *51* 2950

[123] Stokes R.H., Mills R., Viscosity of Electrolytes and Related Properties, The International Encyclopedia of Physical and Chemical Physics Volume 3, Pergamon Press **1965**

[124] Gurney R.W., Ionic Processes in Solution, Dover Publications Inc., **1962**

[125] Handbook of Chemistry and Physics 55th Edition, CRC Press **1974-1975**

[126] Wilke C.R., Chang P., AIChE **1955** *1* 264

[127] Scheibel E.G., Ind. Eng. Chem. **1954** *46* 2007

[128] Innes K.K., Albright L.F., Ind. Eng. Chem **1957** *49* 1793

[129] Othmer D.F., Thakar M.S., Ind. Eng. Chem **1953** *45* 589

[130] Longsworth L.G., J. Am. Chem. Soc. **1954** *58* 770

[131] Terabe S., Otsuka K., Ando A., Anal. Chem **1985** *57* 834

[132] Atamna I.Z., Metral C.J., Muschik G.M., Issaq H.J., J. Liq. Chrom. **1990** *13* 2517

[133] Özisik M.N., Heat Transfer-A Basic Approach, International Edition **1985**, McGraw-Hill Book Co..

[134] Roberts J. K., Heat and Thermodynamics, 3rd Edition, Blackie, London **1947**

[135] Churchill S.W., Chu H.H.S., Int. Journal Heat Mass Transfer **1975** *18* 1049

[136] Morgan, Advances in Heat Transfer,**1975** *16* 199

[137] Handbook of tables for Applied Engineering Science, Chemical Rubber Co., **1970**

[138] McAdams W.H., Heat Transmission, 3rd edition, McGraw-Hill

[139] Philip J.R., Wooding R.A., J. Phys. Chem. **1970** *52* 953